Efficient New Routes to Leading Ruthenium Catalysts, and Studies of Bimolecular Loss of Alkylidene

Craig Day

A thesis submitted
in partial fulfillment of the requirements for the Master's degree in
Chemistry

Master of Science

Center for Catalysis Research and Innovation
Department of Chemistry and Biomolecular Science
Ottawa-Carleton Chemistry Institute
Faculty of Science
University of Ottawa

Table of Contents

Abstract

Olefin metathesis is an exceptionally versatile and general methodology for the catalytic assembly of carbon-carbon bonds. Ruthenium metathesis catalysts have been widely embraced in academia, and are starting to see industrial uptake. However, the challenges of reliability, catalyst productivity, and catalyst cost have limited implementation even in value-added technology areas such as pharmaceutical manufacturing. Key to the broader adoption of metathesis methodologies is improved understanding of catalyst decomposition. Many studies have focused on phenomenological relationships that relate catalyst activity to substrate structure, and on the synthesis of new catalysts that offer improved activity. Until recently, however, relatively little attention was paid to catalyst decomposition. The first part of this thesis explores a largely overlooked decomposition pathway for "second-generation" olefin metathesis catalysts bearing an *N*-heterocyclic carbenes (NHC) ligand, with a particular focus on identifying the Ru decomposition products. Efforts directed at the deliberate synthesis of these products led to the discovery of a succinct, high-yielding route to the second-generation catalysts.

Multiple reports, including a series of detailed mechanistic studies from our group, have documented the negative impact of phosphine ligands in Ru-catalyzed olefin metathesis. Phosphine-free derivatives are now becoming widely adopted, particularly in pharma, as recognition of these limitations has grown. Decomposition of the phosphine-free catalysts, however, was little explored at the outset of this work. The only documented pathway for *intrinsic* decomposition (i.e. in the absence of an external agent) was β-hydride elimination of the metallacyclobutane (MCB) ring as propene. An alternative mechanism, well established for group 3-7 and first-generation ruthenium metathesis catalysts, is bimolecular coupling (BMC) of the four-coordinate methylidene intermediate. However, this pathway was widely viewed as irrelevant to decomposition of second-generation Ru catalysts. This thesis work complements parallel studies from the Fogg group, which set out to examine the relevance and extent of BMC for this important class of catalysts. First, β-hydride elimination was quantified, to assess the importance of the accepted pathway. Even at low catalyst concentrations (2 mM Ru), less than 50% decomposition was shown to arise from β-hydride elimination. Parallel studies by Gwen Bailey demonstrated ca. 80% BMC for the fast-initiating catalyst $RuCl_2H_2IMes(=CHPh)(py)_2$ **GIII**. Second, the ruthenium products of decomposition were isolated and characterized. Importantly, and in contrast to inferences drawn from the serendipitous isolation of crystalline

byproducts (which commonly show a cyclometallated NHC ligand), these complexes show an intact H_2IMes group. This rules out NHC activation as central to catalyst decomposition, suggesting that catalyst redesign should not focus on NHC cyclometallation as a core problem. Building on historical observations, precautions against bimolecular coupling are proposed to guide catalyst choice, redesign, and experimental setup.

The second part of this thesis work focused on the need for more efficient routes to second-generation Ru metathesis catalysts, and indeed a general lack of convenient, well-behaved precursors to $RuCl_2(H_2IMes)$. This challenge was met by building on early studies in which metathesis catalysts were generated in situ by thermal or photochemical activation of $RuCl_2$(*p*-cymene)(PCy_3) in the presence of diazoesters. Such piano-stool complexes (including the IMes analogue) have also been applied more broadly as catalysts, inorganic drugs, sensors, and supramolecular building blocks. However, $RuCl_2$(*p*-cymene)(H_2IMes), which should in principle offer access to the $RuCl_2(H_2IMes)$ building block, has been described as too unstable for practical use. The basis of the instability of $RuCl_2$(*p*-cymene)(H_2IMes) toward loss of the *p*-cymene ring was examined. Key factors included control over reaction stoichiometry (i.e. limiting the proportion of the free NHC), limiting exposure to light, and maintaining low concentrations to inhibit bimolecular displacement of the *p*-cymene ring. A near-quantitative route to $RuCl_2$(*p*-cymene)(H_2IMes) was achieved using appropriate dilutions and rates of reagent addition, and taking precautions against photodecomposition. This approach was used to develop atom-economical syntheses of the Hoveyda catalyst, $RuCl_2(H_2IMes)$(=CHAr) (Ar = 2-isopropoxybenzylidene) and $RuCl_2(H_2IMes)(PPh_3)$(=CHPh), a fast-initiating analogue of **GII**. Related *p*-cymene complexes bearing bulky, inflexible imidazolidene or other donors may likewise be accessible.

List of Contributions

Publications (F = Full Paper, C = Communication)

2C. High-Yield Synthesis of a Long-Sought, Labile Ru-NHC Reagent, and Its Application to the Concise Synthesis of Second-Generation Metathesis Catalysts. **Craig S. Day** and Deryn E. Fogg. *Organometallics* **2018**, 37, 4551-4555 (ACS Editor's Choice)

1F. Bimolecular Coupling as a Vector for Decomposition of Fast-Initiating Olefin Metathesis Catalysts. Gwendolyn A. Bailey, Marco Foscato, Carolyn S. Higman, **Craig S. Day**, Vidar R. Jensen, and Deryn E. Fogg. *J. Am. Chem. Soc.* **2018**, 140, 22, 6931-6944

Presentations (O = Oral, P = Poster)

O1. **Day, C**; Fogg, D. E. "An Improved Route to a Versatile Piano-Stool Complex Bearing an N-Heterocyclic Carbene". 100^{th} Ottawa-Carlton Chemistry Institute Research Day, Ottawa, Canada: May 22, 2018

P3. **Day, C**; Fogg, D. E. "Ruthenium Metathesis Catalysts Containing Cyclic (Alkyl)(Amino) Carbene (CAAC) Ligands: Robustness to External Assault". 50th Inorganic Discussion Weekend, Toronto, Canada: Nov 4-6, 2017

P2. **Day, C**; Bailey, G. A.; Fogg, D. E "Bimolecular Decomposition of Rapidly-Initiating Ruthenium Metathesis Catalysts". 100th Canadian Chemistry Conference and Exhibition, Toronto, Canada: May 28- June 1, 2017

P1. **Day, C**; Bailey, G. A.; Fogg, D. E "Bimolecular Decomposition of Rapidly-Initiating Ruthenium Metathesis Catalysts". Ottawa-Carlton Chemistry Institute Research Day, Ottawa, Canada: May 25, 2017

Acknowledgments

Firstly I would like to thank my supervisor Deryn Fogg for continually pushing me to succeed and develop as a chemist and person. The lessons I learned during my time here will be invaluable to my life moving forward.

I would also like to thank my mentors at York University. Dr. Organ taught me the importance of hard work and dedication, Dr. Orellana inspired my love of chemistry and Dr. Wilson showed me tremendous support.

This thesis wouldn't have been possible without the amazing faculty at uOttawa. Dr. Baker has been an incredible role model for me - showing a balance between passion for chemistry and the importance of kindness and interpersonal relationships. Dr. Glenn Facey is thanked for the incredible technical assistance with NMR, along with Dr. Gambarotta, Dr. Richeson, and Dr. Hemmer for useful discussions about chemistry.

I would also like to thank my labmates who kept me sane for the last two years and provided a place I looked forward to going each and every day. Daniel Nascimento, Stephanie Rufh, and Alex Goudreault, thank you for the warm welcome to uOttawa and the great friendships. Stephanie Ton for the lunch trips and most importantly taking care of Puppers. Andrew White for the continual joviality and discussions about chemistry. Finally I'd like to thank Carolyn Higman and Gwendolyn Bailey for training me in how to perform organometallic chemistry in a methodical manner.

To my friends Jee Kwak, Minhao Zhang, Faizan Rasheed, and Arthur Kwok among others who have really stood out to me for their support and grounding perspectives. You guys have been like family to me, thank you for your generosity and kindness.

My family who has always been there, Mom, Dad, Mike, Em, Jess thank you for your endless support. If I ever have a problem, I know you have my back which has allowed me to push myself to pursue the unknown.

In the field of observation, chance favors the prepared mind.

- **Louis Pasteur**

Organic and main group compounds

H_2IMes	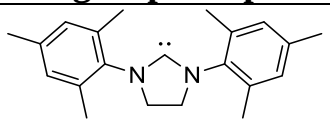	**1**	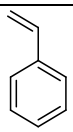
2	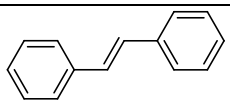	**3**	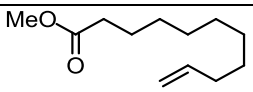
4	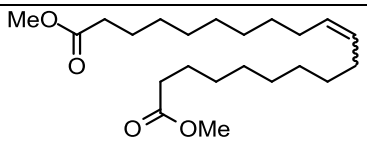	DMT	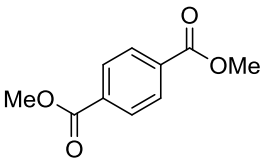
KTp	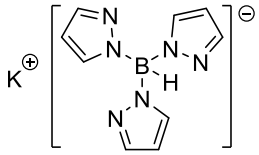	Anthracene	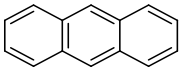
TMB	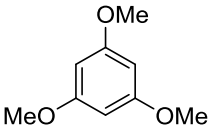		

Transition-metal complexes

Ti-1	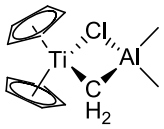	**Mo-1**	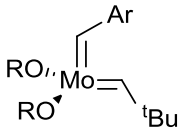
W-1	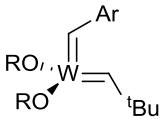	**Mo-2**	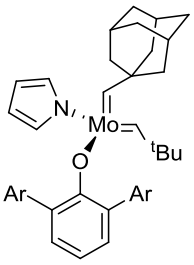
GI	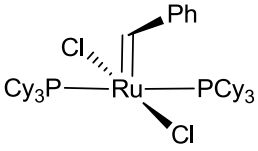	**GII**	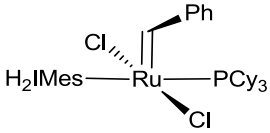
HII	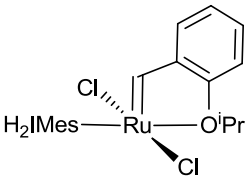	**GIII'**	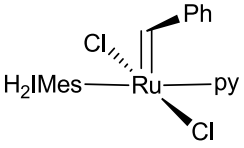
GIII	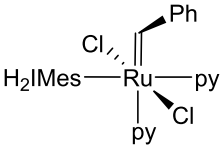	**GII-PPh_3**	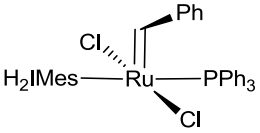
GreII	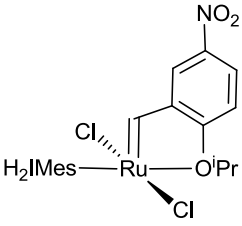	**DA**	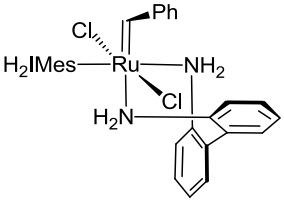

PII	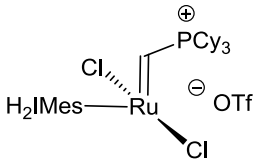	**CAAC-Hov**	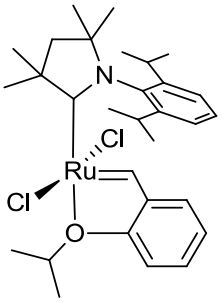
Ru-1	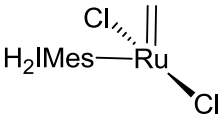	**Ru-2**	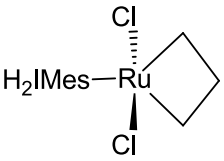
Ru-3	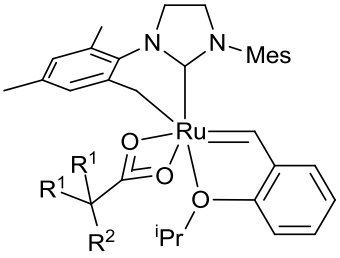	**Ru-4**	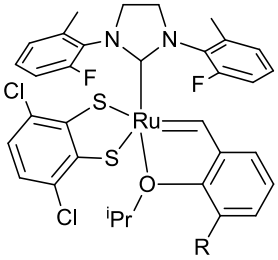
Ru-5	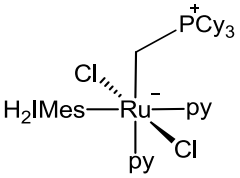	**Ru-6**	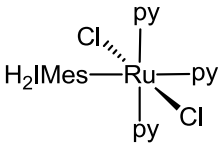
Ru-7	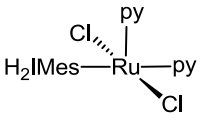	**Ru-8**	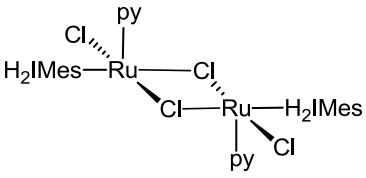
Ru-9	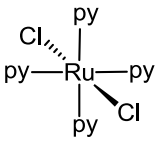	**Ru-10**	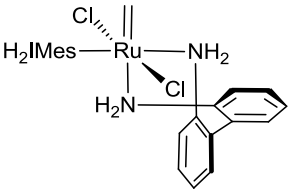

Ru-11	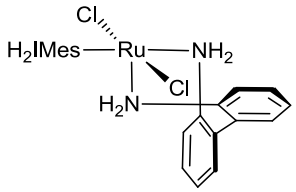	**Ru-12**	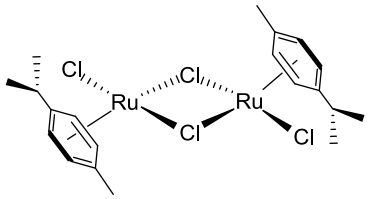
Ru-13	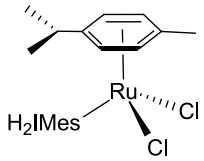	**Ru-14**	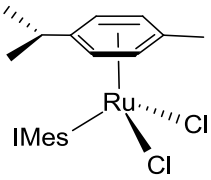
Ru-15	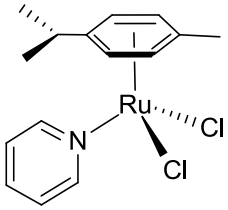		

Chapter 1. Introduction

1.1 Olefin Metathesis

1.1.1 History of Olefin Metathesis

Olefin (alkene) metathesis is a metal-catalyzed chemical reaction that has become an essential part of the chemist's toolbox.[1-4] Metathesis catalysts redistribute carbon-carbon double bonds via scission and reformation[1] (Figure 1.1). The reaction has been widely adopted in organic chemistry, material and polymer science, along with green chemistry and biochemistry. Uptake of metathesis began with ill-defined heterogeneous catalyst "recipes" used in petroleum processing nearly 60 years ago.[5,6] Well-defined molecular catalysts are now widely used to construct C-C bonds.[7]

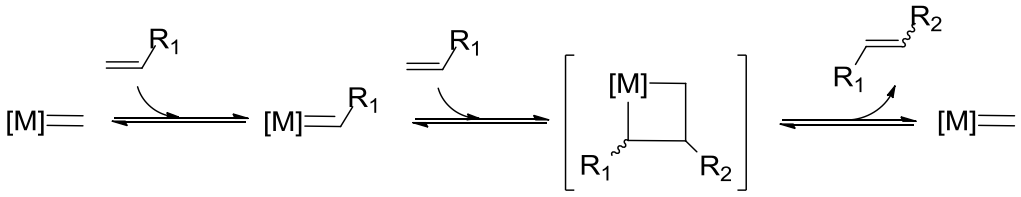

Figure 1.1 The Olefin Metathesis Reaction

The metathesis catalysts first discovered in the 1950s at DuPont consisted of heterogeneous mixtures of W and Mo oxides,[5] which gave 1-butene and ethylene from propene when heated.[5,6] Implementation of heterogeneous catalysts in industrial processes followed shortly, with Eleuterio's 1960 report of the polymerization of norbornene using $WCl_6/AlEt_2Cl$ systems.[6] In 1967, Calderon coined the term "olefin metathesis" for such reactions.[8-10]

These discoveries were followed by many attempts to elucidate the mechanism. Postulated intermediates include a four-centered cyclobutane-metal species,[10] a tetra(methylene)metal complex,[11] and metallocyclopentane intermediate.[12] Chauvin put together three key findings to formulate a mechanism wherein olefin metathesis could occur via successive [2+2] cycloadditions/ cycloreversions (Figure 1.1) in 1971.[13] The first was a report by Fischer[14] of tungsten-carbene complex $[W(CO)_5(C(CH_3)(OCH_3))]$. Second was Natta's polymerization of cyclopentene by WCl_6 and $AlEt_3$,[15] and thirdly the observed formation of ethylene and 2-butene from propene, catalyzed by $[W(CO)_6]$ on alumina.

The Chauvin mechanism postulates that a metal species bearing an alkylidene coordinates to an incoming olefin, and then undergoes a [2+2] cycloaddition forming a metallacyclobutane.[13] This metallacyclobutane then undergoes a [2+2] cycloreversion to either reform the starting alkylidene and olefin (this resulting in unproductive metathesis), or to liberate a new alkylidene and olefin (productive metathesis). The search for well-defined intermediates was aided by the discovery of stable metal carbenes such as $W(CO)_5(COCH_3)(CH_3)$[14,16] which led to synthesis of metathesis-active catalysts[17,18] (Figure 1.2).

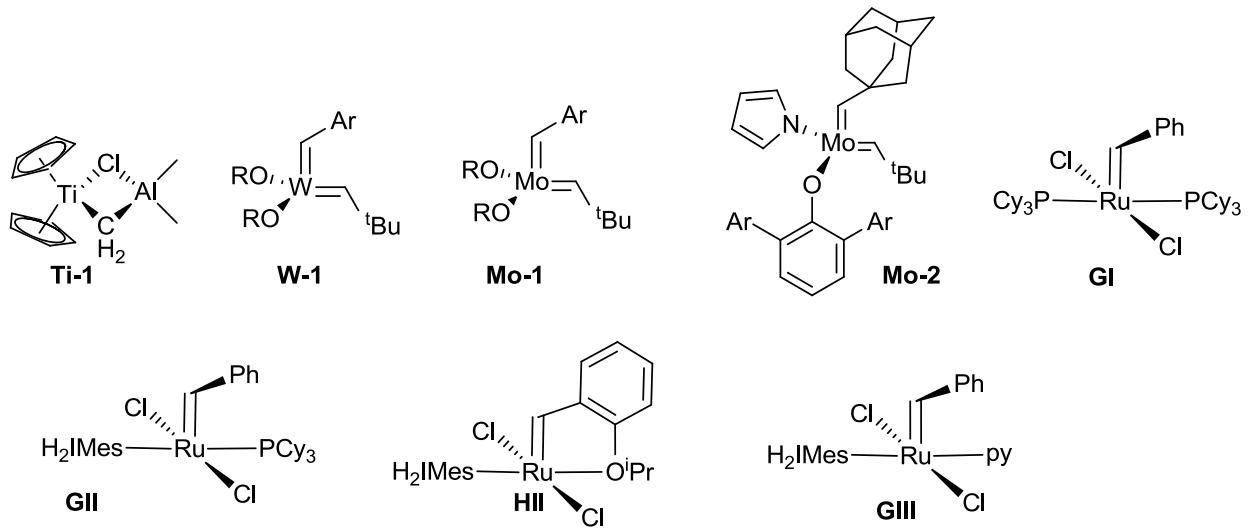

Figure 1.2 Olefin Metathesis Catalysts

Despite the opportunities revealed by early transition-metal catalysts (Mo, W, Re, Ti), their applications in synthetic organic chemistry have been limited. These catalysts are incompatible with oxophilic or protic functionalities, and are challenging to handle. Systems such as **W-1**, **Mo-1**, and **Ti-1** are highly oxophilic, and readily decompose in air. Ruthenium catalysts are less air-sensitive and more functional-group tolerant, which allowed these methodologies to be implemented by synthetic organic chemists in less rigorous conditions.

1.1.2 Metathesis Reaction

In recent years, olefin metathesis has emerged as a general methodology for carbon-carbon bond formation.[7] For their contribution to the development of olefin metathesis as a practical methodology Robert Grubbs, Richard Schrock, and Yves Chauvin were awarded the 2005 Nobel Prize in Chemistry.[2-4] An attractive feature of olefin metathesis is its versatility. Olefin

metathesis is commonly employed to form terminal, internal, cyclic, macrocyclic olefins and polymers (Figure 1.3). Successful implementation of olefin metathesis typically requires a thermodynamic driving force (e.g volatile products, release of ring strain, or the formation of stable products). Metathesis catalysts are routinely used in ring-closing metathesis (RCM) of α,ω-dienes to form cyclic olefins of interest in the pharmaceutical[19,20] and fine-chemical sectors.[21] Polymers can also be accessed via acyclic diene metathesis (ADMET) or ring-opening metathesis polymerisation (ROMP) of strained cyclic olefins. Furthermore, intermolecular reactions of two olefins in cross metathesis (CM) reactions are highly desirable in commodity manufacturing. Of interest is the transformation of plant oils to building-block chemicals[22-24] as well as CM of essential oils to yield value-added products.[25,26]

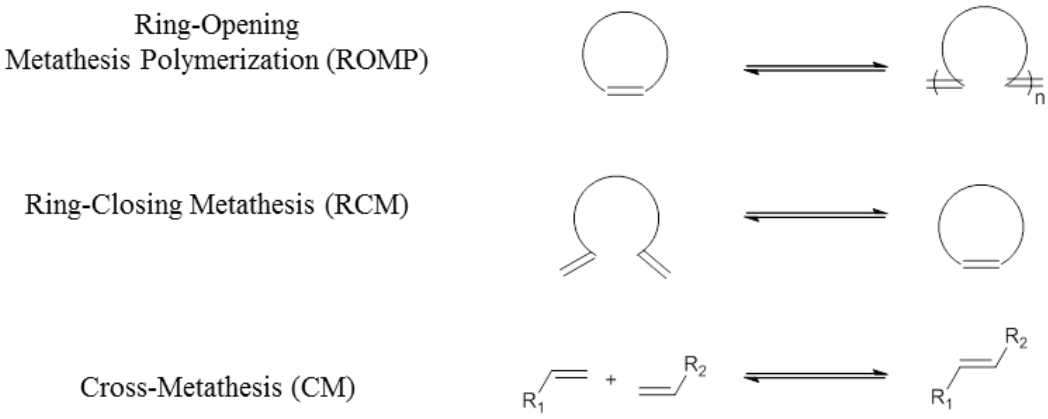

Figure 1.3 Common Metathesis Reactions

Though the thermodynamic driving force of olefin metathesis has been used with great success, escaping this paradigm is at the forefront of scientific research, since the thermodynamically favoured products are not always desirable. These challenges are highlighted in articles on resolving cis/trans selectivity of olefins, where trans (thermodynamic) olefins are favored over cis olefins. Among other challenging problems is the formation of dimers at higher concentrations in ring-closing metathesis. Attempts to alleviate these constraints are highlighted by work on kinetic E-selective macrocyclic ring-closing metathesis and Z-selective catalysts along with RCM at higher concentrations.

1.1.3 Well-Defined Ruthenium Metathesis Catalysts

The first molecular ruthenium-carbene complex, $RuCl_2(PPh_3)(=CH\text{-}CH=CPh_2)$, was synthesized by Grubbs in 1992.[27] It was found to promote ROMP of low-strain olefins and RCM of functionalized dienes. In 1995, this was followed by[28] $[RuCl_2(PCy_3)_2(=CHPh)]$ **GI**, commercialized as the first-generation Grubbs catalyst. Both catalysts are less reactive than their Mo counterpart (**Mo-1**) but exhibit better air stability and functional-group compatibility.[29] These precatalysts have been shown to initiate by loss of phosphine, forming a 14-electron active species which can then coordinate an olefin. With the intention of promoting phosphine dissociation, Grubbs introduced an N-heterocyclic carbene (NHC) ligand, which was anticipated to have a trans-labilizing effect.[30] While this assumption proved inaccurate, the increase in electron density at Ru associated with the stronger donor ability of the NHC (Figure 1.4) promoted olefin binding, and greatly improving activity over the first-generation catalysts.

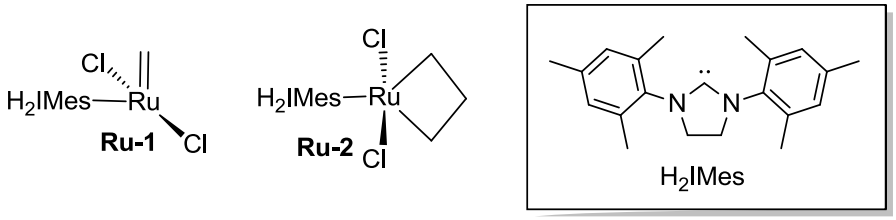

Figure 1.4 Catalytically-Active Intermediates for Second-Generation Ruthenium Metathesis Catalysts

The increased activity of second-generation catalysts can be rationalized by increased back-donation to the incoming olefin,[31-33] one of the driving forces behind olefin metathesis. Multiple iterations of these catalysts were pursued, and select examples are highlighted in Figure 1.5. Modification of the benzylidene to include a chelating isopropoxy substituent that replaces PCy_3 gives the Hoveyda catalyst **HII**,[34] which avoids the limitations associated with the stabilizing phosphine ligand.[35] Grela's analogue **GreII**, in which the *p*-nitro functionality weakens the Ru-OR bond, enabling faster initiation, has also been widely adopted. Other noteworthy alternatives are fast-initiating derivatives that replace the phosphine ligand with nitrogen donors. **GIII** has been extensively implemented in ROMP.[36] Our group[37] analyzed its limitations (as well as those of **GII**, **HII**, etc.), and used this knowledge to design the dianiline-stabilized catalyst **DA**. The latter exhibited standout performance via hydrogen-bonding assisted macrocyclization. Less

successful redesign efforts involved use of unsaturated NHCs.[38,39] Much more promising are cyclic alkyl amino carbenes, as well as approaches pioneered by our group[40-43] involving the use of "pseudohalide" ligands.[38,39]

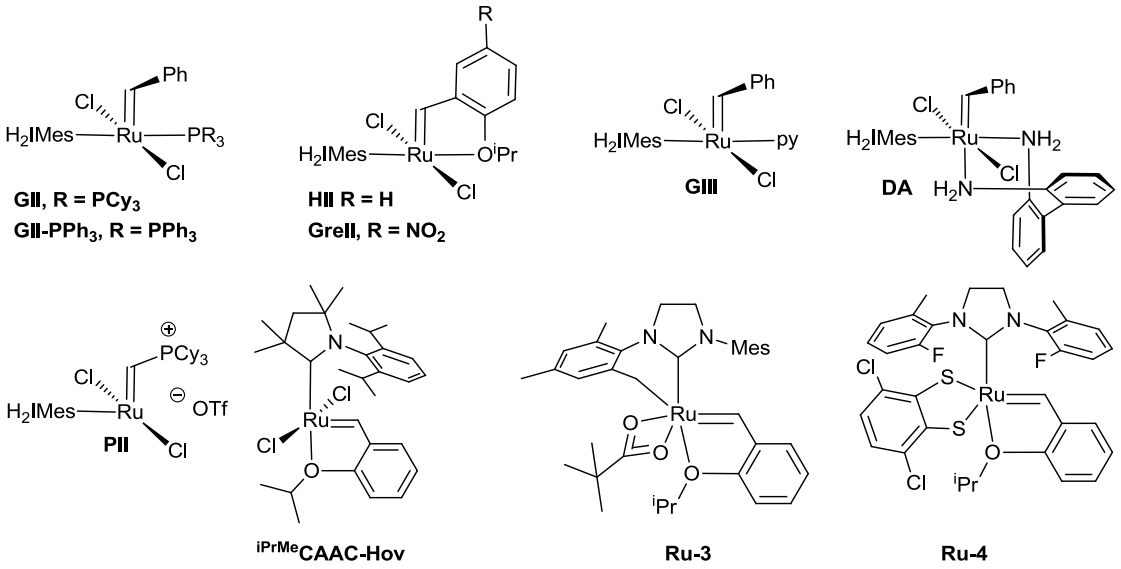

Figure 1.5 Novel Catalyst Structures

Large scale use of ruthenium metathesis catalysts has primarily been in RCM of active pharmaceutical ingredients (APIs).[44] HCV inhibitors with ring sizes ranging from 14-20 atoms have been accessed by this methodology at 0.2-0.05 M substrate. Other arenas of metathesis include the synthesis of high-density aviation fuels. RCM of neat linalool at room temperature with **HII** followed by further modifications provides a rocket propellant. Self-metathesis of soybean oil (triglycerides) with **GII** in 0.005 mol% followed by hydrogenation provides oligomeric products used in personal care products.

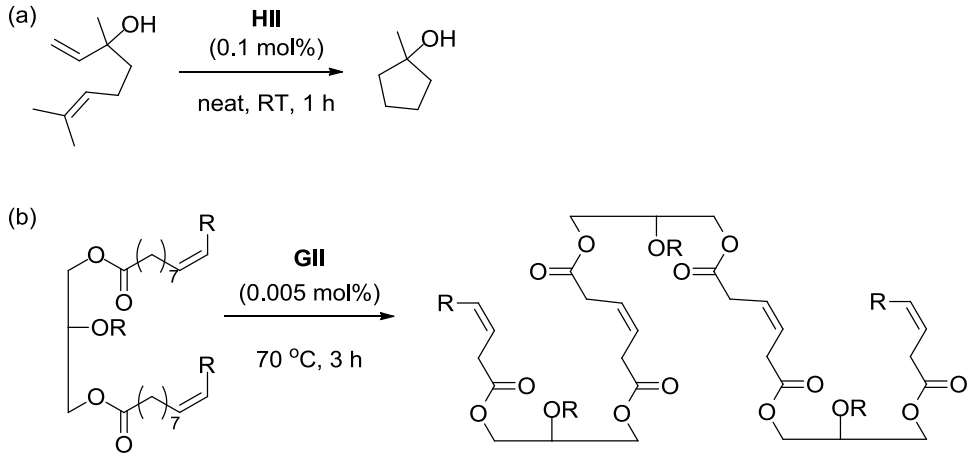

Figure 1.6 Industrial Metathesis Reactions

1.1.4 Mechanism and Mechanistic Intermediates in Ru-Based Olefin Metathesis

For the most common phosphine-bearing precatalysts, entry into the catalytic cycle starts with phosphine dissociation forming the active 14-electron Ru-alkylidene intermediate **Ru-1**. This is followed by either re-binding of the phosphine to reform the pre-catalyst, or η^2 binding of an incoming olefin. In keeping with the Chauvin mechanism,[45,46] the bound olefin undergoes a [2+2] cycloaddition with the Ru-alkylidene to form the metallacyclobutane. Cycloreversion from the metallacyclobutane eliminates the desired metathesis product and the active Ru-alkylidene intermediate.

Kinetic studies have established that phosphine dissociation in catalysts such as **GII** is rate-determining.[32] For catalysts with chelating alkylidenes (e,g **HII**, or **GreII**), oxygen dissociation or olefin binding may be rate-determining, depending on the nature of the catalyst and the bulk of the incoming olefin.[47-49] Once initiation occurs, the rate-determining step is less clear (Figure 1.7).[45,46] Altering the NHC, substrate or even solvent seems to drastically alter selectivity and reactivity profiles. Each of these conditions therefore must be optimized to achieve maximum selectivity, and productivity. A "general catalyst" in olefin metathesis appears to be an unrealizable goal. As noted by Schrock and Hoveyda, the more readily modifiable a catalyst class, and the larger the number of available catalysts, the better the odds of obtaining desirable results.[50]

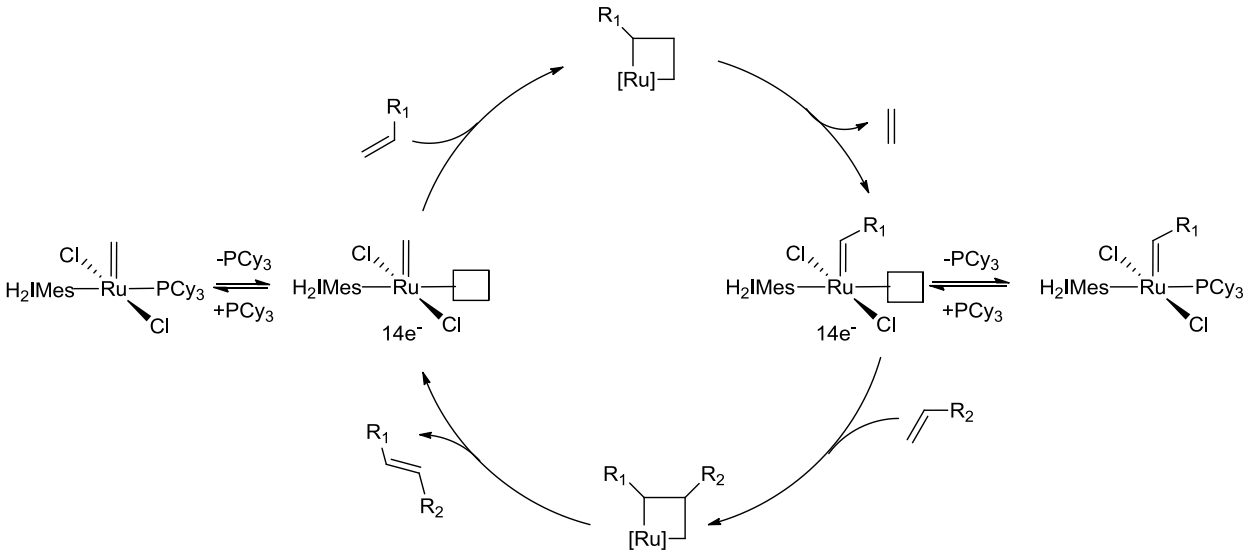

Figure 1.7 Catalytic Cycle for Ru Olefin Metathesis Including Important Intermediates

1.1.5 Decomposition of Ru Catalysts

Catalyst decomposition – i.e. loss of the alkylidene from [M]=CHR or the MCB ring – is problematic because higher catalyst loadings are therefore required, often leading to difficulties in product isolation.[41,44,51,52] The ruthenium products of decomposition are also problematic, as they promote undesirable olefin isomerization.[53-58] Understanding these decomposition pathways is required to inform catalyst and process design.[44] Most studies of the decomposition of metathesis catalysts have focused on the easily-accessible precatalysts.[59,60] Justin Lummiss' development of the first clean, high-yield synthesis[61,62] of **GIIm**, the resting-state species for **GII**, opened the door to detailed examination of the latter. Empirical studies had shown that contaminants such as N-donors[63] and phosphines[64] are detrimental to catalyst productivity: the availability of **GIIm** was a major advance in enabling direct examination of the mechanism by which this complex and its 14-electron derivative are decomposed. Below will be addressed the most substantive work on catalyst decomposition.

The poor performance of the second-generation Grubbs catalyst **GII** is largely due to the stabilizing PCy_3 ligand. The low lability of PCy_3 impedes entry of the precatalyst into the catalytic cycle.[32] Moreover, recapture of PCy_3 by methylidene intermediate **Ru-1** forms an off-cycle resting-state species **GIIm**. Re-entry into the cycle from **GIIm** is nearly 300 times slower than entry of **GII**,[65] owing to Ru→PCy_3 backbonding, compounded by the limited steric

pressure exerted by the methylidene ligand (compared to benzylidene) on the phosphine ligand.[66] A role for alkylidene rotation has also been suggested.[67,68] Finally, the nucleophilicity of PCy_3 is a challenge. It severely limits metathesis of electron-deficient olefins,[69] and also participates in nucleophilic abstraction of the methylidene, which forms the phosphonium salt $[MePCy_3]Cl$ as a by-product (Figure 1.8).[70,71]

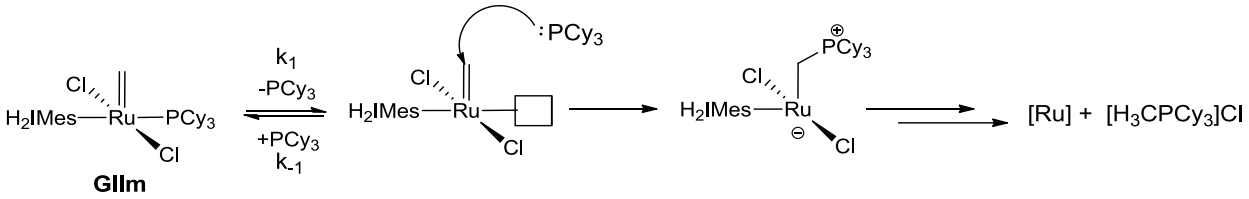

Figure 1.8 Nucleophilic Abstraction of the Methylidene Ligand by Dissociated Phosphine

The mechanistic basis for the latter reaction was established by our group in studies involving ^{13}C-labeling of the methylidene ligand in **GI**.[61] Liberation of $[^{13}CH_3PCy_3]Cl$ confirmed the origin of the methyl ligand in the phosphonium salt, while direct insight into the deactivation event was enabled by treating **GIm** with pyridine, this giving near-quantitative access to the σ-alkyl species, which was characterized by NMR analysis and X-ray crystallography. The relevance of these results to NHC systems was confirmed by treating **GIIm-IMes** and **GIIm-H_2IMes-d_{22}** with pyridine (Figure 1.9). This effects immediate formation of a short-lived σ-alkyl species, which rapid liberates $[MePCy_3]Cl$ by cyclometallation of a mesityl ring. Importantly, our group demonstrated that nucleophilic abstraction of the methylidene is greatly accelerated by donor groups ranging from pyridines to water.[35] These promote *associative* loss of phosphine, overcoming the rate barrier to PCy_3 loss, and stabilizing the methylidene species for attack by free phosphine.

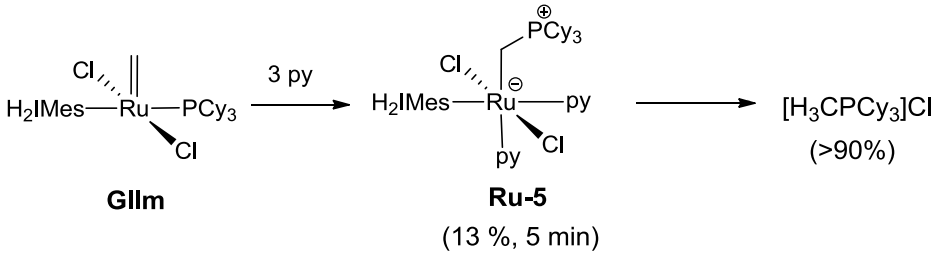

Figure 1.9 Formation of a σ-Alkyl Complex

The bulkier ethylidene ([Ru]=CHMe) intermediate, generated by treating **GII** with cis-2-butene, did not liberate the ethylphosphonium salt [$EtPCy_3$]Cl, indicating that modest steric protection aids in inhibiting nucleophilic abstraction of the methylidene ligand. However, [$MePCy_3$]Cl was slowly generated, presumably via isomerization to 1-butene and subsequent methylidene formation. In addition, it should be noted that small nucleophiles such as unhindered primary amines can abstract even benzylidene ligands.[61,72,73]

An alternative decomposition pathway involves deprotonation of the metallacyclobutane by Bronsted base. Addition of DBU to precatalyst **GII** or resting state **GIIm** yielded stable DBU adducts.[72] In the presence of an olefin, however, rapid decomposition occurred. Similar results were observed with **HII**.[73] Kinetics, labelling, and computational studies subsequently demonstrated that decomposition proceeds via deprotonation of the metallacyclobutane ring at the β position.[74]

The MCB can also decompose in the absence of base. Direct study of the MCB was aided by Piers' discovery of the four-coordinate phosphonium alkylidene complex **PII**, which initiates irreversibly.[75–78] Treating **PII** with ethylene at –78 °C enabled direct observation of the unsubstituted MCB. When ^{13}C-labelled ethylene was used, ^{13}C-propene was observed on warming. This confirmed MCB decomposition via β-hydride elimination (Figure 1.10). This was the first direct evidence for such decomposition of the MCB, although others had previously suggested such a pathway to account for the observation of propene on ethenolysis of **GIIm** and **HII**.[79,80] (It should be noted that **GIIm** normally decomposes by another pathway involving methylidene abstraction: see below. The observation of propene for this species implies that the PCy_3 was converted to its oxide by trace air). Computational analysis suggested an energy barrier of 24.3 kcal/mol for β-hydride elimination.

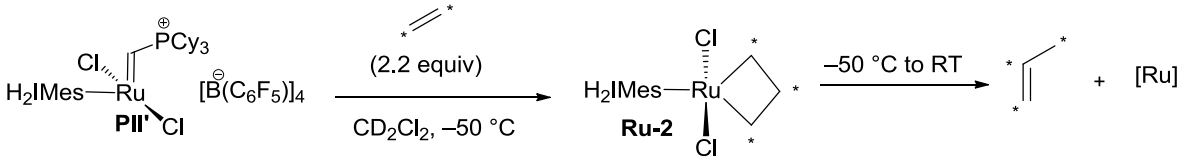

Figure 1.10 Propenes Originating in **Ru-2**

Another widely discussed decomposition pathway is bimolecular coupling. This pathway has been proposed for first-generation systems stabilized with PPh_3 ligands. An early drawback of

these catalysts was that they underwent bimolecular coupling at room temperature, losing the alkylidene ligand. Once PCy_3 ligands were installed, the precatalysts were more robust to this pathway. However, studies by Grubbs show that by treating **GI** with CuCl, second-order decomposition occurs. These results were rationalized by abstraction of PCy_3 from **GI** forming a four coordinate alkylidene that then undergoes bimolecular coupling.[81-85] Bimolecular coupling of second-generation systems has been dismissed, as discussed in more detail in Chapter 3.

1.2 Scope of thesis work

Olefin metathesis is now a powerful tool for the assembly of carbon-carbon bonds. The metathetical behaviour of the active species is now generally well understood. Deactivation pathways, however, have attracted less attention. Understanding intrinsic decomposition pathways, and developing ways to reduce them, is central to rational catalyst design or use. Reduced decomposition could promote broader implementation of metathesis in pharmaceutical manufacturing and elsewhere. To put the economic impact in perspective, the cost of the important catalyst **HII**, at $472 /g, is significantly higher than the Pd-PEPPSI^{IPr} catalyst also used for carbon-carbon bond-forming methodologies ($151/g).

This thesis seeks to contribute to the practice of olefin metathesis by examining an intrinsic decomposition pathway for important phosphine-free ruthenium metathesis catalysts. Chapter 2 presents all experimental details, following which Chapter 3 outlines these efforts, as well as efforts to characterize the ruthenium decomposition products to gain further insight. A promising Ru precursor, $RuCl_2(H_2IMes)$(*p*-cymene), was identified in the course of this synthetic work. Chapter 4 examines the instability of this valuable Ru-H_2IMes building block, and describes a high-yield synthesis of this complex. Its utility as a precursor to two second-generation metathesis catalysts, **HII** and **GII-PPh_3**, was demonstrated. Chapter 5 summarizes the key advances and contributions of this thesis and suggests future work.

1.3 References

(1) Grubbs, R. H.; Wenzel, A. G., *Handbook of Metathesis*. 2nd ed.; Wiley-VCH: Weinheim, 2015.
(2) Chauvin, Y. *Angew. Chem., Int. Ed.* **2006**, *45*, 3741–3747.
(3) Schrock, R. R. *Angew. Chem., Int. Ed.* **2006**, *45*, 3748–3759.
(4) Grubbs, R. H. *Angew. Chem., Int. Ed.* **2006**, *45*, 3760–3765.
(5) Banks, R. L.; Bailey, G. C. *Ind. Eng. Chem. Prod. Res. Dev.* **1964**, *3*, 170–173.
(6) Eleuterio, H. S. *J. Mol. Catal.* **1991**, *65*, 55-61.
(7) Grela, K., *Olefin Metathesis-Theory and Practice*. Wiley: Hoboken, NJ, 2014.
(8) Calderon, N.; Chen, H. Y.; Scott, K. W. *Tetrahedron Lett.* **1967**, 3327–3329.
(9) Calderon, N. *Acc. Chem. Res.* **1972**, *5*, 127–132.
(10) Calderon, N.; Ofstead, E. A.; Ward, J. P.; Judy, W. A.; Scott, K. W. *J. Am. Chem. Soc.* **1968**, *90*, 4133–4140.
(11) Lewandos, G. S.; Pettit, R. *J. Am. Chem. Soc.* **1971**, *93*, 7087-7088.
(12) Grubbs, R. H.; Brunck, T. K. *J. Am. Chem. Soc.* **1972**, *94*, 2538-2540.
(13) Hérisson, J. L.; Chauvin, Y. *Makromol. Chem.* **1971**, *141*, 161–176.
(14) Fischer, E. O.; Maasbol, A. *Angew. Chem., Int. Ed.* **1964**, *3*, 580–581.
(15) Natta, G.; Dall'Asta, G.; Mazzanti, G. *Angew. Chem., Int. Ed.* **1964**, *3*, 765–772.
(16) Schrock, R. R. *Adv. Synth. Catal.* **2002**, *344*, 571–572.
(17) Katz, T. J.; McGinnis, J. *J. Am. Chem. Soc.* **1975**, *97*, 1592–1594.
(18) Grubbs, R. H.; Burk, P. L.; Carr, D. D. *J. Am. Chem. Soc.* **1975**, *97*, 3265-3267.
(19) Giordanetto, F.; Kihlberg, J. *J. Med. Chem.* **2014**, *57*, 278-295.
(20) Villar, E. A.; Beglov, D.; Chennamadhavuni, S.; Porco, J. A.; Kozakov, D.; Vajda, S.; Whitty, A. *Nat. Chem. Biol.* **2014**, *10*, 723-731
(21) Heinis, C. *Nat. Chem. Biol.* **2014**, *10*, 696-698
(22) Rybak, A.; Meier, M. A. R. *Green Chem.* **2007**, *9*, 1356–1361.
(23) Miao, X.; Dixneuf, P. H.; Fischmeister, C.; Bruneau, C. *Green Chem.* **2011**, *13*, 2258–2271.
(24) Miao, X.; Malacea, R.; Fischmeister, C.; Bruneau, C.; Dixneuf, P. H. *Green Chem.* **2011**, *13*, 2911–2919.
(25) Santos, A. G.; Bailey, G. A.; dos Santos, E. N.; Fogg, D. E. *ACS Catal.* **2017**, *7*, 3181−3189.
(26) Lummiss, J. A. M.; Oliveira, K. C.; Pranckevicius, A.; Santos, A.; dos Santos, E. N.; Fogg, D. E. *J. Am. Chem. Soc.* **2012**, *134*, 18889–18891.
(27) Nguyen, S. T.; Johnson, L. K.; Grubbs, R. H.; Ziller, J. W. *J. Am. Chem. Soc.* **1992**, *114*, 3974–3975.
(28) Schwab, P.; France, M. B.; Ziller, J. W.; Grubbs, R. H. *Angew. Chem., Int. Ed. Engl.* **1995**, *34*, 2039–41.
(29) Wolf, J.; Stuer, W.; Grunwald, C.; Werner, H.; Schwab, P.; Schulz, M. *Angew. Chem., Int. Ed.* **1998**, *37*, 1124–1126.
(30) Scholl, M.; Ding, S.; Lee, C. W.; Grubbs, R. H. *Org. Lett.* **1999**, *1*, 953–956.
(31) McGuinness, D. S.; Cavell, K. J.; Skelton, B. W.; White, A. H. *Organometallics* **1999**, *18*, 1596–1605.
(32) Sanford, M. S.; Love, J. A.; Grubbs, R. H. *J. Am. Chem. Soc.* **2001**, *123*, 6543–6554.
(33) Hoveyda, A. H.; Zhugralin, A. R. *Nature* **2007**, *450*, 243–251.

(34) Kingsbury, J. S.; Harrity, J. P. A.; Bonitatebus, P. J.; Hoveyda, A. H. *J. Am. Chem. Soc.* **1999**, *121*, 791–799.
(35) McClennan, W. L.; Rufh, S. A.; Lummiss, J. A. M.; Fogg, D. E. *J. Am. Chem. Soc.* **2016**, *138*, 14668−14677.
(36) Love, J. A.; Sanford, M. S.; Day, M. W.; Grubbs, R. H. *J. Am. Chem. Soc.* **2003**, *125*, 10103–10109.
(37) Higman, C. S.; Nascimento, D.; Ireland, B. J.; Audorsch, S.; Bailey, G. A.; Fogg, D. E. *J. Am. Chem. Soc.* **2018**, *140*, 1604−1607.
(38) Samojlowicz, C.; Bieniek, M.; Grela, K. *Chem. Rev.* **2009**, *109*, 3708–3742.
(39) Vougioukalakis, G. C.; Grubbs, R. H. *Chem. Rev.* **2010**, *110*, 1746–1787.
(40) Conrad, J. C.; Amoroso, D.; Czechura, P.; Yap, G. P. A.; Fogg, D. E. *Organometallics* **2003**, *22*, 3634–3636.
(41) Conrad, J. C.; Parnas, H. H.; Snelgrove, J. L.; Fogg, D. E. *J. Am. Chem. Soc.* **2005**, *127*, 11882–11883.
(42) Monfette, S.; Blacquiere, J. M.; Conrad, J. C.; Beach, N. J.; Fogg, D. E., Ru-Aryloxide Catalysts for Olefin Metathesis. In *NATO Sci. Ser. A*, Imamoglu, Y.; Dragutan, V., Eds. Springer Verlag: Berlin, 2007; Vol. 243, pp 79–89.
(43) Monfette, S.; Camm, K. D.; Gorelsky, S. I.; Fogg, D. E. *Organometallics* **2009**, *28*, 944–946.
(44) Higman, C. S.; Lummiss, J. A. M.; Fogg, D. E. *Angew. Chem., Int. Ed.* **2016**, *55*, 3552–3565.
(45) Arlie, J. P.; Chauvin, Y.; Commereuc, D.; Soufflet, J. P. *Makromol. Chem.* **1974**, *175*, 861–872.
(46) Adlhart, C.; Chen, P. *J. Am. Chem. Soc.* **2004**, *126*, 3496–3510.
(47) Vorfalt, T.; Wannowius, K. J.; Plenio, H. *Angew. Chem., Int. Ed.* **2010**, *49*, 5533 –5536.
(48) Ashworth, I. W.; Hillier, I. H.; Nelson, D. J.; Percy, J. M.; Vincent, M. A. *Chem. Commun.* **2011**, *47*, 5428–5430.
(49) Thiel, V.; Hendann, M.; Wannowius, K.-J.; Plenio, H. *J. Am. Chem. Soc.* **2012**, *134*, 1104–1114.
(50) Schrock, R. R.; Hoveyda, A. H. *Angew. Chem., Int. Ed.* **2003**, *42*, 4592–4633.
(51) Wheeler, P.; Phillips, J. H.; Pederson, R. L. *Org. Process Res. Dev.* **2016**, *2*-, 1182−1190.
(52) Cho, J. H.; Kim, B. M. *Org. Lett.* **2003**, *5*, 531–533.
(53) Higman, C. S.; Lanterna, A. E.; Marin, M. L.; Scaiano, J. C.; Fogg, D. E. *ChemCatChem* **2016**, *8*, 2446–2449.
(54) Higman, C. S.; Plais, L.; Fogg, D. E. *ChemCatChem* **2013**, *5*, 3548-3551.
(55) van Lierop, B. J.; Lummiss, J. A. M.; Fogg, D. E., Ring-Closing Metathesis. In *Olefin Metathesis-Theory and Practice*, Grela, K., Ed. Wiley: Hoboken, NJ, 2014; pp 85–152.
(56) Fandrick, K. R.; Savoie, J.; Jinhua, N. Y.; Song, J. J.; Senanayake, C. H., Challenges and Opportunities for Scaling the Ring-Closing Metathesis Reaction in the Pharmaceutical Industry. In *Olefin Metathesis – Theory and Practice*, Grela, K., Ed. Wiley: Hoboken, 2014; pp 349-366.
(57) Alcaide, B.; Almendros, P.; Luna, A. *Chem. Rev.* **2009**, *109*, 3817–3858.
(58) Larionov, E.; Li, H.; Mazet, C. *Chem. Commun.* **2014**, *50*, 9816–9826.
(59) Crabtree, R. H. *Chem. Rev.* **2015**, *115*, 127–150.
(60) Schrodi, Y., Mechanisms of Olefin Metathesis Catalyst Decomposition and Methods of Catalyst Reactivation. In *Handbook of Metathesis*, Grubbs, R. H.; Wenzel, A. G., Eds. Wiley-VCH: Weinheim, 2015; pp 323–342.

(61) Lummiss, J. A. M.; Botti, A. G. G.; Fogg, D. E. *Catal. Sci. Technol.* **2014**, *4*, 4210–4218.
(62) Lummiss, J. A. M.; Beach, N. J.; Smith, J. C.; Fogg, D. E. *Catal. Sci. Technol.* **2012**, *2*, 1630–1632.
(63) Wang, H.; Goodman, S. N.; Dai, Q.; Stockdale, G. W.; Clark, W. M. *Org. Process Res. Dev.* **2008**, *12*, 226–234.
(64) Farina, V.; Horváth, A., Ring-Closing Metathesis in the Large-Scale Synthesis of Pharmaceuticals. In *Handbook of Metathesis*, Grubbs, R. H.; Wenzel, A. G., Eds. Wiley-VCH: Weinheim, 2015; Vol. 2, pp 633–658.
(65) Lummiss, J. A. M.; Higman, C. S.; Fyson, D. L.; McDonald, R.; Fogg, D. E. *Chem. Sci.* **2015**, *6*, 6739–6746.
(66) Lummiss, J. A. M.; Perras, F. A.; Bryce, D. L.; Fogg, D. E. *Organometallics* **2016**, *35*, 691–698.
(67) Straub, B. F. *Angew. Chem., Int. Ed.* **2005**, *44*, 5974–5978.
(68) Yang, H.-C.; Huang, Y.-C.; Lan, Y.-K.; Luh, T.-Y.; Zhao, Y.; Truhlar, D. G. *Organometallics* **2011**, *30*, 4196–4200.
(69) Bailey, G. A.; Fogg, D. E. *J. Am. Chem. Soc.* **2015**, *137*, 7318–7321.
(70) Hong, S. H.; Day, M. W.; Grubbs, R. H. *J. Am. Chem. Soc.* **2004**, *126*, 7414–7415.
(71) Hong, S. H.; Wenzel, A. G.; Salguero, T. T.; Day, M. W.; Grubbs, R. H. *J. Am. Chem. Soc.* **2007**, *129*, 7961–7968.
(72) Lummiss, J. A. M.; Ireland, B. J.; Sommers, J. M.; Fogg, D. E. *ChemCatChem* **2014**, *6*, 459–463.
(73) Ireland, B. J.; Dobigny, B. T.; Fogg, D. E. *ACS Catal.* **2015**, *5*, 4690−4698.
(74) Bailey, G. A.; Lummiss, J. A. M.; Foscato, M.; Occhipinti, G.; McDonald, R.; Jensen, V. R.; Fogg, D. E. *J. Am. Chem. Soc.* **2017**, *139*, 16446–16449.
(75) Romero, P. E.; Piers, W. E.; McDonald, R. *Angew. Chem., Int. Ed.* **2004**, *43*, 6161–6165.
(76) Romero, P. E.; Piers, W. E. *J. Am. Chem. Soc.* **2005**, *127*, 5032–5033.
(77) Romero, P. E.; Piers, W. E. *J. Am. Chem. Soc.* **2007**, *129*, 1698–1704.
(78) van der Eide, E. F.; Piers, W. E. *Nature Chem.* **2010**, *2*, 571–576.
(79) Nizovtsev, A. V.; Afanasiev, V. V.; Shutko, E. V.; Bespalova, N. B. *NATO Sci. Ser. II* **2007**, *243*, 125–135.
(80) van Rensburg, W. J.; Steynberg, P. J.; Meyer, W. H.; Kirk, M. M.; Forman, G. S. *J. Am. Chem. Soc.* **2004**, *126*, 14332–14333.
(81) Schwab, P.; Grubbs, R. H.; Ziller, J. W. *J. Am. Chem. Soc.* **1996**, *118*, 100–110.
(82) Ulman, M.; Grubbs, R. H. *J. Org. Chem.* **1999**, *64*, 7202–7207.
(83) Dias, E. L.; Grubbs, R. H. *Organometallics* **1998**, *17*, 2758–2767.
(84) Dinger, M. B.; Mol, J. C. *Organometallics* **2003**, *22*, 1089–1095.
(85) Wang, H.; Metzger, J. O. *Organometallics* **2008**, *27*, 2761–2766.

Chapter 2. Experimental Methods

2.1 General Procedures

2.1.1 Reaction Conditions

Reactions were carried out under N_2 using standard glovebox and Schlenk techniques,[1] unless otherwise noted. Clean glassware was oven-dried at 110 °C for at least 4 h, then allowed to cool under vacuum prior to use. Room temperature is ca. 25 °C for glovebox work, or 23 °C for Schlenk work. Reactions above RT were carried out using a thermostatted oil bath.

2.1.2 Reagents

Reagents PPh_3 (Strem, 99%), styrene (Aldrich, 99%), methyl 10-undecenoate (Aldrich, 96%), ethylene (BOC Ultra-High Purity Grade 3.0, 99.9%, Linde), 1,3,5-trimethoxybenzene (TMB, Sigma-Aldrich), dimethyl terephthalate (DMT, >99%) dodecane (>99%, Sigma-Aldrich), potassium hydrotris(1-pyrazolyl)borate (KTp, >99%, Sigma-Aldrich), anthracene (97%, Sigma-Aldrich), pyridine (>99%, Fisher) were used as received. The following materials were prepared according to literature procedures: $[RuCl_2(p\text{-cymene})]_2$,[2] $CHArN_2$ (Ar = *o*-$C_6H_4O^iPr$),[3] $PhCHN_2$,[4] and H_2IMes,[5] *o*-dianiline (**ODA**; [1,1'-biphenyl]-2,2'-diamine),[6] $RuCl_2(py)_4$,[7] the third-generation Grubbs catalyst (**GIII**),[8] the second-generation Hoveyda catalyst (**HII**),[9] and the second-generation Piers catalyst (**PII**; trifluoromethanesulfonate salt)[10] were prepared according to literature procedures unless otherwise stated.

2.1.3 Solvents

Dry, oxygen-free hexanes, THF, C_6H_6, CH_2Cl_2, C_7H_8, and Et_2O were obtained using a Glass Contour or Anhydrous Engineering solvent purification system (SPS), and stored in the glovebox. Karl-Fisher titrations were performed prior to sieve treatment on hexanes (4 ppm), THF (4 ppm), C_6H_6 (4 ppm), CH_2Cl_2 (5 ppm) biannually to validate drying column status as well as these solvent-drying protocols. Standard distillation methods[11] were used to purify and degas other solvents: MeOH from I_2-activated Mg turnings, acetone from $CaSO_4$, and pentane (Fisher ACS grade, pre-dried for 24 h over $MgSO_4$) from P_2O_5. All organic solvents were stored in the glovebox over activated 4 Å sieves for at least 16 h prior to use.

2.1.4 Deuterated Solvents

Deuterated solvents (Cambridge Isotopes or Sigma Aldrich) were used as received for the NMR analysis of air-stable species. For analysis of oxygen- and moisture-sensitive compounds,

deuterated solvents were degassed by five consecutive freeze-pump-thaw cycles, and stored in the glovebox over activated 4 Å sieves for at least 16 h prior to use.

2.1.5 Instrumentation

2.1.5.1 NMR Spectroscopy

NMR spectra were recorded on a Bruker Avance 300, Avance II 300, or Avance 400 spectrometer, at RT unless otherwise noted. ^{1}H and $^{13}C\{^{1}H\}$ spectra were referenced to the residual proton or carbon signal of the deuterated solvent used; $^{31}P\{^{1}H\}$ spectra were referenced externally to 85% H_3PO_4 at 0 ppm. For oxygen- and moisture-sensitive samples, spectra were acquired in screw-top (J. Young or Rotoflo) NMR tubes.

2.1.5.2 Gas Chromatography

Gas chromatography (GC) quantification was performed using an Agilent 7890A or 7683B Series autosampling GC, each equipped with a flame ionization detector (FID) and an Agilent HP-5 polysiloxane column (30 m length, 320 μm diameter). An inlet split ratio of 10:1 was used, with an inlet temperature of 250 ºC. Helium (UHP grade) was used as the carrier gas to maintain a column pressure of 11.5 psi, and the FID response was maintained between 5 – 2000 ρA. Samples were diluted with CH_2Cl_2 (ACS reagent grade) prior to injection, to give analyte concentrations of ca. 5 mM. Retention times for substrates, products, and internal standards were confirmed by GC-MS and NMR analysis. For GC quantification, calibration curves (peak area vs. concentration) were constructed for substrates and products relative to internal standard (decane or dodecane) in the relevant concentration regime, to account for the dependence of signal intensity on detector response. Conversions and yields for catalytic runs were measured by integration of peak areas for the analyte relative to internal standard, and compared to the initial ratios.

2.2 Experimental Data for Chapter 3

2.2.1 Representative Procedure for Quantification of Propenes Formed During Styrene Metathesis.

To maximize retention of volatile propene, these experiments were conducted in filled J. Young NMR tubes. A small headspace (0.15 mL; ca. 5% of the tube volume) was provided to accommodate any unintended thermal expansion of the solvent in these nominally isothermal (23

°C) experiments. A stock solution of **HII** (10.5 mg, 0.017 mmol) and anthracene (ca. 0.5 mg; internal standard) was dissolved in 0.5 mL C_6D_6. 155 µL of the stock solution was added to a J. Young NMR tube and diluted to 700 µL. A ^{1}H NMR spectrum was measured to establish the starting ratio of **HII** vs anthracene. Styrene (595 µL, 8.36 mmol, 1000 equiv) was then added, and the tube was inverted several times to mix the solution. An immediate color change from green to brown occurred. ^{1}H NMR (C_6D_6, 300 MHz; diagnostic signals only; Figure A2): δ 16.72 (s, 1H, [Ru]=CHAr of **HII**; none remaining), 8.19 (s, 2H, Ar C*H* of anthracene), 7.00 (s, 2H, =C*H* of stilbene), 6.58 (dd, $^3J_{HH}$ = 18 Hz, $^3J_{HH}$ = 11 Hz, =C*H*Ph of styrene), 6.19 (dt, $^3J_{HH}$ = 16 Hz, $^3J_{HH}$ = 7 Hz, 1H, =C*H*CH$_2$Ph of 1,3- diphenylpropene;[12] not observed), 6.03 (dq, $^3J_{HH}$ = 15.9 Hz, $^3J_{HH}$ = 6.8 Hz, 1H, =C*H*CH$_3$ of β-methylstyrene;[12] 12%), 5.27 (s, C_2H_4), 5.01–4.92 (m, three-quarters of the propene =C*H*$_2$ pattern;[13] the remaining multiplet is partially obscured by signal for excess styrene; 18%). The propenes arising from elimination of the isopropoxyphenyl-substituted metallacyclobutane[12] were not observed, perhaps reflecting the large excess of styrene present in solution, which indicates ethenolysis of stilbene is occurring.

Quantification of propenes formed during styrene metathesis by **GIII** was carried out as above. The yield of propenes was assessed at complete loss of [Ru]=C*H*R (1 h).

2.2.2 Metathesis of Methyl 10-Undecenoate: Formation of "False" Propene Markers .

Quantification of propenyl products can be invaluable as a means of quantifying β-hydride elimination from the MCB. This presumes, however, that no propenes form by isomerization-metathesis. The experiments below were designed to assess whether (and to what extent) such "false" propenyl markers were generated in metathesis of a standard aliphatic 1-olefin (Table A1). Accordingly, a J. Young NMR tube was charged with **HII** (21 mg, 0.034 mmol) and DMT (ca. 1 mg) in 0.70 mL C_6D_6, and methyl 10-undecenoate (**3**) (1.00 mL, 4.45 mmol, 130 equiv) was added via syringe. The tube was shaken to effect mixing, and the progress of reaction was examined after 1 h, at which point no further catalyst signals remained.

After 1 h: ^{1}H NMR (C_6D_6, 300 MHz; diagnostic signals only): δ 16.72 (s, 1H, [Ru]=C*H*Ar of **HII**; none remaining), 5.73 (m, 1H, =C*H*R of **3**), 5.37 (m, 2H, =C*H*R of **4**), 5.28 (s, 4H, C_2H_4), 4.95 (dq, $^3J_{HH}$ = 17.0, $^4J_{HH}$ = 1.8 Hz, 1H, RCH=C*H*$_a$H$_b$ of **3**), 4.89 (dm, $^3J_{HH}$ = 10.3 Hz, 1H, RCH=CH$_a$*H*$_b$ of **3**), 1.51 (m, 2H, C*H*$_2$CH$_2$CO$_2$Me of **3**). As signals due to **3** obscure any propene formed (for the values reported for **3**,[13] see text), GC analysis was conducted instead (Table A1).

This indicates a combined yield of 6% propene products, whereas a 0.7% maximum would be obtained if they originated solely in β-elimination of metallacyclobutane **Ru-2**. Isomerization-metathesis thus indeed prevents accurate quantitation of β-elimination.

2.2.3 Quantification of Organic Products from GIII Metathesis

As in Section 2.2.1, a solution of **GIII** (14 mg, 0.019 mmol) and anthracene (ca. 3 mg; internal standard) in 1.9 mL C_6D_6 was added to a J. Young NMR tube and a ^{1}H NMR spectrum was measured to establish the starting ratio of **GIII** vs anthracene. Styrene (4.2 µL, 0.037 mmol, 2 equiv) was then added, and the tube was inverted several times to mix the solution and heated at 60 °C for 30 minutes. A color change from green to brown occurred. Complete loss of **GIII** was evident at this point. Comparing the integrations of starting **GIII** to organic products observed upon complete decomposition, a ca. 96% of **GIII** decomposed via bimolecular coupling. ^{1}H NMR (C_6D_6, 300 MHz; diagnostic signals only; Figure A3): δ 19.72 (s, 1H, [Ru]=C*H*Ar of **GIII**; none remaining), 8.19 (s, 2H, Ar C*H* of anthracene), 7.00 (s, 2H, =C*H* of stilbene), 6.58 (dd, $^3J_{HH}$ = 18 Hz, $^3J_{HH}$ = 11 Hz, =C*H*Ph of styrene), 5.25 (s, 4H, =C*H* of ethylene).

2.2.4 Isolation of $RuCl_2(H_2IMes)(py)_3$ Ru-6 from GIII

In a glovebox, a 25 mL Schlenk flask was charged with **GIII** (194 mg, 0.267 mmol) and 4 mL C_6H_6. To the stirred solution, styrene (61 µL, 0.534 mmol, 2 equiv) was added and then the solution was heated at 60 °C for 30 minutes. A colour change from green to yellow occurred within the first 5 minutes, and solvent was removed under vacuum after 30 minutes. ^{1}H NMR spectra revealed a mixture of pyridine-ligated ruthenium products and no **GIII** signals remained. The remaining solid was dissolved in 4 mL benzene and 0.1 mL pyridine was added. **Ru-6** was then precipitated with 10 mL cold hexanes. The yellow product was filtered off, and washed with cold Et_2O (1 mL) and cold hexanes (2 x 2 mL), and dried under vacuum to afford spectroscopically pure **Ru-6**. Yield: 141 mg (85%).

$RuCl_2(H_2IMes)(py)_3$ Ru-6. ^{1}H NMR (C_6D_6, 300 MHz): δ 9.62 (dt, $^3J_{HH}$ = 5.2 Hz, $^4J_{HH}$ = 1.5 Hz, 4H, py *o*-C*H*), 9.39 (dt, $^3J_{HH}$ = 4.9 Hz, $^4J_{HH}$ = 1.6 Hz, 2H, py *o*-C*H*), 6.53 (tt, $^3J_{HH}$ = 7.5 Hz, $^4J_{HH}$ = 1.6 Hz, 1H, py *p*-C*H*), 6.41 (tt, $^3J_{HH}$ = 7.4 Hz, $^4J_{HH}$ = 1.5 Hz, 2H, py *p*-C*H*), 6.28 (m, 2H, py *m*-C*H*; overlapping with Mes C*H*), 6.28 (s, 4H, Mes C*H*; overlapping with py *m*-C*H*), 5.98 (m, 4H, py *m*-C*H*), 3.64 (s, 4H, NCH_2), 2.77 (s, 12H, *o*-CH_3), 1.89 (s, 6H, *p*-CH_3).

2.2.5 High Conversion to $RuCl_2(H_2IMes)(py)_2$ Ru-7 from GIII

In a glovebox, a 10 mL Kontes flask was charged with **GIII'** (130 mg, 0.179 mmol) and 1 mL of C_6H_6. The solvent was degassed and connected to an ethylene cylinder via a T-joint. The solution was stirred open to the cylinder for 2 h, over which time a colour change from green to yellow occurred. The solvent was removed under vacuum. The remaining solid was dissolved in a minimal volume of CH_2Cl_2 (ca. 0.2 mL) and precipitated with 2 mL cold hexanes. The yellow product was filtered off, and washed with cold Et_2O (0.2 mL) and cold hexanes (2 x 0.4 mL) and dried under vacuum. A 1:4 mixture of **Ru-6** and **Ru-7** was obtained, which was used to characterize **Ru-7**.

$RuCl_2(H_2IMes)(py)_2$ Ru-7. ^{1}H NMR (C_6D_6, 300 MHz): δ 9.40 (br s, 2H, py *o*-C*H*; overlapping with py *o*-C*H* of **Ru-6**), 9.16 (br s, 2H, py *o*-C*H*), 6.54 (br s, 1H, py *p*-C*H*; overlapping with py *p*-C*H* of **Ru-6**), 6.47 (br s, 1H, py *p*-C*H*; overlapping with py *p*-C*H* of **Ru-6**), 6.29 (br s, 2H, py *m*-C*H*), 6.28 (s, 4H, Mes C*H*; overlapping with Mes C*H* of **Ru-6**), 6.03 (br s, 2H, py *m*-C*H*; overlapping with py *m*-C*H* of **Ru-6**), 3.48 (br s, 4H, NCH_2), 2.75 (br s, 12H, *o*-CH_3), 1.99 (br s, 6H, *p*-CH_3).

2.2.6 Isolation of $RuCl_2(H_2IMes)(ODA)$ Ru-11 from DA

In a glovebox, the **DA** catalyst (22 mg, 0.039 mmol) was dissolved in 1.5 mL C_6D_6. Styrene (33 µL, 0.028 mmol, 10 equiv) was then added. The green solution was heated to 50 °C for 16 h, after which it was yellow in colour and no signals for **DA** were apparent (^{1}H NMR). The solvent was removed under vacuum. The residue was precipitated from CH_2Cl_2/hexanes to afford a yellow solid, which was filtered off, washed with cold hexanes (2 x 1 mL) and dried under vacuum. **Ru-11** was obtained with minor impurities present, in yields too low to accurately measure.

2.3 Experiments for Chapter 4

2.3.1 Synthesis of $RuCl_2$(*p*-cymene)(H_2IMes), Ru-13.

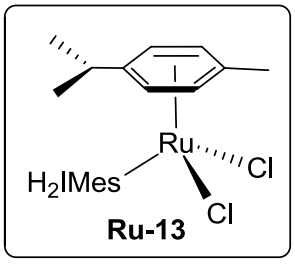

Ru-13

In a dark glovebox, a foil-wrapped 100 mL Schlenk flask was charged with $[RuCl_2(p\text{-cymene})]_2$ **Ru-12** (436 mg, 0.711 mmol) and 25 mL THF. To the stirred red suspension was added a solution of H_2IMes (458 mg, 1.49 mmol, 2.1 equiv per dimer) in 30 mL THF, at a rate of 1 mL/min (total delivery time 30 min). The colour deepened within 5 min, and a clear dark red

solution was present when addition of H_2IMes was complete. The solvent was removed under vacuum, and the residue was reprecipitated from CH_2Cl_2-hexanes (5 CH_2Cl_2; 35 mL hexanes) at –35 °C. The red precipitate was filtered off, washed with cold pentane (2 x 3 mL), and dried under vacuum. Yield of **Ru-13**: 812 mg (96%). NMR data in C_6D_6 are in good agreement with values reported:[14] they are reproduced here for convenience. Also given are values in $CDCl_3$ (Figure A9), which have not previously been reported.

^{1}H NMR (C_6D_6, 300 MHz): δ 6.77 (s, 4H, Mes *sp*^{2}-C*H*), 4.86 (d, $^3J_{HH}$ = 6.9 Hz, 2H, cym *sp*^{2}-C*H*), 4.39 (d, $^3J_{HH}$ = 6.9 Hz, 2H, cym *sp*^{2}-C*H*), 3.20 (s, 4H, NCH_2), 2.48 (s, 12H, Mes *o*-CH_3), 2.13 (s, 6H, Mes *p*-CH_3), 1.72 (s, 3H, cym *p*-CH_3), 1.31 (m, 1H, ^{i}Pr *CH*) 1.06 (d, $^3J_{HH}$ = 6.9 Hz, 6H, ^{i}Pr *CH*$_3$).

^{1}H NMR ($CDCl_3$, 300 MHz): δ 6.91 (s, 4H, Mes *sp*^{2}-C*H*), 5.02 (d, $^3J_{HH}$ = 6.6 Hz, 2H, cym *sp*^{2}-C*H*), 5.63 (d, $^3J_{HH}$ = 6.6 Hz, 2H, cym *sp*^{2}-C*H*), 3.86 (s, 4H, NCH_2), 2.47 (s, 12H, Mes *o*-CH_3), 2.40 (m, 1H, ^{i}Pr *CH*), 2.30 (s, 6H, Mes *p*-CH_3), 1.75 (s, 3H,cym *p*-CH_3), 1.07 (d, $^3J_{HH}$ = 6.9 Hz, 6H, ^{i}Pr CH_3).

^{1}H-^{1}H NOESY ($CDCl_3$, 300 MHZ, 1 s mixing time). NOE cross-peaks correlate the Mes *o*-C*H*$_3$ and cymene CH_3, C*H*, and CH(C*H*$_3$)$_2$ signals: Figure A10.

2.3.2 Synthesis of $RuCl_2(H_2IMes)(=CH\text{-}o\text{-}C_6H_4O^iPr)$, HII.

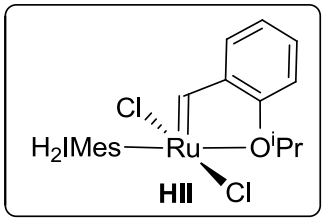

In a dark glovebox, dark red $RuCl_2$(*p*-cymene)(H_2IMes) **Ru-13** (319 mg, 0.53 mmol) was dissolved in CH_2Cl_2 (13 mL) in a foil-wrapped Schlenk flask. The flask was removed to a Schlenk line and the solution was chilled to –78 °C. The foil was then removed, and ice-cold $ArCHN_2$ (Ar = *o*-$C_6H_4O^iPr$) (255 mg, 2.7 equiv) in 4 mL pentane was added dropwise by cannula to the stirred solution. After 1 h, the solution was allowed to warm to 0 °C, and irradiated at 254 nm for 10 min using a portable UV lamp mounted 5 cm from the flask. The solvent was then evaporated, and the residue subjected to flash chromatography (silica gel, CH_2Cl_2). A green band was collected, stripped of solvent, and washed with pentane (2 x 5 mL). Yield of **HII** after drying under vacuum: 275 mg (82%). NMR data in $CDCl_3$ (see Figure A11) agree with those reported:[3] values are reproduced here for convenience.

^{1}H NMR ($CDCl_3$, 300 MHz): δ 16.56 (s, 1H, [Ru]=C*H*R), 7.48 (d, $^3J_{HH}$ = 8.4 Hz, 1H, Ar *sp*^{2}-C*H*), 7.07 (s, 4H, Mes C*H*), 7.01-6.70 (m, 3H, Ar *sp*^{2}-C*H*), 4.90 (m, 1H, ^{i}Pr C*H*), 4.18 (s, 4H,

Mes NC*H*$_2$), 2.47 (s, 12H, Mes *o*-C*H*$_3$), 2.40 (s, 6H, Mes *p*-C*H*$_3$), 1.27 (d, $^3J_{HH}$ = 6.0 Hz, 6H, ^{i}Pr C*H*$_3$).

2.3.3 Synthesis of $RuCl_2(H_2IMes)(PPh_3)(=CHR)$, GII-$PPh_3$.

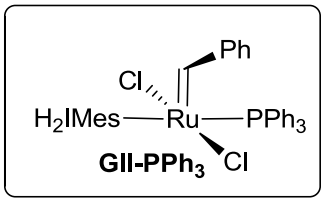

As above, but with addition of PPh_3 (215 mg, 1.48 equiv) to **Ru-13** at –78 °C prior to removing the foil and adding the $PhCHN_2$ solution. Workup as above, but with 1:1 hexane:EtOAc as the eluant in flash chromatography, and collection of a brown band. Yield of **GII-PPh_3**: 365 mg (81%). NMR data in C_7D_8 are in good agreement with values reported.[15] Below are values in $CDCl_3$ (see Figure A12), which have not previously been reported.

$^{31}P\{^1H\}$ NMR ($CDCl_3$, 300 MHz): δ 33.86 (s). ^1H NMR ($CDCl_3$, 300 MHz): δ 19.26 (s, 1H, [Ru]=C*H*R), 7.4-6.7 (m, Ph, 22H), 6.35 (s, 2H, Mes C*H*), 4.01 (m, 4H, Mes NC*H*$_2$), 2.65 (s, 6H, Mes *o*-C*H*$_3$), 2.42 (s, 3H, Mes *p*-CH_3), 2.25 (s, 6H, Mes *o*-C*H*$_3$), 1.96 (s, 3H, Mes *p*-C*H*$_3$).

2.3.4 Decomposition of H_2IMes by CH_2Cl_2.

In a 4 mL vial, H_2IMes (12.5 mg, 0.04 mmol) was dissolved in 0.15 mL CH_2Cl_2. An immediate colour change to pale yellow occurred. After 10 min, C_6D_6 (1 mL) was added. A white precipitate deposited, which was presumed to be the imidazolinum salt. ^1H NMR analysis of the solution revealed no remaining H_2IMes. A number of broad signals assigned to $H_2IMes{=}CH_2$ were present.[16]

NMR data for starting H_2IMes: ^1H NMR (C_6D_6, 300 MHz): δ 6.84 (s, 4H, Mes C*H*), 3.27 (s, 4H, Mes NC*H*$_2$), 2.31 (s, 12H, Mes *o*-C*H*$_3$), 2.17 (s, 6H, Mes *p*-CH_3).

NMR data for $H_2IMes{=}CH_2$: ^1H NMR (C_6D_6, 300 MHz):): δ 6.82 (s, 4H, Mes C*H*), 3.31 (s, 4H, Mes NC*H*$_2$), 2.59 (s, 2H, C=C*H*$_2$) 2.34 (s, 12H, Mes *o*-C*H*$_3$), 2.14 (s, 6H, Mes *p*-CH_3).

2.3.5 Decomposition of Isolated $RuCl_2$(*p*-cymene)(H_2IMes) Ru-13 by Reaction with H_2IMes.

In a dark glovebox, a solution of H_2IMes (7 mg, 0.02 mmol) in 1 mL C_6D_6 was added dropwise to a stirred solution of **Ru-13** (13 mg, 0.02 mmol) in 1 mL C_6D_6 in a foil-wrapped 4 mL vial. An immediate colour change from red to purple was observed. The reaction was continued for 10

min, after only trace **Ru-13** was observable by ^{1}H NMR analysis (Figure A13), and no signals for free H_2IMes.

2.3.6 Decomposition of Isolated $RuCl_2$(*p*-cymene)(H_2IMes) Ru-13.

In a dark glovebox, **Ru-13** (24 mg, 0.04 mmol) and anthracene (ca. 2 mg) was dissolved in 2 mL C_6D_6 was in a foil-wrapped 20 mL vial. The solution was divided between two foil-wrapped J. Young NMR tubes, and the initial integration ratio of **Ru-13** vs. anthracene was measured. The foil was removed from one NMR tube, which was placed in a fumehood illuminated with fluorescent light; the other was left wrapped except when NMR spectra were measured (Fig. A14a). Loss of **Ru-13** was monitored by ^{1}H NMR analysis over 21 h, over which time the colour changed from red to dark brown (both samples). The order of decomposition with respect to [Ru] is shown in Fig. A14b (for reaction in the dark) and Fig. A14c (for reaction in the light).

2.3.7 Photolytic Decomposition of $RuCl_2$(*p*-cymene)(H_2IMes) Ru-13: UV-Vis Studies.

The photolability of **Ru-13** was examined further by LED irradiation. Solutions in CH_2Cl_2 were made up in a foil-wrapped vessel in a darkened glovebox, and transferred to a quartz cuvette, which was sealed with a Teflon stopper. For spectra at a range of concentrations (0.1–2 mM **Ru-13**), see Fig. A15a. Decomposition was monitored spectrophotometrically for ca. 1 mM solutions (2 mg **Ru-13** in 4 mL CH_2Cl_2; 0.8 mM, with irradiation in the UV (365 nm, 6882.44 mW•m^{-2}; Fig. A15b) or the visible (blue) region (465 nm, 1669 mW•m^{-2}; Fig. A15c). Under UV irradiation, significant broadening of the absorption bands was apparent after 14 min. Under blue light irradiation, the lowest-energy absorption band at 445 nm exhibited broadening after 15 min, and complete loss by 42 min. In both cases a black suspension formed, suggesting nanoparticle formation and agglomeration.

2.4 References

(1) Shriver, D. F.; Drezdzon, M. A., *The Manipulation of Air-Sensitive Compounds*. 2nd Ed. ed.; John Wiley & Sons: New York, 1986.
(2) Herrmann, W. A.; Elison, M.; Fischer, J.; Koecher, C.; Artus, G. R. J. *Chem. – Eur. J.* **1996**, *2*, 772–780.
(3) Kingsbury, J. S.; Harrity, J. P. A.; Bonitatebus, P. J.; Hoveyda, A. H. *J. Am. Chem. Soc.* **1999**, *121*, 791–799.
(4) Schwab, P.; Grubbs, R. H.; Ziller, J. W. *J. Am. Chem. Soc.* **1996**, *118*, 100–110.
(5) Arduengo, A. J.; Harlow, R. L.; Kline, M. *J. Am. Chem. Soc.* **1991**, *113*, 361–363.
(6) Jung, K.-H.; Kim, H.-K.; Lee, G. H.; Kang, D.-S.; Park, J.-A.; Kim, K. M.; Chang, Y.; Kim, T.-J. *J. Med. Chem.* **2011**, *54*, 5385–5394.
(7) Bottomley, F.; Mukaida, M. *J. Chem. Soc., Dalton Trans.* **1982**, 1933–1937.
(8) Sanford, M. S.; Love, J. A.; Grubbs, R. H. *Organometallics* **2001**, *20*, 5314–5318.
(9) van Lierop, B. J.; Reckling, A. M.; Lummiss, J. A. M.; Fogg, D. E. *ChemCatChem* **2012**, *4*, 2020–2025.
(10) Dubberley, S. R.; Romero, P. E.; Piers, W. E.; McDonald, R.; Parvez, M. *Inorg. Chim. Acta* **2006**, *359*, 2658–2664.
(11) Armarego, W. L. F.; Perrin, D. D., *Purification of Common Laboratory Chemicals*. 4th Ed. ed.; Butterworth-Heinemann: Oxford, 1997.
(12) Ireland, B. J.; Dobigny, B. T.; Fogg, D. E. *ACS Catal.* **2015**, *5*, 4690−4698.
(13) Fulmer, G. R.; Miller, A. J. M.; Sherden, N. H.; Gottlieb, H. E.; Nudelman, A.; Stoltz, B. M.; Bercaw, J. E.; Goldberg, K. I. *Organometallics* **2010**, *29*, 2176–2179.
(14) Engel, J.; Smit, W.; Foscato, M.; Occhipinti, G.; Törnroos, K. W.; Jensen, V. R. *J. Am. Chem. Soc.* **2017**, *139*, 16609–16619.
(15) Love, J. A.; Sanford, M. S.; Day, M. W.; Grubbs, R. H. *J. Am. Chem. Soc.* **2003**, *125*, 10103–10109.
(16) Arduengo, A. J.; Davidson, F.; Dias, H. V. R.; Goerlich, J. R.; Khasnis, D.; Marshall, W. J.; Prakasha, T. K. *J. Am. Chem. Soc.* **1997**, *119*, 12742–12749.

Chapter 3. Bimolecular Coupling of Fast-Initating Metathesis Catalysts: Exploring Additional Evidence and the Nature of the Ru Products

This chapter describes findings by CSD that contributed to the article "*Bimolecular Coupling as a Vector for Decomposition of Fast-Initiating Olefin Metathesis Catalysts"* (authors Gwendolyn A. Bailey, Marco Foscato, Carolyn S. Higman, **Craig S. Day**, Vidar R. Jensen, and Deryn E. Fogg), *J. Am. Chem. Soc.* **2018**, 140, 22, 6931-6944. Copyright 2018 American Chemical Society; reprinted with permission.

Author Contributions: The experiments described in this chapter have all been performed by CSD or will explicitly describe the contributions of experiments this author did not perform. This manuscript was conceived, written, edited, and revised by GAB and DEF with contributions from CSD. MF performed the computational analysis, with input from VRJ. CSH first demonstrated the susceptibility of the benzylidene complex **GIII** to bimolecular coupling, and participated in drafting an early version of the paper. Metathesis studies aimed at quantifying β-hydride elimination via analysis of product distributions were initially conceived and performed by CSD in early drafts of the paper and repeated by GAB with controlled mixing. The Ru-pyridine products generated following loss of the methylidene functionality (**Ru-6**, **Ru-7**, and **Ru-9**) were initially isolated and characterized by CSD.

3.1 Introduction

The deleterious impact of phosphine ligands on olefin metathesis has been increasingly documented.[1,2] As discussed in Chapter 1, the most widely used second-generation catalyst, **GII**, suffers from several problems that are due to the PCy_3 ligand. First, the low lability of this ligand inhibits initiation,[3] and even more severely inhibits re-entry into the catalytic cycle from the resting-state methylidene species $RuCl_2(H_2IMes)(PCy_3)(=CH_2)$ **GIIm**.[4] The nucleophilicity of PCy_3 is also problematic, as free PCy_3 abstracts the methylidene ligand from the active species **Ru-1** (Chart 3.1(a)) as $[MePCy_3]Cl$. In studies of **GIm** and deuterated **GIIm-d_{22}**, our group presented spectroscopic and crystallographic evidence that decomposition proceeds by nucleophilic attack at the methylidene carbon to generate a σ-alkyl complex, [55] and ensuing liberation of the $[MePCy_3]Cl$ by NHC cyclometallation. Phosphine-free catalysts such as **HII** (Chart 3.1(b)) circumvent both problems. Such catalysts are now widely used in challenging metathesis reactions[6-10] (although they remain under-used relative to **GII** in organic synthesis in

academia). However, decomposition of the phosphine-free systems has been little studied. While recent studies from our research group described decomposition of **HII** and related catalysts by nucleophiles or base,[11,12] only two prior reports in the literature discussed intrinsic decomposition pathways.

Chart 3.1 Metathesis Catalysts and Active Species.

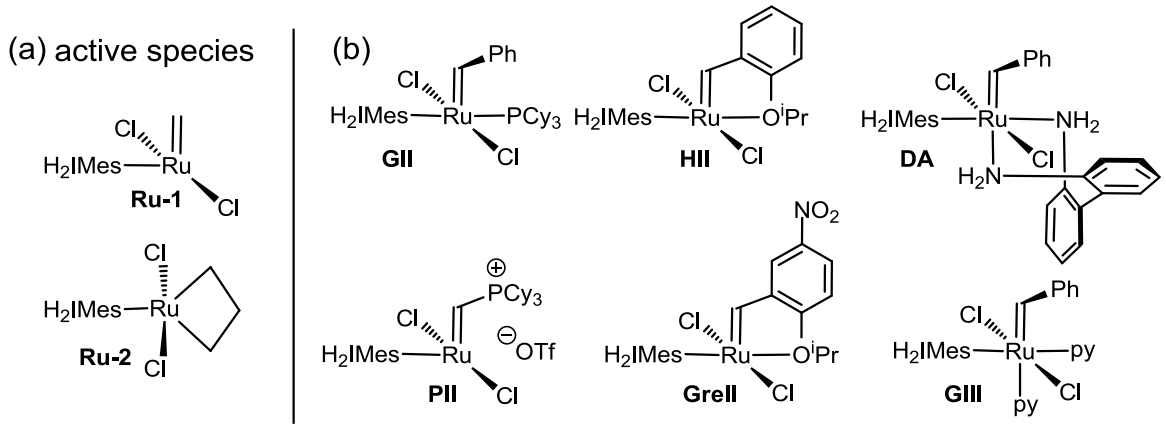

In the first of these, Bespalova reported that **HII** produced propene on metathesis with ethylene (ethenolysis), and suggested that this was due to β-hydride elimination from the metallacyclobutane (MCB).[11,12] Piers provided the first mechanistic evidence for this pathway (Figure. 3.1), by synthesizing the ^{13}C-labelled MCB at low temperature (–78 °C) from the Piers catalyst **PII**. Liberation of ^{13}C labeled propene on warming supports the proposed β-hydride elimination pathway.

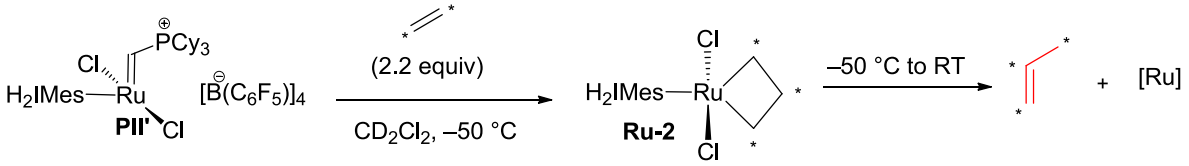

Figure 3.1 Propenes originating from MCB in **Ru-2**

At the outset of this thesis work, MCB elimination was the only *intrinsic* decomposition pathway reported for the phosphine-free catalysts. Our group suspected, however, that bimolecular decomposition might also be relevant. Quantifying the propenes formed by β–hydride elimination during metathesis was therefore a priority. Experiments to that end (initially conceived by myself, but improved upon by Gwen Bailey with mixing to improve

reproducibility) showed 0–40% decomposition via this pathway for all catalysts studied: **HII**, **GreII**, **PII**, **DA**, and **GIII** (Chart 3.1b). Higher-dilution versions of these experiments, which more closely simulate conditions employed in metathesis macrocyclization will be discussed in Section 3.2.2.

The role of bimolecular coupling in decomposition of second-generation catalysts has been largely dismissed, despite its documented role with earlier transition metals.[13,14] Early hints of bimolecular coupling also appear in synthesis of first-generation systems stabilized by PPh_3 ligands, some of which decomposed at room temperature with liberation of stilbene[13] or (for vinylalkylidene catalysts) a triene.[15,16] Likewise consistent with bimolecular coupling was the observation of a second-order dependence of decomposition on [Ru] when **GI** was treated with CuCl to abstract PCy_3, although no pathway was suggested.[17-21] Bimolecular coupling of many second-generation systems was thought to be unlikely on the basis of the slow initiation of the catalysts.[22,23b,24] In the case of **HII**, rapid recapture of the active species by isopropoxystyrene (the long-debated and ultimately validated boomerang mechanism)[25] reduces the concentration of the active species present, and it was again assumed that this precludes methylidene coupling.

Experiments by Carolyn Higman and Gwen Bailey of the Fogg group demonstrated that bimolecular decomposition occurs even for the benzylidene species. Thus, stilbene was observed in 74% yield after heating a in C_6D_6 solution of **GIII** at 60 °C for 5 days, while $RuCl_2(H_2IMes)(py)(CHMe)$ decomposed in ca. 30 min under the same conditions. The ruthenium products in the **GIII** reaction (Scheme 3.1) were tentatively assigned on the basis of ^1H NMR analysis as the tris-py complex **Ru-6** and chloride-bridged dimer $[RuCl_2(H_2IMes)(py)_2]_2$ **Ru-8**. The latter is corrected in the work below (Section 3.2.6) to a bis-py analogue of **Ru-6**.

Scheme 3.1. Ru Products Reportedly Formed in Thermolysis of **GIII**.

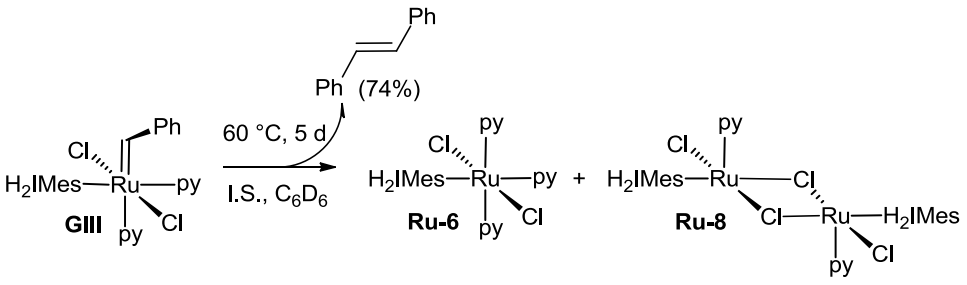

The synthesis, isolation, and controlled decomposition of a transiently-stabilized methylidene complex by Gwen Bailey provided the first direct evidence for bimolecular coupling of the active, four-coordinate methylidene intermediate. (While the resting-state methylidene species **GIm** and **GIIm** had previously been isolated, decomposition of these species proceeds primarily by PCy_3-induced methylidene abstraction; Chapter 1). Two such complexes were isolated, stabilized by either pyridine or an *o*-dianiline ligand.[26] Liberation of ethylene from these complexes provides the key evidence for bimolecular coupling. Early attempts at the synthesis and isolation of $RuCl_2(H_2IMes)(ODA)(CH_2)$ **Ru-10** were aided by myself.

Scheme 3.2. Synthesis of *o*-Dianiline Adduct **Ru-10.**

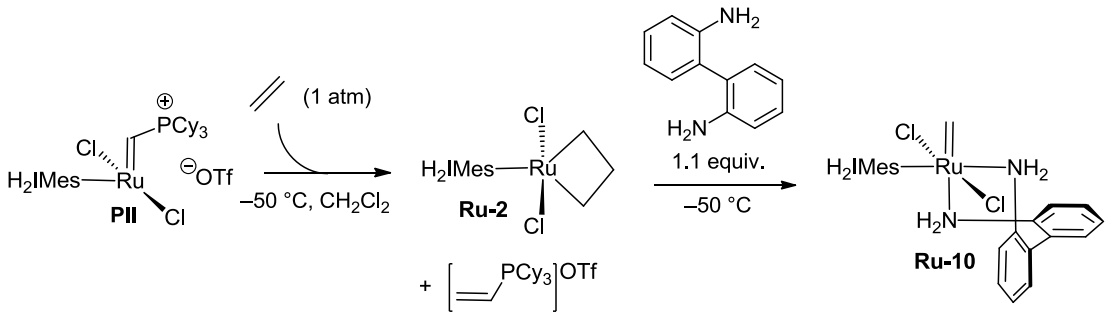

Decomposition of **Ru-10** exhibits a second-order dependence on [Ru], further supporting the proposed bimolecular decomposition pathway. Computational work by our collaborators Marco Foscato and Vidar Jensen revealed a transition state at 17.5 kcal/mol. Previously-suggested Ru intermediates, including a "dimetallacyclobutane" structure identified by Schrock,[27] were too high in energy to contribute to the observed decomposition.

Alternative decomposition pathways have been proposed based largely on the serendipitous isolation of crystalline products. A common feature is cyclometallation of the NHC N-mesityl substituents, leading many to believe that this plays a causal role in catalyst decomposition. The fate of the NHC ligand reports directly on these pathways: if this structure is intact in the products obtained immediately following the decomposition step, these pathways are not operative. Identification of the Ru-NHC products is thus critical to assessing the relevance of these pathways. Described below are efforts to assess the extent of bimolecular coupling during metathesis, and to evaluate the relevance of competing decomposition pathways involving NHC cyclometallation.

3.2 Results and Discussion

3.2.1 Quantifying Isomerization of 1-Olefins

As noted above, quantifying the propene products generated during metathesis would report on the extent to which **Ru-2** decomposes via β–hydride elimination. However, the majority of 1-olefins that undergo metathesis also isomerize pre- and/or post-metathesis, which may thus also liberate propenes. The validity of this concern was confirmed by performing the self-metathesis of methyl 10-undecenoate (Scheme 3.3(a)). Isomerization results in an apparent propene yield of over 800% relative to Ru (Scheme 3.3(b)). It is therefore critical to use a non-isomerizable olefin such as styrene to assess the contribution of BMC to catalyst decomposition.

Scheme 3.3 (a) Metathesis of Methyl 10-Undecenoate; showing metathesis products and propene byproducts. (b) Pathway depicting formation of propene byproducts via metathesis-isomerization.

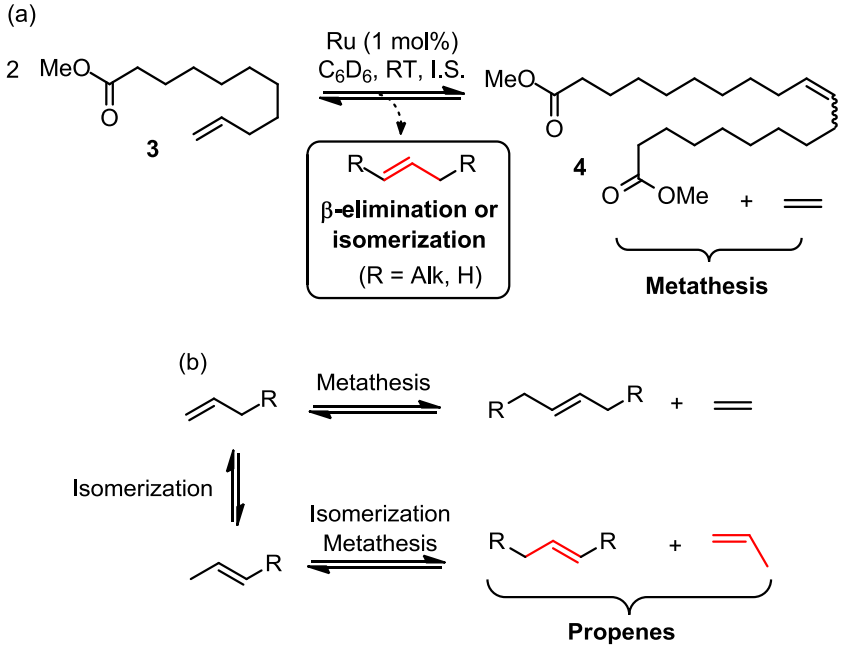

3.2.2 Decomposition via β-Elimination at Low Ruthenium Concentrations.

The experiments outlined in the introduction found that the extent of β-hydride elimination at 20 mM [Ru] was drastically lower than expected from the literature. Added experiments were directed at assessing the proportion of propenes at lower, more catalytically relevant catalyst concentrations. The proportion of β-hydride elimination (a unimolecular pathway) vs.

bimolecular coupling is expected to increase as Ru concentrations decrease. However, metathesis of styrene at a tenfold lower concentration (2 mM Ru, 0.1 mol% catalyst), revealed 0% and 46% propenes relative to ruthenium for **GIII** or **HII**, respectively. While this could be taken to suggest that bimolecular coupling is operative at unexpectedly low concentrations, a more likely explanation is that contaminants present in minor quantities promote other decomposition pathways. Parallel work by Alexandre Goudreault and Daniel do Nascimento of this research group has found that at low Ru concentrations (0.005 mol%), water or other contaminants significantly reduce the RCM performance of all catalysts studied, including **GII** and **HII**.

Scheme 3.4 Quantification of β–Hydride Elimination at High Dilutions (0.002 M Ru).

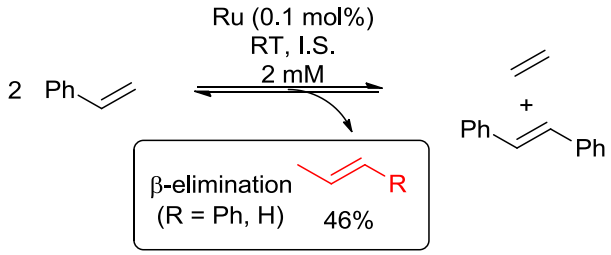

3.2.3 Insight from the Nature of the Ru Decomposition Products.

The py ligands in **GIII** offer opportunities to trap the Ru products of decomposition. Of particular interest is the fate of the H_2IMes ligand in these products, as NHC activation and/or cyclometallation are common features in pathways proposed on the basis of small amounts of serendipitously-crystallized materials.[13] Identifying the methylidene-free Ru species formed on reaction of **GIII** with styrene would indicate whether these pathways occur on any significant scale during spontaneous decomposition of methylidene species **Ru-1**. Scheme 3.5 depicts the major products observed: the known tris-pyridine complex **Ru-6** and its bis-pyridine analog $RuCl_2(H_2IMes)(py)_2$ **Ru-7**. The latter was originally assigned as chloride-bridged $[RuCl_2(H_2IMes)(py)_2]_2$ **Ru-8** (see Higman's preliminary studies of the thermolysis of **GIII** in the Introduction, as depicted in Scheme 3.1). However further characterization (see Section 3.2.6 below) revealed monomeric, fluxional complex **Ru-7** in both cases. Upon treating the mixture of ruthenium products formed with pyridine, 98% conversion to **Ru-6** was observed, ruling out other decomposition pathways that involve the NHC.

Scheme 3.5. Bimolecular Decomposition of **GIII** During Metathesis.

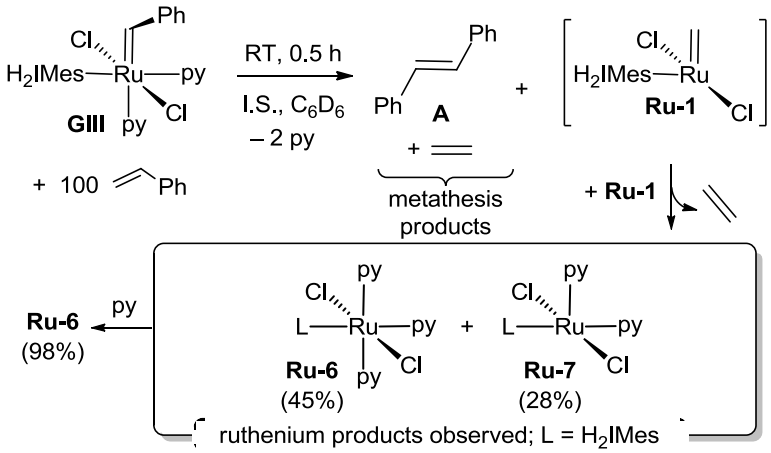

3.2.4 Quantifying Decomposition via Bimolecular Coupling.

The relatively low proportion of β-hydride elimination identified in Section 3.2.2 above indicates the operation of alternative pathway(s) in olefin metathesis. Bimolecular coupling is one possible contributor. However, our original experiments, in which bimolecular coupling was measured by thermolysis of **GIII** in the absence of olefin, are a poor comparison to standard conditions of metathesis. Directly investigating bimolecular coupling under catalytic conditions is desirable, but extremely challenging because ethylene generated by methylidene coupling is concealed by ethylene generated by metathesis of 1-olefin. Under catalytic conditions, the ethylene produced from bimolecular coupling is too small to be quantified. In an attempt to quantify bimolecular coupling while metathesis is proceeding, stoichiometric reactions of **GIII** with 2 equiv styrene were undertaken in NMR tubes filled with solvent (to retain ethylene in solution). Any ethylene from alkylidene coupling (0.5 equiv) would add to that generated by metathesis. The reversibility of metathesis and the closed system ensures continual metathesis even at low proportions of styrene. The yield of organic products (styrene, stilbene, ethylene) after decomposition of **GIII** reports on the extent of alkylidene coupling. If all the catalyst decomposes by bimolecular coupling, an additional 0.5 equivalents (Scheme 3.6 (b)) of organic products are added to the 2 equivalents (Scheme 3.6 (a)) of styrene for a total of 2.5 equivalents (Scheme 3.6; blue) relative to internal standard. Less than 2.5 equivalents would suggest the operation of alternative decomposition pathways, whether β-hydride elimination (Scheme 3.6 - red), NHC activation or others. Interestingly, after 30 min at 60 °C, no alkylidene of **GIII** was present by ^{1}H NMR

analysis and 2.43 equiv of the expected 2.5 equiv (ca. 97%) of organic products were formed, indicating a high proportion of alkylidene coupling.

Scheme 3.6. Quantifying Bimolecular Coupling of **GIII** in the Presence of Olefin.[a] (a) Metathesis of styrene generating 2 equiv olefins. (b) Bimolecular coupling of **Ru-1** generating ca. 0.5 equiv ethylene.

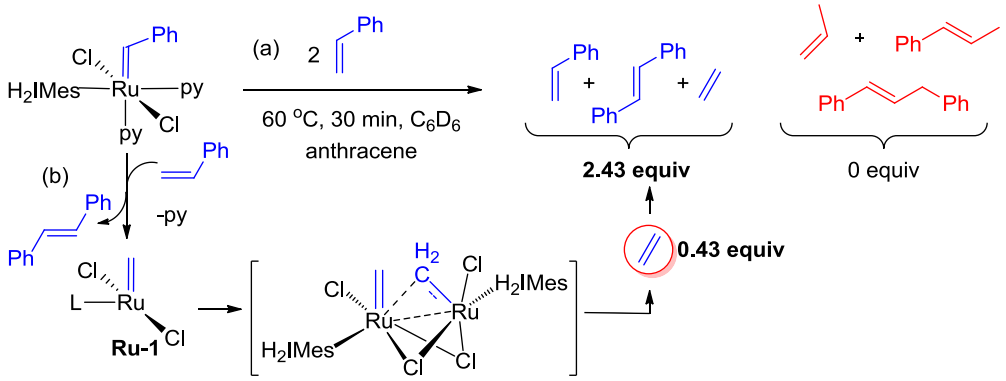

[a]Ru products are omitted.

3.2.5 Synthesis of Decomposition Products from Commercial Starting Materials

The Ru decomposition products described in the Introduction were identified on the basis of in situ ^{1}H NMR analysis. The independent synthesis of $RuCl_2(H_2IMes)(py)_2$ **Ru-7** and $RuCl_2(H_2IMes)(ODA)$ **Ru-11** was pursued to verify these assignments. Access to the known tris-pyridine complex **Ru-6** was envisioned by treating tetrakis-pyridine complex **Ru-9** with one equivalent of H_2IMes in C_6D_6 (Scheme 3.7). No reaction was evident after 24 h at room temperature, or 16 h at 75 °C, suggesting that the starting complex **Ru-9** is inert. The unexpectedly low lability of the py ligands may reflect the absence of any steric pressure that would promote ligand loss, and the weak trans effect of pyridine.

Scheme. 3.7 Attempted Synthesis of **Ru-6** by Ligand Exchange with **Ru-9.**

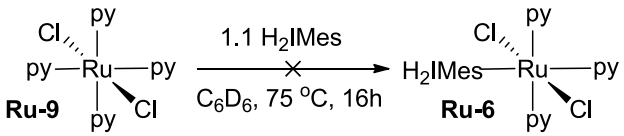

The complementary approach, installing H_2IMes followed by pyridine, was also attempted. A challenge in such reactions, unless a bulky, strongly-bound ligand is already in place at the Ru center, is the tendency to form bis-H_2IMes products. Few mono-H_2IMes complexes are known

outside the **GII**-class metathesis catalysts. The latter, accessed from bis(PCy_3) species **GI**, benefit from the strong binding of mutually trans NHC and PCy_3 ligands.[4] Rare examples outside the context of metathesis are the mono-NHC piano-stool complexes synthesized from the *p*-cymene dimer **Ru-12** (Scheme 3.8; **Ru-13** and **Ru-14**).[28,29,30]

Scheme 3.8. Synthesis of $RuCl_2$(*p*-cymene)(NHC) Complexes.

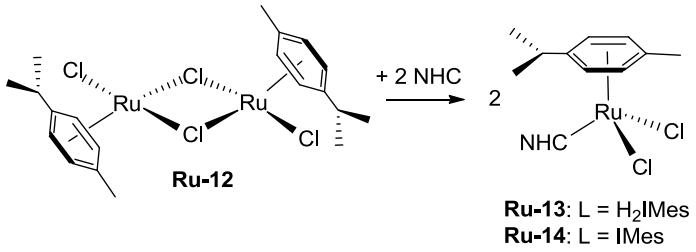

Particularly interesting is H_2IMes derivative $RuCl_2$(*p*-cymene)(H_2IMes) **Ru-13**, despite difficulties in isolation that limit its yield to 26%.[31] The basis of the poor yield, and an improved synthesis, are discussed in Chapter 4. Reaction of **Ru-13** with pyridine at room temperature gives H_2IMes complex **Ru-6** and a product tentatively assigned as the pyridine-bound *p*-cymene complex **Ru-15** (ratio 5:2 ratio), accompanied by traces of tetrakis-pyridine complex **Ru-9** (Figure 3.9(a)). Assignment of $RuCl_2$(*p*-cymene)(py) is proposed based on observation of a diagnostic pyridine *o-H* doublet at 9.03 ppm, the *p*-cymene Ar-C*H* doublets at 4.91 and 4.51 ppm, in the expected 1:1:1 ratio. This suggests, rather unexpectedly, that loss of H_2IMes competes with the desired displacement of the *p*-cymene ring. The low yields hampered isolation of tris-py complex **Ru-6** by precipitation or crystallization. Further modifications did not improve conversion and showed poor reproducibility, perhaps due to the photosensitivity of **Ru-13** (see Chapter 4). Attempts to adapt this method to generate $RuCl_2$(H_2IMes)(ODA) **Ru-11** by dropwise addition of *o*-dianiline to $RuCl_2$(*p*-cymene)(H_2IMes) **Ru-13** at room temperature (Scheme 3.9b) showed no reaction after 30 min. After heating the solution to 40 °C for 2 h, decomposition of **Ru-13** was inferred from the emergence of broad ^{1}H NMR signals: no **Ru-11** was observed.

Scheme 3.9 Attempted Synthesis of Ru Decomposition Species from $RuCl_2$(*p*-cymene)(H_2IMes) **Ru-13.**

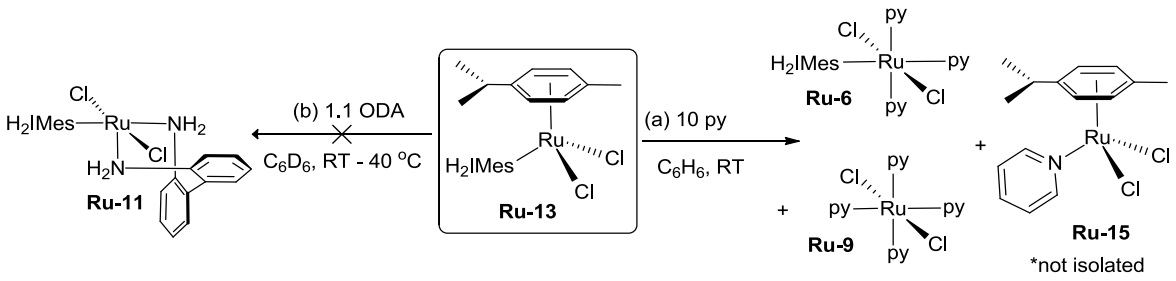

3.2.6 Isolation of NHC-Ligated Complexes from Ru Precatalysts

With the independent synthesis of these complexes unsuccessful, the more costly isolation of bis-py complex **Ru-7** and **Ru-11** from the precatalysts was pursued. Tris-py derivative **Ru-6** is reportedly formed as the thermodynamic product from decomposition of **GIIm** with pyridine in 29% yield.[32] Transformation to **Ru-7** by abstraction of one pyridine ligand was envisaged. Accordingly, **GIII** was treated with 2 equiv styrene at 60 °C (Scheme 3.10). Loss of the alkylidene ^{1}H NMR signal was complete after 30 min. Adding pyridine effected convergence on **Ru-6**, which on workup (reprecipitation followed by washing with Et_2O and hexanes) gave clean **Ru-6** in 85% yield.

Scheme 3.10 Isolation of Thermodynamic Product $RuCl_2(H_2IMes)(py)_3$ **Ru-6**

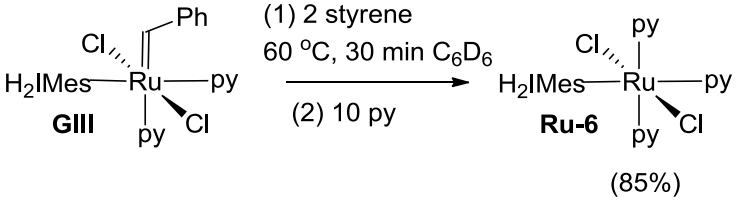

Synthesis of bis-pyridine complex **Ru-7** from its tris-py analogue **Ru-6** by azeotropic removal of pyridine was then attempted. The strong trans effect of the H_2IMes ligand was expected to labilize the trans pyridine ligand in **Ru-6**, giving equilibrium access to bis-pyridine species **Ru-7**. However, no conversion to **Ru-7** was observed by ^{1}H NMR analysis after repeatedly (5 cycles) dissolving **Ru-6** in benzene and evaporating to remove pyridine. Attempts to precipitate **Ru-6** from CH_2Cl_2/hexanes also proved unsuccessful. A third approach involved treatment of **Ru-6** with HCl to protonate pyridine. This method gave access **Ru-7**, but a competing side reaction,

protonation of H_2IMes, led to co-formation of tetrakis pyridine **Ru-9** (28% to **Ru-6**) and other undefined species. These results suggest that the pyridine ligand is non-labile, and that no equilibrium exists between **Ru-6** and **Ru-7**.

Scheme 3.11 Attempted Isolation of bis-Pyridine Complex **Ru-7**

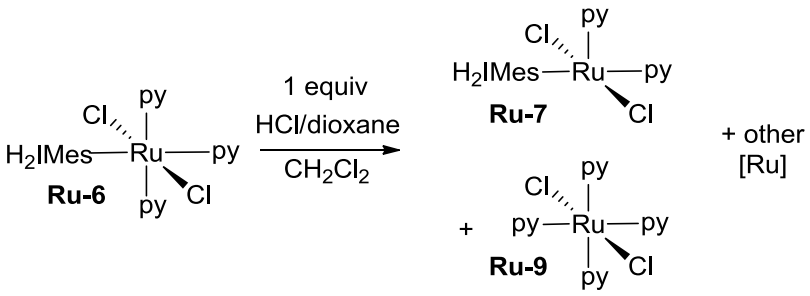

Ru-7 was ultimately accessed from **GIII** via metathesis. A pyridine ligand was first removed from **GIII** by reprecipitation, affording the mono-pyridine complex **GIII'** in 90% yield. On exposing to ethylene for 2 h, this species underwent a color change from green to yellow. A mixture of tris- and bis-pyridine products, **Ru-6** and **Ru-7**, was obtained in 1:4 ratio on reprecipitation from CH_2Cl_2/hexanes.

Scheme 3.12 Attempted Isolation of bis-Pyridine Complex **Ru-7** from **GIII**

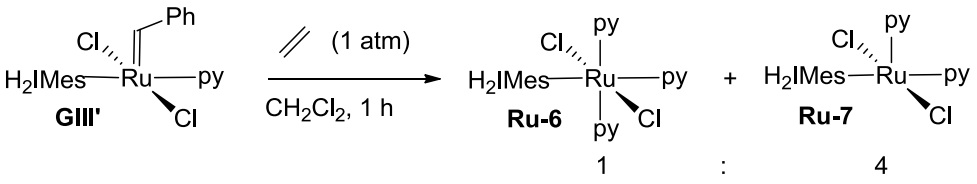

The presence of **Ru-6** proved an asset in identifying **Ru-7** as a bis-py complex, as opposed to the dimeric structure originally proposed ($[RuCl_2(H_2IMes)(py)_2]_2$, Scheme 3.1). DOSY analysis of the mixture revealed that the two components diffused at similar rates (Appendix A8), supporting a mono-Ru formulation. The pyridine signals were assigned by ^1H–^1H COSY correlations between adjacent protons on each unique pyridine ring: δ_H 9.15 / 6.29 / 6.54 ppm, and 9.40 / 6.03 / 6.47 ppm (Scheme 3.13). Two inequivalent pyridine ligands were observed, consistent with a square pyramidal geometry.

Scheme 3.13. ^{1}H-^{1}H COSY Spectra of $RuCl_2(H_2IMes)(py)_2$ **Ru-7**

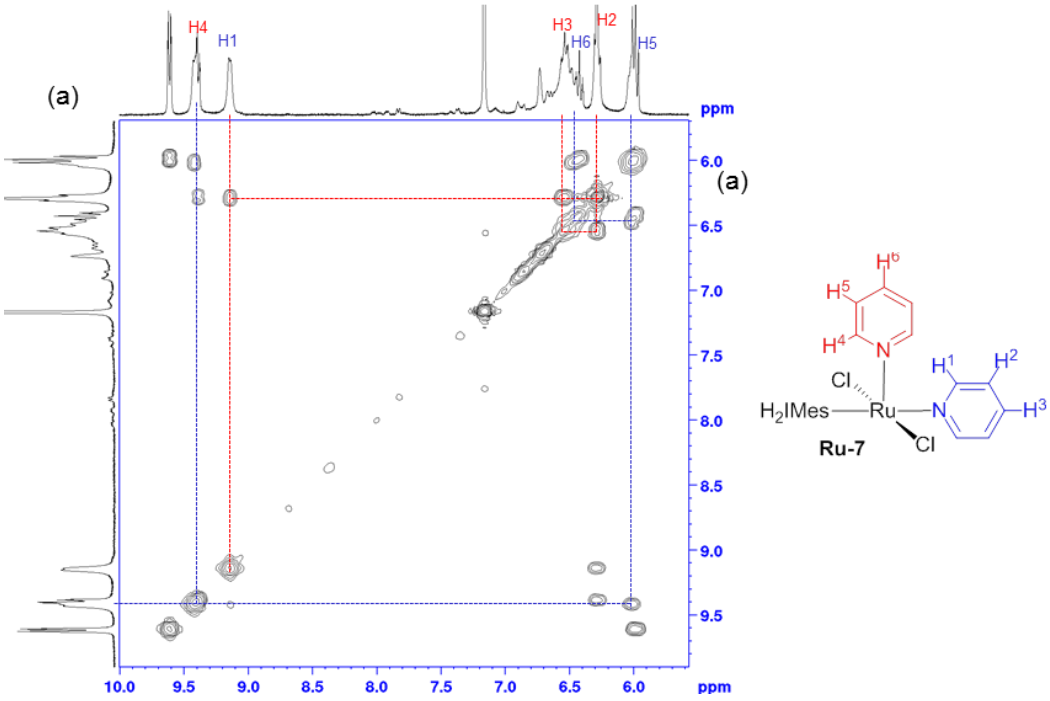

All of the discrete ^{1}H NMR signals for **Ru-7** are broad ($\omega_{1/2}$ ~5–50 Hz), suggesting fluxionality at RT. Consistent with this, exchange of the two pyridine ligands is observed by ^{1}H – ^{1}H EXSY spectroscopy (δ 9.40 / 9.16 ppm, 6.29 / 6.03 ppm, and 6.54 / 6.47 ppm) and NOE cross-peaks are observed between both of the pyridine ligands and the (equivalent) mesityl rings by ^{1}H – ^{1}H NOESY spectroscopy in C_6D_6 with 1s mixing times (Appendix A6 and A7).

Isolation of the corresponding dianiline complex $RuCl_2(H_2IMes)(ODA)$ **Ru-11** likewise proved challenging. Preliminary NMR experiments in which the precatalyst **DA** was treated with ethylene led to broad, unresolved ^{1}H NMR signals; 5 hydride signals were evident at complete decomposition, with no signals for **Ru-11**. However, metathesis of **DA** with styrene (10 equiv) at 50 °C for 16 h, followed by precipitation from CH_2Cl_2/hexanes, yielded **Ru-11** with minor impurities. Diagnostic signals for **Ru-11** are the diastereotopic NH_aH_b pairs at 4.89 / 3.95 ppm, and 4.20 / 4.04 ppm.

3.3 Conclusion

At the outset of this work, the sole decomposition pathway considered for phosphine-free catalysts was β-elimination of the metallacyclobutane. The relevance of this pathway was assessed at low Ru concentrations (2 mM; 0.1 mol % Ru), conditions designed to approach those employed in ring-closing macrocyclization. Bimolecular coupling is expected to be minimal at these dilutions. Under these conditions, the propene markers for this pathway account for <50% of the initial catalyst charge. These findings strongly suggest that alternative pathways beyond β-elimination are operative under catalytic conditions, and point toward the importance of understanding decomposition by ubiquitous contaminants such as water.

Characterization of the Ru products of decomposition via bimolecular coupling was also undertaken. The NHC ligands are intact in these species, indicating that widely-accepted pathways such as NHC cyclometallation are not in fact relevant under these conditions. Efforts to synthesize these complexes from commercially available starting materials pointed toward the potential utility of $RuCl_2(H_2IMes)$(*p*-cymene) as a Ru-H_2IMes building block. Realization of that potential forms the subject of the next Chapter.

3.4 References

(1) (a) Hong, S. H.; Wenzel, A. G.; Salguero, T. T.; Day, M. W.; Grubbs, R. H. *J. Am. Chem. Soc.* **2007**, *129*, 7961–7968. (b) Hong, S. H.; Day, M. W.; Grubbs, R. H. *J. Am. Chem. Soc.* **2004**, *126*, 7414–7415.

(2) (a) McClennan, W. L.; Rufh, S.; Lummiss, J. A. M.; Fogg, D. E. *J. Am. Chem. Soc.* **2016**, *138*, 14668−14677. (b) Lummiss, J. A. M.; McClennan, W. L.; McDonald, R.; Fogg, D. E. *Organometallics* **2014**, *33*, 6738–6741. (c) Lummiss, J. A. M.; Ireland, B. J.; Sommers, J. M.; Fogg, D. E. *ChemCatChem* **2014**, *6*, 459–463. (d) Lummiss, J. A. M.; Botti, A. G. G.; Fogg, D. E. *Catal. Sci. Technol.* **2014**, *4*, 4210–4218.

(3) Rate constants for initiation (k_i; x 10^{-3} s^{-1}) at 5 °C: **GII**, 0.0032; **HII**, 2.6; **GIII**, >200. See: Love, J. A.; Morgan, J. P.; Trnka, T. M.; Grubbs, R. H. *Angew. Chem., Int. Ed.* **2002**, *41*, 4035–4037, and references therein. % Recapture = proportion of the resting-state species at 50% catalyst decomposition during styrene metathesis (100 equiv styrene, 22 °C, C_6D_6). Data for selected Class A–C catalysts: **GII**, 15%; **HII**, 100%; **GIII**, 0%. The resting states are, respectively, $RuCl_2(H_2IMes)(PCy_3)(=CH_2)$ **GIIm**, **HII** itself, and (see below) $RuCl_2(H_2IMes)(py)_n(=CH_2)$.

(4) Lummiss, J. A. M.; Higman, C. S.; Fyson, D. L.; McDonald, R.; Fogg, D. E. *Chem. Sci.* **2015**, *6*, 6739–6746.

(5) Lummiss, J. A. M.; McClennan, W. L.; McDonald, R.; Fogg, D. E. *Organometallics* **2014**, *33*, 6738–6741.

(6) Bailey, G. A.; Fogg, D. E. *J. Am. Chem. Soc.* **2015**, *137*, 7318–7321.

(7) Rybak, A.; Meier, M. A. R. *Green Chem.* **2007**, *9*, 1356–1361.

(8) Schweitzer, D.; Snell, K. D. *Org. Process Res. Dev.* **2015**, *19*, 715−720.

(9) Bilel, H.; Hamdi, N.; Zagrouba, F.; Fischmeister, C.; Bruneau, C. *Green Chem.* **2011**, *13*, 1448–1452.

(10) Lafaye, K.; Nicolas, L.; Guérinot, A.; Reymond, S. b.; Cossy, J. *Org. Lett.* **2014**, *16*, 4972−4975.

(11) Ireland, B. J.; Dobigny, B. T.; Fogg, D. E. *ACS Catal.* **2015**, *5*, 4690−4698.

(12) Bailey, G. A.; Lummiss, J. A. M.; Foscato, M.; Occhipinti, G.; McDonald, R.; Jensen, V. R.; Fogg, D. E. *J. Am. Chem. Soc.* **2017**, *139*, 16446–16449.

(13) (a) Schrodi, Y., Mechanisms of Olefin Metathesis Catalyst Decomposition and Methods of Catalyst Reactivation. In ref 1b, pp 323–342. (b) Chadwick, J. C.; Duchateau, R.; Freixa, Z.; van Leeuwen, P. W. N. M., Alkene Metathesis. In *Homogeneous Catalysts: Activity – Stability – Deactivation*, Wiley-VCH: Weinheim, 2011; pp 347-396.

(14) (a) Schrock, R. R.; Copéret, C. *Organometallics* **2017**, *36*, 1884–1892. An important early analysis noted the striking propensity of $M=CH_2$ species to eliminate ethylene: (b) Merrifield, J. H.; Lin, G.-Y.; Kiel, W. A.; Gladysz, J. A. *J. Am. Chem. Soc.* **1983**, *105*, 5811–5819. For crystallographically characterized examples of methylidene complexes derived from group 6 metathesis catalysts, see: (c) Arndt, S.; Schrock, R. R.; Muller, P. *Organometallics* **2007**,

26, 1279–1290. (d) Tsang, W. C. P.; Jamieson, J. Y.; Aeilts, S. L.; Hultzsch, K. C.; Schrock, R. R.; Hoveyda, A. H. *Organometallics* **2004**, *23*, 1997–2007.

(15) Amoroso, D.; Yap, G. P. A.; Fogg, D. E. *Organometallics* **2002**, *21*, 3335–3343.

(16) Amoroso, D.; Snelgrove, J. L.; Conrad, J. C.; Drouin, S. D.; Yap, G. P. A.; Fogg, D. E. *Adv. Synth. Catal.* **2002**, *344*, 757–763.

(17) Schwab, P.; Grubbs, R. H.; Ziller, J. W. *J. Am. Chem. Soc.* **1996**, *118*, 100–110.

(18) Ulman, M.; Grubbs, R. H. *J. Org. Chem.* **1999**, *64*, 7202–7207.

(19) Dias, E. L.; Grubbs, R. H. *Organometallics* **1998**, *17*, 2758–2767.

(20) Dinger, M. B.; Mol, J. C. *Organometallics* **2003**, *22*, 1089–1095.

(21) Wang, H.; Metzger, J. O. *Organometallics* **2008**, *27*, 2761–2766.

(22) Adlhart, C.; Chen, P. *Helv. Chim. Acta* **2003**, *86*, 941–949.

(23) (a) Romero, P. E.; Piers, W. E. *J. Am. Chem. Soc.* **2005**, *127*, 5032–5033. (b) Romero, P. E.; Piers, W. E. *J. Am. Chem. Soc.* **2007**, *129*, 1698–1704. (c) van der Eide, E. F.; Piers, W. E. *Nature Chem.* **2010**, *2*, 571–576.

(24) (a) Fürstner, A.; Ackermann, L.; Gabor, B.; Goddard, R.; Lehmann, C. W.; Mynott, R.; Stelzer, F.; Thiel, O. R. *Chem. – Eur. J.* **2001**, *7*, 3236–3253. (b) Huang, J.; Schanz, H.-J.; Stevens, E. D.; Nolan, S. P. *Organometallics* **1999**, *18*, 5375–5380.

(25) For evidence of "boomerang" recapture of isopropoxystyrene, see: (a) Bates, J. M.; Lummiss, J. A. M.; Bailey, G. A.; Fogg, D. E. *ACS Catal.* **2014**, *4*, 2387−2394. (b) Griffiths, J. R.; Keister, J. B.; Diver, S. T. *J. Am. Chem. Soc.* **2016**, *138*, 5380−5391. For the original proposal, see: (c) Garber, S. B.; Kingsbury, J. S.; Gray, B. L.; Hoveyda, A. H. *J. Am. Chem. Soc.* **2000**, *122*, 8168–8179.

(26) The excellent Lewis basicity of *o*-dianiline is evident from over a dozen reports of its Ru complexes. Selected examples: (a) Crimmin, M. R.; Bergman, R. G.; Toste, F. D. *Angew. Chem., Int. Ed.* **2011**, *50*, 4484–4487. (b) Faller, J. W.; Fontaine, P. P. *Organometallics* **2005**, *24*, 4132–4138. (c) Aikawa, K.; Mikami, K. *Angew. Chem., Int. Ed.* **2003**, *42*, 5455–5458. A pK_a of 3.81 in 70% aqueous EtOH is reported for the conjugate acid of *o*-dianiline; cf. 3.66 for pyridine. See, respectively: (a) Grantham, P. H.; Weisburger, E. K.; Weisburger, J. H. *J. Org. Chem.* **1961**, *26*, 1008–1017. (b) McDaniel, D. H.; Özcan, M. *J. Org. Chem.* **1968**, *33*, 1922–1923. The pK_a reported for pyridine in acetonitrile is considerably higher: see ref 24.

(27) Arndt, S.; Schrock, R. R.; Muller, P. *Organometallics* **2007**, *26*, 1279–1290.

(28) Jafarpour, L.; Huang, J.; Stevens, E. D.; Nolan, S. P. *Organometallics* **1999**, *18*, 3760–3763.

(29) Wanzlick, H.-W.; Lachmann, B.; Schikora, E. *Chem. Ber.* **1965**, 3170–3177.

(30) Delaude, L.; Demonceau, A.; Noels, A. F. *Chem. Commun.* **2001**, 986–987.

(31) Denk, M. K.; Gupta, S.; Brownie, J.; Tajammul, S.; Lough, A. J. *Chem. - Eur. J.* **2001**, *7*, 4477–4486.

(32) Hong, S. H.; Wenzel, A. G.; Salguero, T. T.; Day, M. W.; Grubbs, R. H. *J. Am. Chem. Soc.* **2007**, *129*, 7961–7968.

Chapter 4. High-Yield Synthesis of a Long-Sought, Labile Ru-NHC Reagent, and Its Application to the Concise Synthesis of Second-Generation Metathesis Catalysts

The work in this Chapter forms the manuscript of a Communication published in *Organometallics* (selected as ACS Editors' Choice) authored by CSD and DEF.

Author Contributions: The manuscript was written by CSD and DEF. All experimental work was carried out by CSD.

4.0 Preface

The work in this chapter was aimed at providing access to complexes based on the $RuCl_2(H_2IMes)$ core, which could be broadly expanded upon in catalyst synthesis. Preliminary efforts to target this core structure from standard ruthenium precursors ($RuCl_2(PPh_3)_3$, $[RuCl_2(PPh_3)_2]_2$, $[RuCl_2(COD)]_n$, $RuCl_2(L)_4$ or $RuCl_2(PPh_3)_2(L)_2$, where L = pyridine or 3-picoline, and $RuCl_2(PPh_3)_2(L)$, where L = phenathroline or *o*-dianiline), met with limited success. Access to $RuCl_2(H_2IMes)(py)_3$ **Ru-6** was possible by reaction of $RuCl_2(PPh_3)_2(py)_2$ with H_2IMes and pyridine, but in yields that prevented isolation. In complementary work aimed at synthesizing metathesis catalysts, $RuCl_2(PPh_3)(py)_2$ did not react with phenyldiazomethane at –78 °C. On warming to -41 °C, a reaction was observed, as indicated by a colour change and evolution of N_2. These results suggest that octahedral complexes are poor precursors in the target reaction, as the required ligand loss is inhibited at low temperatures. Coordinatively unsaturated or labile precursors are required, accounting for prior successes with $RuCl_2(PPh_3)_3$.

4.1 Abstract

Controlled reaction of $[RuCl_2(p\text{-cymene})]_2$ with H_2IMes generates the previously challenging precatalyst and Ru synthon $RuCl_2(p\text{-cymene})(H_2IMes)$ **Ru-13** in 96% isolated yield. Critical to success is inhibiting premature *p*-cymene displacement. This is achieved by carrying out the synthesis at ambient temperatures, protected from light, and at sufficient dilutions (25 mM in THF) to enable stoichiometric control and inhibit bimolecular decomposition. The ease with which *p*-cymene loss can be *deliberately* induced, however, is key to the utility of **Ru-13** in both catalysis and catalyst synthesis. Transformation of **Ru-13** into two second-generation olefin metathesis catalysts is described. $RuCl_2(H_2IMes)(=CH(o\text{-}C_6H_4\text{-}O^iPr))$ **HII** and $RuCl_2(H_2IMes)(PPh_3)(=CHPh)$ **GII-PPh$_3$** (a desirable, faster-initiating analogue of **GII**) are accessible in ca. 80% yield over 2 steps from commercially available $[RuCl_2(p\text{-cymene})]_2$.

Synthesis from $RuCl_2(PPh_3)_3$, in comparison, requires 3 or 4 steps for **HII** or **GII-PPh$_3$**, respectively, and proceeds in lower yields.

4.2 Introduction

Piano-stool complexes of the group 8 metals are privileged structures in catalysis, bioinorganic, and medicinal chemistry.[1-7] *p*-Cymene complexes of ruthenium dominate, owing to their ease of access from commercially available $[RuCl_2(p\text{-cymene})]_2$ (**Ru-12**), although expanding roles for iron complexes[8] and functionalized arene derivatives[9] are documented in recent reviews. In particular, attention has focused on catalysis via *N*-heterocyclic carbene (NHC) derivatives of **Ru-12** (Chart 4.1).[1-6]

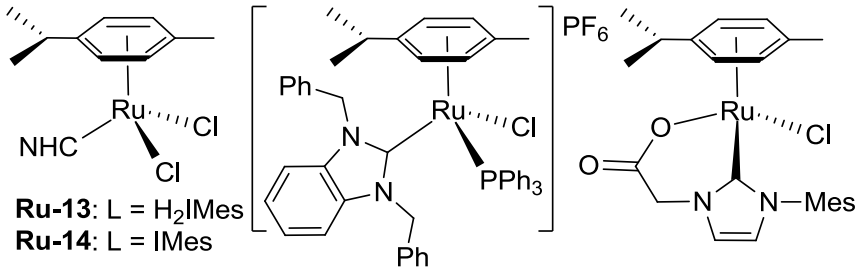

Chart 4.1. Exemplary *p*-cymene/NHC catalysts.[10-15]

Notably sparse, however, are reports of high-performing *p*-cymene catalysts containing *N,N'*-diarylimidazolidin-2-ylidenes, of which the H_2IMes complex **Ru-13** (Chart 4.1) may be regarded as an exemplar. This is particularly striking given early advances establishing a convenient in situ synthesis of **Ru-13**,[13] for use in olefin metathesis and atom-transfer radical polymerization.[13,16-18] Ledoux and co-workers subsequently described **Ru-13** as too unstable to isolate.[19] The Jensen group recently succeeded in isolating the complex,[10,20] albeit in yields (26%) that support this view. The *N*-*o*-phenol analogue of **Ru-13** also decomposes rapidly.[19] In contrast, IMes analogue **Ru-14** is stable, and indeed isolable in ca. 80-90% yield.[11,12]

The behavioral difference between these complexes is critical to their informed deployment. In some cases (e.g. outer-sphere transfer hydrogenation),[21] retention of the arene ligand is critical. In other contexts (e.g., metathesis, arylation, alkylation or hydrogen-borrowing catalysis, or synthesis of new catalysts by elaboration of the $RuCl_2(H_2IMes)$ core), *p*-cymene loss is essential, and its facile, *controlled* displacement represents a key potential asset. In the present work, we sought to clarify and control the instability of **Ru-13**, as an essential step toward harnessing the

potential of this and related *p*-cymene complexes in synthesis and catalysis. Here we identify key factors that promote loss of the *p*-cymene ring; we report the successful development of a high-yield route to **Ru-13**, and we demonstrate the exceptional utility of this complex in enabling a concise, efficient route to high-performing second-generation Ru metathesis catalysts.

Literature reports describe the use of thermal and photolytic triggers to displace the *p*-cymene ligand from phosphine[22] and NHC derivatives of **Ru-12**.[12,13] In the case of **Ru-13**, we suspected that steric pressure exerted by the H_2IMes mesityl groups might add to the lability of the η^6-arene ligand. While rotation about the Ru–H_2IMes bond is restricted[23-25] (a consequence of the π-acceptor character of the saturated NHC),[26,27] N–Mes bond rotation is facile. In contrast, the IMes ligand has a higher barrier to N–Mes rotation,[28,29] as well as a lower buried volume.[30] These factors could account for the improved stability of **Ru-14**. NOE experiments on isolated **Ru-13** (Fig. A10; generated as described below) confirm the presence of steric interactions between the mesityl *o*-Me groups and the *p*-cymene ligand in solution.

4.3 Results and Discussion

We bore the above points in mind in seeking to synthesize **Ru-13** for direct study. The thermal lability of the *p*-cymene ring rules out, for example, in situ production of H_2IMes from its imidazolinium salt,[19] which typically requires high temperatures as well as strong base. Instead, **Ru-13** was prepared by adding free H_2IMes to dimeric **Ru-12**, under conditions designed to minimize exposure of the product to light and heat: that is, at 22 °C in a foil-wrapped vessel, with the glovebox light switched off.

The stoichiometry of the reaction – and hence the solubility of **Ru-12** – emerged as a key additional criterion. Synthesis of **Ru-13** in CH_2Cl_2, in which **Ru-12** is fully soluble, is precluded by the rapid reaction of H_2IMes with CH_2Cl_2.[31] THF was therefore employed, despite only partial solubility of **Ru-12** in this solvent even at millimolar concentrations. An important insight was offered by the observation of negligible yields of **Ru-13** when solid H_2IMes was added to the **Ru-12** suspension, but greatly improved yields when THF *solutions* of H_2IMes were added. We infer that a local excess of H_2IMes is able to displace the *p*-cymene ligand from **Ru-13**. In an optimized synthetic protocol (Scheme 4.1), we therefore slowly infused a solution of the free carbene (1 mL/min; 25 mM) into a THF suspension of **Ru-12** (ca. 15 mg/mL). Addition was complete after 30 min, at which point a clear deep red solution was present. Evaporation of the solvent and reprecipitation of the residue from CH_2Cl_2-hexanes afforded **Ru-13** as a dark red

powder, in 96% yield.

Scheme 4.1. High-Yield Synthesis of **Ru-13.**

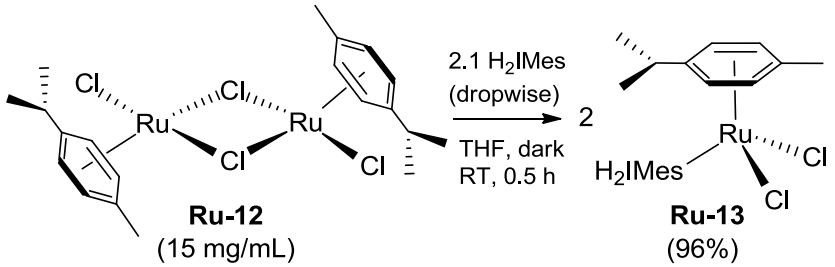

With clean **Ru-13** in hand, we examined its stability. As anticipated from the experiments above, adding H_2IMes to **Ru-13** caused extensive loss of the *p*-cymene ring (minutes at RT; Figure 4.1a). Exposing C_6D_6 solutions of **Ru-13** to fluorescent laboratory light at RT caused nearly 70% decomposition over 5 h, vs. 10% for a foil-wrapped sample over the same period (Figure 4.1b,c). Of note, the photolytic reaction showed a first-order rate dependence on [**Ru-13**], while decomposition in the dark was second order, albeit slower (Figure 4.1d). The latter, bimolecular reaction underscores the importance of maintaining low concentrations during synthesis of **Ru-13**. Irradiating CH_2Cl_2 solutions of **Ru-13** at 465 or 365 nm led to broadening of the absorption bands (Fig. A15) and formation of a black suspension, suggesting nanoparticle formation.[32]

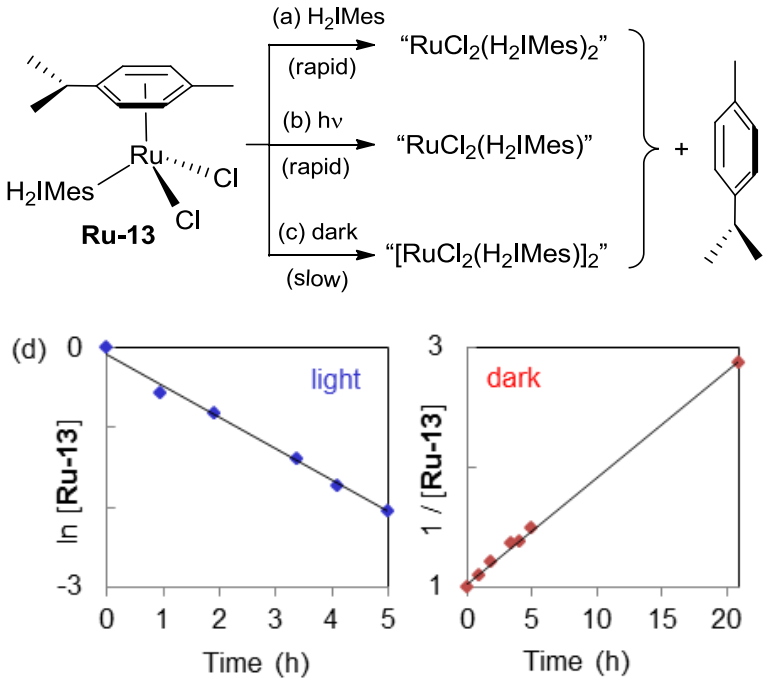

Figure 4.1. (a–c) Decomposition of **Ru-13** (20 mM; C_6D_6, RT), with plausible initial products. (d) Order of reaction with respect to Ru in the light and dark.

The historical difficulties in isolating **Ru-13** noted above are unsurprising, given the need to inhibit loss of *p*-cymene by protecting from (i) light and heat, (ii) uptake of a second H_2IMes ligand, and (iii) bimolecular decomposition. Once recognized, however, these conditions are readily met, as indicated by near-quantitative isolation of **Ru-13** on nearly 1 g scale via the protocol of Scheme 4.1.

From a complementary perspective, the ease with which the *p*-cymene ring can be displaced is a core asset that enables use of **Ru-13** as a clean source of "$RuCl_2(H_2IMes)$" in catalysis or catalyst synthesis. A final aspect of this work focused on the latter opportunity: specifically, use of **Ru-13** as an entry point to olefin metathesis catalysts. The important "second-generation" metathesis catalysts are typically accessed via multiple steps (Scheme 4.2),[33-39] commencing with transformation of hydrated $RuCl_3$ into $RuCl_2(PPh_3)_3$, then the first-generation Grubbs catalyst **GI**.[36a] $RuCl_2(PPh_3)_3$ is attractive relative to many alternative Ru precursors for its ease of handling,[36b] and because the bulk of the stabilizing phosphine ligands provides leverage for ligand exchange.[40]

Scheme 4.2. Dominant Routes to **HII** and **GII-PPh$_3$.**[a,b]

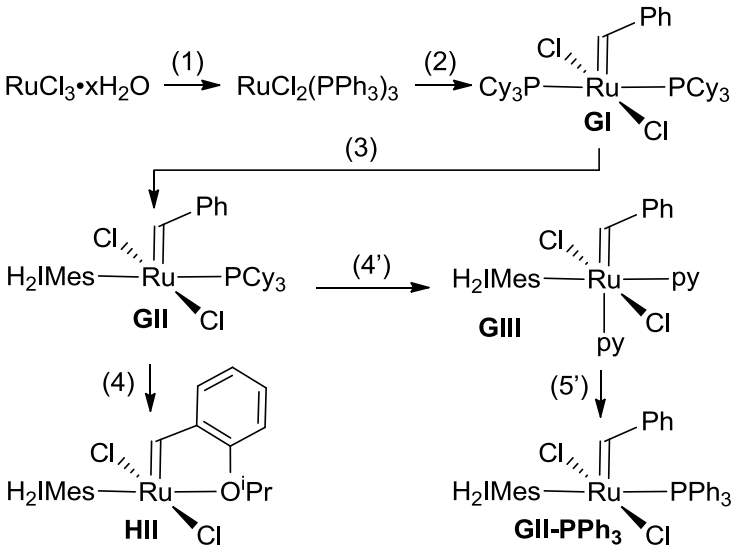

[a]Overall yields: 34-52% for **HII**, 29-33% for **GII-PPh$_3$**: see Appendix. [b]Conditions: (1) 6 PPh_3, refluxing MeOH.[41] (2) 2 $PhCHN_2$ + 2.2 PCy_3, CH_2Cl_2, –78 °C to RT.[36a] (3) 1.1 H_2IMes, THF, Merrifield resin.[38] (4) 1.1 $ArCH{=}CH_2$, 1.3 CuCl, refluxing CH_2Cl_2.[37] (4') 1:3 toluene-py;[42] the product is a mono/bis-py mixture.[43] (5') 1.1 PPh_3, C_6H_6.[42] For further details, see Appendix. Steps 3 and 4 in the synthesis of **HII** can be advantageously reversed.[38,39]

A major drawback, however, is the need to first install, and then remove, the PPh_3 ligands and one or more PCy_3 ligands. While phosphine scavengers can significantly improve isolated

yields,[38] the net process is laborious and wasteful.[44] More efficient routes to Ru metathesis catalysts, which circumvent reliance on $RuCl_2(PPh_3)_3$ as a precursor,[36b] are highly desirable.

In important early work, metathesis-active allenylidene or indenylidene complexes were generated by treating **Ru-12** or **Ru-14** with terminal alkynes,[11,45,46] and piano-stool Os complexes were prepared using phenyldiazomethane.[47,48] Here we sought to build on these advances by displacing the arene ring from **Ru-13**, while simultaneously introducing a benzylidene ligand and a stabilizing donor. We envisaged that this could offer access to the second-generation Hoveyda catalyst **HII** (Scheme 4.3a),[33,34] for example, in a single step.

Scheme 4.3. One-Step Synthesis of High-Performing Metathesis Catalysts from **Ru-13.**

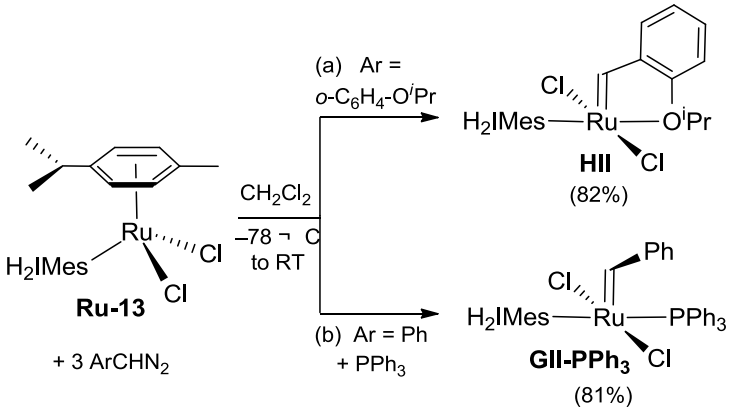

Accordingly, we adapted to **Ru-13** a procedure used by the Hoveyda group to install chelating benzylidene ether ligands on $RuCl_2(PPh_3)_3$.[33] Adding $ArCHN_2$ (Ar = *o*-C_6H_4-O^{i}Pr)[49] to a CH_2Cl_2 solution of **Ru-13** at –78 °C caused evolution of N_2, accompanied by a colour change from red to green over the ca. 20 min time of addition. The solution was then allowed to warm to 0 °C, and irradiated for 10 min at 365 nm using a standard portable UV lamp mounted 5 cm away. (It should be noted that Pyrex or borosilicate glass blocks light below 325 nm). **HII** was obtained following flash chromatography in 82% isolated yield, or ca. 70% overall yield from the ultimate precursor $RuCl_3$. This compares favourably with the dominant route shown in Scheme 4.1, which required 4 steps and 3-5 days from $RuCl_3$, and gave a maximum net yield of ca. 50%.

Chelation of the stabilizing ligand is not essential, as demonstrated by the synthesis of **GII-PPh$_3$** (Scheme 4.3b), an analogue of the Grubbs catalyst **GII**. Such PPh_3 derivatives are attractive for the higher lability[50] and reduced nucleophilicity[51] of the phosphine ligand, which helps inhibit catalyst decomposition.[52] Owing to their cumbersome synthesis,[42,53] however, these catalysts see little use.[54] **GII-PPh$_3$** was synthesized as above, but with addition of PPh_3 to the cold solution of

Ru-13 prior to cannula addition of $PhCHN_2$. **GII-PPh$_3$** was obtained in 81% yield after flash chromatography. In comparison, the literature route[42a] to **GII-PPh$_3$** requires 5 steps from $RuCl_3$, and proceeds in overall yields of 29–33%. From the perspective of atom efficiency, the new route represents an improvement of more than threefold (see Appendix).

4.4 Conclusion

The foregoing describes the successful synthesis and isolation of the long-sought precatalyst and synthon $RuCl_2$(*p*-cymene)(H_2IMes) **Ru-13**. This previously intractable complex is readily generated in high yields at RT by controlling reaction stoichiometry, limiting exposure to light, and keeping concentrations low to inhibit bimolecular displacement of the *p*-cymene ring. We anticipate that these precautions may likewise afford access to related *p*-cymene complexes bearing bulky, inflexible imidazolidene or other donors, and hence expand the deployment of such complexes in catalysis.

Importantly, the lability of the η^6-arene ring represents a major asset to use of **Ru-13** as a precatalyst or a building block. An exceptionally efficient route to high-performing phosphine-free and phosphine-stabilized metathesis catalysts from **Ru-13** is demonstrated. Attractive features are its brevity (just 2 synthetic steps from commercially available **Ru-12**), time-efficiency, and high yields (ca. 70% from $RuCl_3$). In comparison, existing routes proceed in overall yields of ca. 30–50% over 4-5 steps, and require up to a week. These findings are anticipated to open the door to new, efficient transformations based on **Ru-13** as a precatalyst, and to improve the efficiency, economy, and reliability of synthetic routes to leading metathesis catalysts.

4.5 Future work

In parallel with the work described above, the known complex $RuCl_2$(*p*-cymene)(IMe_4)[55] (IMe_4 = tetramethylimidazol-2-ylidene) was synthesized and isolated. The isolated complex underwent no reaction with $ArCHN_2$ (Ar = *o*-C_6H_4-O^{i}Pr) via the protocol described above, however. This observation tends to reinforce the role of NHC-cymene steric interactions in promoting loss of *p*-cymene, as required for installation of the alkylidene ligand. In further efforts to expand the scope of this work, the H_2IPr analogue of **Ru-13** (a new complex) was prepared via to the optimized protocol developed for **Ru-13** (H_2IPr = *N,N*'-bis-(2,6-diisopropylphenyl)imidazolin-2-ylidene). Preliminary NMR experiments indicated quantitative in situ yields of $RuCl_2$(*p*-

cymene)(H_2IPr) relative to internal standard. Time constraints precluded transformation of this species to its benzylidene derivative, an experiment that could be usefully explored.

Perhaps more critical are experiments involving cyclic alkylamino carbene (CAAC) ligands. Synthesis of $RuCl_2$(*p*-cymene)(^{IPrMe}CAAC) (Scheme 4.4.) was attempted via in situ generation of the free carbene, and dropwise addition of the latter to a suspension of $[RuCl_2(p\text{-cymene})]_2$. No formation of $RuCl_2$(*p*-cymene)(CAAC) was evident by ^{1}H NMR analysis, however, despite the expected increase in *p*-cymene lability arising from the greater steric bulk of the CAAC relative to H_2IMes [56]. While this could reflect low in situ yields of the free CAAC (which is normally generated in situ, to limit carbene coupling), it is also important to note that no care was taken to limit exposure to light, as the photolytic susceptibility of the *p*-cymene complexes was not fully appreciated at the time. Installation of the CAAC from the free carbene in the dark may thus afford access to $RuCl_2$(*p*-cymene)(CAAC), and hence to CAAC-ligated metathesis catalysts. Further optimization of the initial step will likely be essential, as the increased bulk of the CAAC may retard binding while also promoting p-cymene loss. If $RuCl_2$(*p*-cymene)(CAAC) complexes can be accessed, however, loss of *p*-cymene and alkylidene installation should be facile.

Scheme 4.4. Attempted Synthesis of a CAAC-Ligated Ruthenium *p*-Cymene Complex

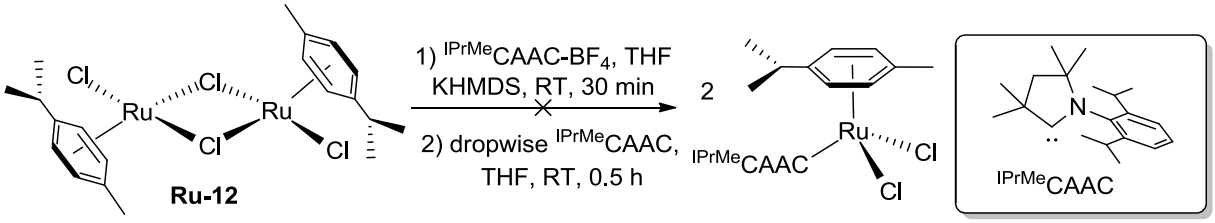

In situ formation of "$RuCl_2(H_2IMes)$" could also aid mechanistic studies, enabling generation of metallacyclobutane **Ru-2** without interference from spectator ligands, via reaction of $RuCl_2$(*p*-cymene)(H_2IMes) with a diazoalkane at –78 °C. Subsequent addition of donor ligands such as PPh_3 to form methylidene derivatives $RuCl_2(H_2IMes)(PPh_3)(=CH_2)$ would allow insight into the rate of recapture, initiation or nucleophilic attack by the added ligand. These experiments would give a more general perspective on these methylidene complexes, beyond the widely-studied complex **GIIm**.

4.6 References

(1) Hey, D. A.; Reich, R. M.; Baratta, W.; Kühn, F. E. *Coord. Chem. Rev.* **2018**, *374*, 114–132.
(2) Hameury, S.; de Fremont, P.; Braunstein, P. *Chem. Soc. Rev.* **2017**, *46*, 632–733.
(3) Delaude, L.; Demonceau, A., NHC–Iron, Ruthenium and Osmium Complexes in Catalysis. In *N-Heterocyclic Carbenes: From Laboratory Curiosities to Efficient Synthetic Tools*, 2nd ed.; Díez-González, S., Ed. Royal Society of Chemistry: Cambridge, 2017; pp 268–301.
(4) Diez-Gonzalez, S.; Marion, N.; Nolan, S. P. *Chem. Rev.* **2009**, *109*, 3612–3676.
(5) Chelucci, G. *Coord. Chem. Rev.* **2017**, *331*, 1–36.
(6) Corma, A.; Navas, J.; Sabater, M. J. *Chem. Rev.* **2018**, *118*, 1410−1459.
(7) Hindi, K. M.; Panzner, M. J.; Tessier, C. A.; Cannon, C. L.; Youngs, W. J. *Chem. Rev.* **2009**, *109*, 3859—3884.
(8) Johnson, C.; Albrecht, M. *Coord. Chem. Rev.* **2017**, *352*, 1–14.
(9) Igau, A. *Coord. Chem. Rev.* **2017**, *344*, 299–322.
(10) Engel, J.; Smit, W.; Foscato, M.; Occhipinti, G.; Törnroos, K. W.; Jensen, V. R. *J. Am. Chem. Soc.* **2017**, *139*, 16609–16619.
(11) Jafarpour, L.; Huang, J.; Stevens, E. D.; Nolan, S. P. *Organometallics* **1999**, *18*, 3760–3763.
(12) Lo, C.; Cariou, R.; Fischmeister, C.; Dixneuf, P. H. *Adv. Synth. Catal.* **2007**, *349*, 546—550.
(13) (a) Delaude, L.; Demonceau, A.; Noels, A. F. *Chem. Commun.* **2001**, 986–987. (b) Delaude, L.; Szypa, M.; Demonceau, A.; Noels, A. F. *Adv. Synth. Catal.* **2002**, *344*, 749–756.
(14) Xie, X.; Huynh, H. V. *ACS Catal.* **2015**, *5*, 4143−4151.
(15) Gandolfi, C.; Heckenroth, M.; Neels, A.; Laurenczy, G.; Albrecht, M. *Organometallics* **2009**, *28*, 5112–5121.
(16) Semeril, D.; Bruneau, C.; Dixneuf, P. H. *Adv. Synth. Catal.* **2002**, *344*, 585–595.
(17) Castarlenas, R.; Alaoui-Abdallaoui, I.; Semeril, D.; Mernari, B.; Guesmi, S.; Dixneuf, P. H. *New J. Chem.* **2003**, *27*, 6–8.
(18) Delaude, L.; Delfosse, S.; Richel, A.; Demonceau, A.; Noels, A. F. *Chem. Commun.* **2003**, 1526–1527.
(19) Ledoux, N.; Allaert, B.; Verpoort, F. *Eur. J. Inorg. Chem.* **2007**, 5578–5583.
(20) Of note, the *p*-cymene ligand can be stabilized by electron-withdrawing ligands, as evidenced by the isolation of a bis(trifluoroacetate) derivative of **Ru-2** in 76% yield. See: Zhang, Y.; Wang, D.; Lonnecke, P.; Scherzer, T.; Buchmeiser, M. R. *Macromol. Sympos.* **2006**, 30–37.
(21) Clapham, S. E.; Hadzovic, A.; Morris, R. H. *Coord. Chem. Rev.* **2004**, *248*, 2201–2237.
(22) Hafner, A.; Muhlebach, A.; van der Schaaf, P. A. *Angew. Chem., Int. Ed. Engl.* **1997**, *36*, 2121–2124.
(23) Lummiss, J. A. M.; Higman, C. S.; Fyson, D. L.; McDonald, R.; Fogg, D. E. *Chem. Sci.* **2015**, *6*, 6739–6746.
(24) Gallagher, M. M.; Rooney, A. D.; Rooney, J. J. *J. Organomet. Chem.* **2008**, *693*, 1252–1260.
(25) Leuthaeusser, S.; Schmidts, V.; Thiele, C. M.; Plenio, H. *Chem. – Eur. J.* **2008**, *14*, 5465–5481.
(26) Huynh, H. V. *Chem. Rev.* **2018**, *118*, 9457–9492.

(27) For recent studies assessing the balance between NHC s-donation and π-acidity, see: (a) Back, O.; Henry-Ellinger, M.; Martin, C. D.; Martin, D.; Bertrand, G. *Angew. Chem., Int. Ed.* **2013**, *52*, 2939–2943. (b) Liske, A.; Verlinden, K.; Buhl, H.; Schaper, K.; Ganter, C. *Organometallics* **2013**, *32*, 5269−5272. (c) Vummaleti, S. V. C.; Nelson, D. J.; Poater, A.; Gomez-Suarez, A.; Cordes, D. B.; Slawin, A. M. Z.; Nolan, S. P.; Cavallo, L. *Chem. Sci.* **2015**, 6, 1895–1904.
(28) Fürstner, A.; Ackermann, L.; Gabor, B.; Goddard, R.; Lehmann, C. W.; Mynott, R.; Stelzer, F.; Thiel, O. R. *Chem. – Eur. J.* **2001**, *7*, 3236–3253.
(29) Kotyk, M. W.; Gorelsky, S. I.; Conrad, J. C.; Carra, C.; Fogg, D. E. *Organometallics* **2009**, *28*, 5424–5431.
(30) Hillier, A. C.; Sommer, W. J.; Yong, B. S.; Petersen, J. L.; Cavallo, L.; Nolan, S. P. *Organometallics* **2003**, *22*, 4322–4326.
(31) Decomposition of H_2IMes by neat CH_2Cl_2 is immediate: see SI. A prior report that this reaction is very slow at RT involved the use of 40 equiv CH_2Cl_2 in hexanes. See: Arduengo, A. J.; Davidson, F.; Dias, H. V. R.; Goerlich, J. R.; Khasnis, D.; Marshall, W. J.; Prakasha, T. K. *J. Am. Chem. Soc.* **1997**, *119*, 12742–12749.
(32) For a report of nanoparticle formation on decomposition of **GII**, see: Higman, C. S.; Lanterna, A. E.; Marin, M. L.; Scaiano, J. C.; Fogg, D. E. *ChemCatChem* **2016**, *8*, 2446–2449. Ligand activation may enable the required reduction event in both cases.
(33) Kingsbury, J. S.; Harrity, J. P. A.; Bonitatebus, P. J.; Hoveyda, A. H. *J. Am. Chem. Soc.* **1999**, *121*, 791–799.
(34) Gessler, S.; Randl, S.; Blechert, S. *Tetrahedron Lett.* **2000**, *41*, 9973–9976.
(35) Scholl, M.; Ding, S.; Lee, C. W.; Grubbs, R. H. *Org. Lett.* **1999**, *1*, 953–956.
(36) (a) Schwab, P.; Grubbs, R. H.; Ziller, J. W. *J. Am. Chem. Soc.* **1996**, *118*, 100–110. (b) For a summary of routes to **GI**, see: Fogg, D. E.; Foucault, H. M., Ring-Opening Metathesis Polymerization. In *Comprehensive Organometallic Chemistry III*, Crabtree, R. H.; Mingos, D. M. P., Eds. Elsevier: Oxford, 2007; Vol. 11, pp 623–652.
(37) Bujok, R.; Bieniek, M.; Masnyk, M.; Michrowska, A.; Sarosiek, A.; Stepowska, H.; Arlt, D.; Grela, K. *J. Org. Chem.* **2004**, *69*, 6894–6896.
(38) For a discussion of the advantages of Merrifield resins relative to other phosphine scavengers, including the Amberlyst resin, see: Nascimento, D. L.; Davy, E. C.; Fogg, D. E. *Catal. Sci. Technol.* **2018**, 1535–1544.
(39) Bieniek, M.; Michrowska, A.; Gulajski, L.; Grela, K. *Organometallics* **2007**, *26*, 1096–1099.
(40) For the importance of steric interactions in promoting ligand dissociation in metathesis, see: (a) Lummiss, J. A. M.; Perras, F. A.; Bryce, D. L.; Fogg, D. E. *Organometallics* **2016**, *35*, 691–698. For difficulties in effecting complete displacement of sterically minimal nitrile ligands from Ru centers, see: (b) Fogg, D. E.; James, B. R. *Inorg. Chem.* **1997**, *36*, 1961–1966.
(41) Hallman, P. S.; Stephenson, T. A.; Wilkinson, G. *Inorg. Synth.* **1970**, *12*, 237–40.
(42) While **GII'** is in principle accessible from $RuCl_2(PPh_3)_2$(=CHPh) **G0**, the initial product formed on treating $RuCl_2(PPh_3)_3$ with phenyldiazomethane, such PPh_3 complexes readily undergo bimolecular decomposition during precipitation of the product. See: Amoroso, D.; Snelgrove, J. L.; Conrad, J. C.; Drouin, S. D.; Yap, G. P. A.; Fogg, D. E. *Adv. Synth. Catal.* **2002**, *344*, 757–763.

(43) (a) Walsh, D. J.; Lau, S. H.; Hyatt, M. G.; Guironnet, D. *J. Am. Chem. Soc.* **2017**, *139*, 13644–13647. (b) Bailey, G. A.; Foscato, M.; Higman, C. S.; Day, C. S.; Jensen, V. R.; Fogg, D. E. *J. Am. Chem. Soc.* **2018**, *140*, 6931–6944.
(44) For synthesis of **HII** via the $RuCl_2(PPh_3)_3$ / indenylidene route, see: (a) Fürstner, A.; Guth, O.; Duffels, A.; Seidel, G.; Liebl, M.; Gabor, B.; Mynott, R. *Chem. – Eur. J.* **2001**, *7*, 4811–4820. (b) Randl, S.; Gessler, S.; Wakamatsu, H.; Blechert, S. *Synlett* **2001**, 430–432. The atom economy from $RuCl_3$ is 25%, and the net yield is 36%. .
(45) Castarlenas, R.; Semeril, D.; Noels, A. F.; Demonceau, A.; Dixneuf, P. H. *J. Organomet. Chem.* **2002**, *663*, 235–238.
(46) Castarlenas, R.; Vovard, C.; Fischmeister, C.; Dixneuf, P. H. *J. Am. Chem. Soc.* **2006**, *128*, 4079–4089.
(47) Castarlenas, R.; Esteruelas, M. A.; Oñate, E. *Organometallics* **2005**, *24*, 4343–4346.
(48) Esteruelas, M. A.; González, A. I.; López, A. M.; Oñate, E. *Organometallics* **2003**, *22*, 414–425.
(49) A ca. threefold excess of the diazo reagent was used to effect complete conversion (cf. 2 equiv in synthesis of **GI**; Scheme 2). The excess required in both cases reflects the instability of these reagents.
(50) (a) For an analysis of the synergy between an activating NHC ligand and a labile PPh_3 donor, see: (a) Conrad, J. C.; Yap, G. P. A.; Fogg, D. E. *Organometallics* **2003**, *22*, 1986–1988. For the 50-fold faster loss of PR_3 from **GII'** vs. **GII**, see: (b) Sanford, M. S.; Love, J. A.; Grubbs, R. H. *J. Am. Chem. Soc.* **2001**, *123*, 6543–6554.
(51) Tolman, C. A. *J. Am. Chem. Soc.* **1970**, *92*, 2953–2956.
(52) (a) McClennan, W. L.; Rufh, S. A.; Lummiss, J. A. M.; Fogg, D. E. *J. Am. Chem. Soc.* **2016**, *138*, 14668−14677. (b) Santos, A. G.; Bailey, G. A.; dos Santos, E. N.; Fogg, D. E. *ACS Catal*. **2017**, *7*, 3181−3189. (c) Bailey, G. A.; Fogg, D. E. *J. Am. Chem. Soc.* **2015**, *137*, 7318–7321.
(53) For an efficient diazo-free route to a vinylalkylidene analogue of **GII'**, see: Conrad, J. C.; Yap, G. P. A.; Fogg, D. E. *Organometallics* **2003**, *22*, 1986–1988.
(54) Among the rare exceptions, see: (a) Biondi, I.; Laurenczy, G.; Dyson, P. J. *Inorg. Chem.* **2011**, *50*, 8038—8045. (b) Hanson, P. R.; Chegondi, R.; Nguyen, J.; Thomas, C. D.; Waetzig, J. D.; Whitehead, A. *J. Org. Chem.* **2011**, *76*, 4358–4370.
(55) Herrmann, W. A.; Elison, M.; Fischer, J.; Koecher, C.; Artus, G. R. J. *Chem. – Eur. J.* **1996**, *2*, 772–780.
(56) Clavier, H.; Nolan, S. P. *Chem. Commun.* **2010**, *46*, 841–861.

Chapter 5. Conclusions and Future Work

The broadly used ruthenium metathesis catalysts have found tremendous success in organic synthesis, but low productivity and high cost impede their adoption in, for example, pharmaceutical manufacturing or the industrial harnessing of renewable feedstocks. Understanding the pathways by which these catalysts decompose can help guide implementation of metathesis methodologies, as well as catalyst redesign. The original, phosphine-stabilized catalysts are now recognized as being subject to many problems arising from the nucleophilicity and basicity of the PCy_3 ligand released during metathesis. Phosphine-free catalysts are attractive in that they bypass such pathways. However, decomposition of this catalyst class is little studied. At the outset of this work, β-hydride elimination from the MCB was the only documented pathway, and was presumed to dominate their decomposition.

The first part of this thesis work examines whether spontaneous elimination of the metallacyclobutane ring as propene(s) contributes to decomposition of the important phosphine-free catalysts. This pathway had been widely presumed to dominate decomposition for second-generation, Ru-NHC metathesis catalysts. The present work, in conjunction with studies by Gwen Bailey of this research group, demonstrates that other decomposition pathways are competing. Elimination of propenes was shown to account for less than 50% of decomposition, even under sealed-tube conditions expected to maximize formation of the MCB, which would promote this pathway. Bimolecular coupling is proposed to account for the balance of decomposition (indeed, Bailey's experiments with the isolated methylidene adduct showed that the "fast-initiating" catalyst **GIII** decomposes *principally* by this pathway). Repeating the propene-elimination experiments at catalyst concentrations of 2 mM indicated that this pathway is operative even at high dilution. Characterization of the ruthenium products shows an intact NHC ligand, demonstrating that speculated decomposition pathways involving NHC cyclometallation do not compete.

In these studies, considerable effort was directed at the independent synthesis of the Ru products of decomposition to confirm their assignment in the decomposition chemistry. In the course of that work, a potentially efficient entry point to second-generation metathesis catalysts emerged. The second part of this thesis builds on this finding. It turns to consideration of a simple, cheap

route to highly active second-generation catalysts, which could support their broader use. An easily accessed $RuCl_2(H_2IMes)$(*p*-cymene) complex is described, which serves as a convenient source of $RuCl_2(H_2IMes)$. Such piano-stool complexes have seen success in catalysis, medicinal and materials chemistry. However, $RuCl_2$(*p*-cymene)(H_2IMes) itself has been reported to undergo premature, uncontrolled loss of *p*-cymene, a feature that presents a significant challenge to its synthesis, isolation, and use. Examination of the origin of the poor stability of the complex revealed that loss of *p*-cymene is accelerated by reaction with H_2IMes, bimolecular reaction, and exposure to light. Controlling each of these factors enabled synthesis and isolation of $RuCl_2$(*p*-cymene)(H_2IMes) in high yields.

In addition, the susceptibility to light was harnessed to effect *controlled* liberation of *p*-cymene in the presence of a carbene source (supplied by a diazo reagent), and a stabilizing donor ligand. Two second-generation metathesis catalysts were synthesized via this protocol, including the widely used catalyst **HII** and a fast-initiating analogue of **GII**, in which a PPh_3 ligand replaces the undesirable (nonlabile, nucleophilic) PCy_3 ligand in **GII** itself. Both complexes were synthesized in high yields (>80% from $RuCl_3$). In comparison, existing routes to these catalysts proceed in yields of 29-50%. The total number of steps from the relevant commercial Ru precursor ($RuCl_2(PPh_3)_3$ or $[RuCl_2(p\text{-cymene})]_2$, respectively) was decreased from 3-4 to 2, and the atom economy was increased threefold.

Many questions in the arena of catalyst stability and decomposition remain to be tackled. Our understanding of the impact of ligands on the stability of the active species remains fragmentary. The Piers catalyst offers an intriguing opportunity to gauge such factors for the metallacyclobutane intermediate, by generating the latter via ethenolysis at –78 °C, and examining rates of β-elimination. Specifically, if routes to the appropriate Piers catalysts can be devised (and hence reliable routes to the metallacyclobutane intermediates), the thermal stability of these species could potentially be assessed as a function of the ligands present. Extraction of structure-stability relationships from the half-life of decomposition would aid in evaluating the steric and electronic impact of the ligands (NHC, CAAC, anionic ligands) on MCB stability.

In terms of synthetic routes to novel catalysts, an attractive opportunity lies in expanding the scope of the ancillary ligands in the $RuCl_2$(*p*-cymene)(L) complex to include other NHCs, CAACs, or designer ligands that are challenging to install by the conventional route, ligand exchange of $RuCl_2(PCy_3)$(=CHPh) **GI**. Preliminary attempts to install CAACs onto [$RuCl_2$(*p*-

cymene)]$_2$ via in situ generation of the free CAAC were unsuccessful. Installation via the free carbene (where the latter is sufficiently stable) offers promise as an alternative. Also of interest is the potential of $RuCl_2$(*p*-cymene)(H_2IMes) as a precursor to other Ru-H_2IMes complexes. Photoliberation of *p*-cymene in the presence of other ligands could provide access to a broad family of $RuCl_2(H_2IMes)(L)_n$ (n = 2 for large L, or n = 3 for small L). A wide range of complexes may thus be attainable, which could enable hydrogen transfer, cross-couplings or other catalytic reactions.

Appendix

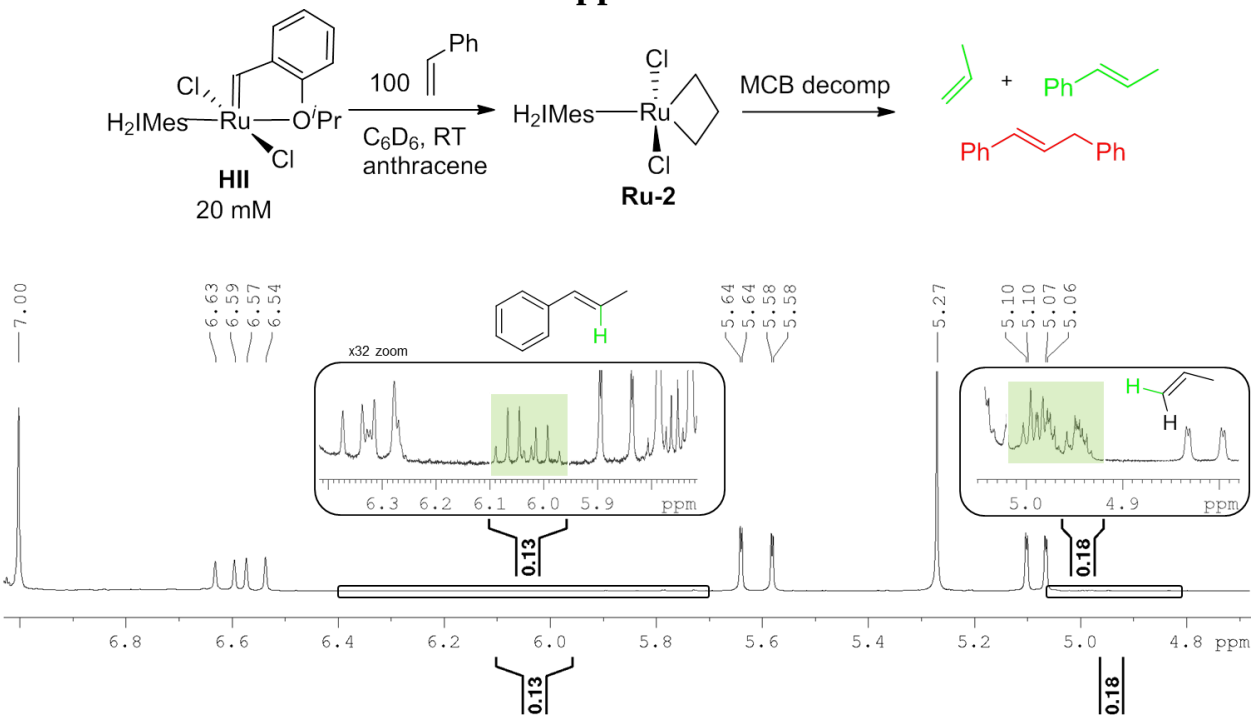

Figure A1. Representative ^{1}H NMR spectrum (C_6D_6, 300 MHz) showing quantification of propenyl products generated on metathesis of styrene by **HII**. Green shading indicates the specific signals used for integration relative to internal standard (anthracene). Integrations are normalized to starting **HII** [Ru]=C*H*Ph (δ_H 16.72, s, 1H).

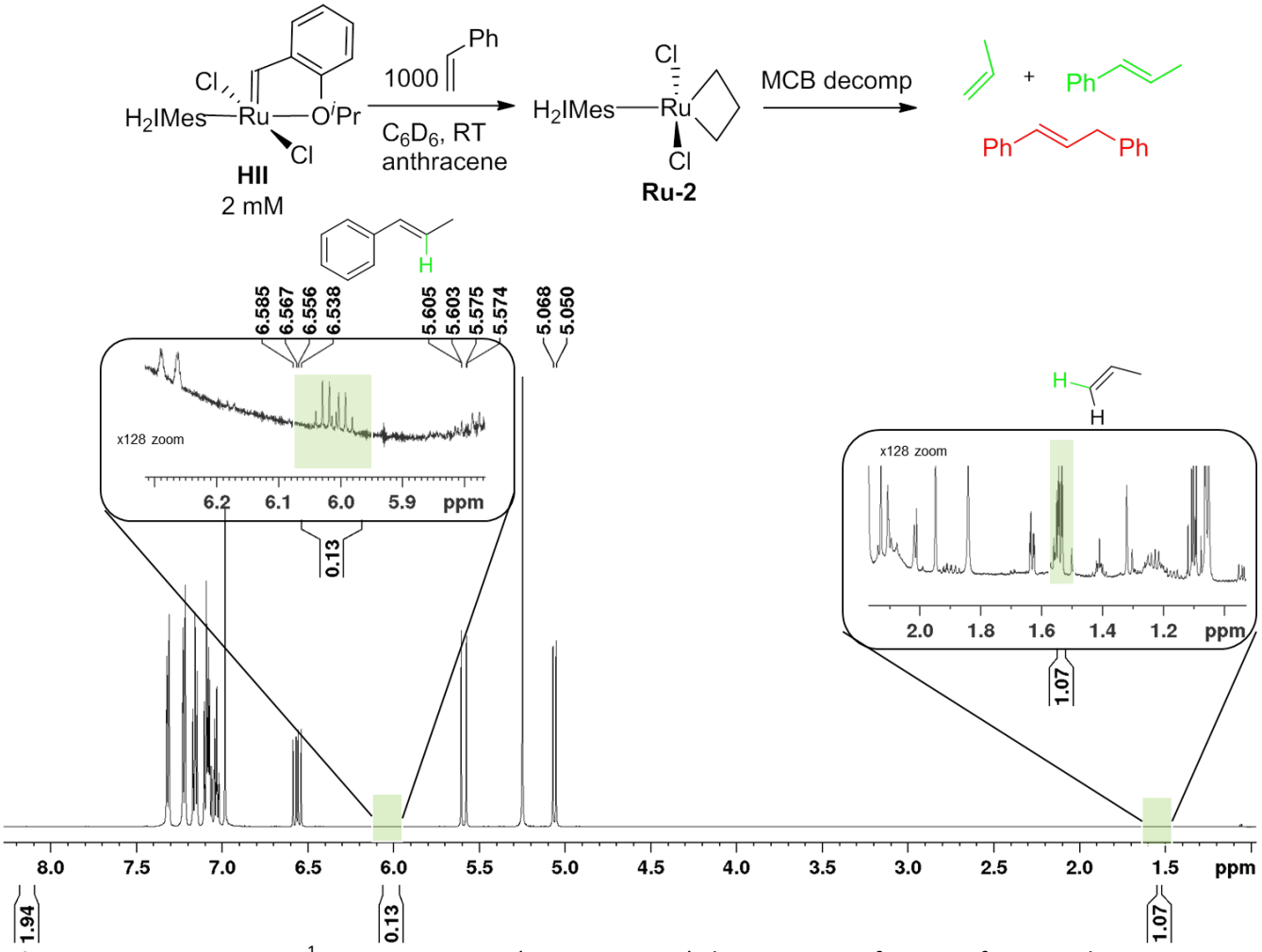

Figure A2. Representative ^{1}H NMR spectrum (C_6D_6, 300 MHz) showing quantification of propenyl products generated on metathesis of styrene by **HII**. Green shading indicates the specific signals used for integration relative to internal standard (anthracene). Integrations are normalized to starting **HII** [Ru]=C*H*Ph (δ_H 16.72, s, 1H).

Table A1. GC signals observed in self-metathesis of methyl 10-undecenoate 3.[a]

Retention time (min)	Assignment	Area %	Basis of Assignment
5.03	**3**–28 Da*	0.8	GC-MS
5.63	**3**–14*	3.0	GC-MS
6.19	**3**	70.8	Co-injection / GC-MS
6.95	**3**+14*	2.1	GC-MS
10.48	Inconclusive (weak)*	2.0	-
10.53	Inconclusive (weak)*	1.5	
10.80	(*E*)-**4**	17.6	NMR
11.08	Inconclusive (weak)*	0.3	-
11.18	Inconclusive (weak)*	0.5	-
11.37	Inconclusive (weak)*	0.3	-

[a] Known or suspected isomerization–metathesis products are denoted with (*).

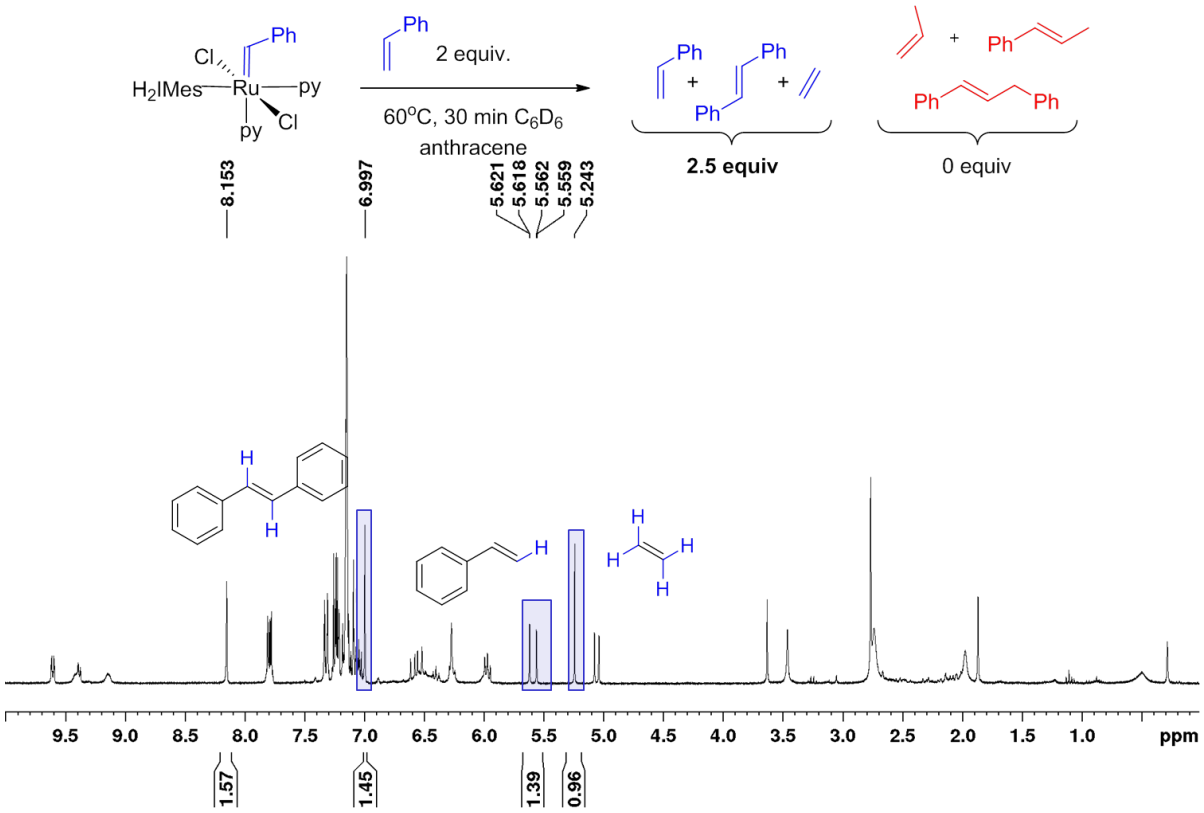

Figure A3. Representative ^{1}H NMR spectrum (C_6D_6, 300 MHz) showing quantification organic products generated on metathesis of styrene by **GIII**. Blue shading indicates the specific signals used for integration relative to internal standard (anthracene). Integrations are normalized to starting **GIII**.

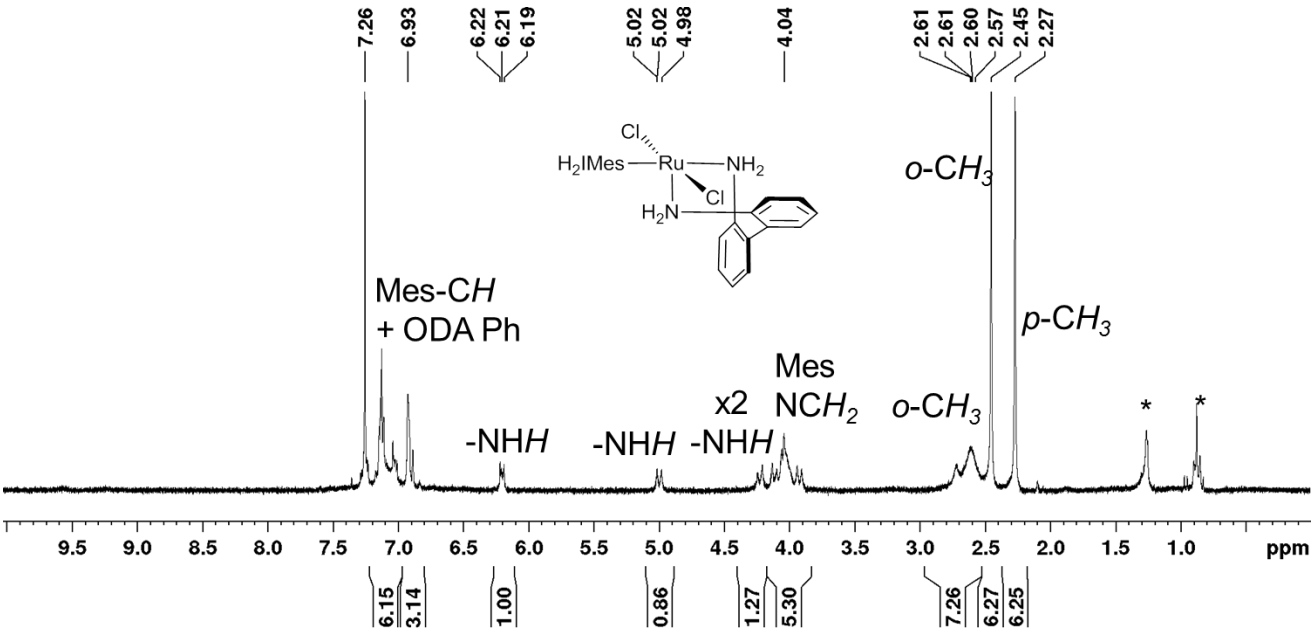

Figure A4. Representative ^{1}H NMR spectrum ($CDCl_3$, 300 MHz) of isolated $RuCl_2(H_2IMes)(ODA)$ **Ru-11**. Residual solvent is denoted: (*) Hexanes

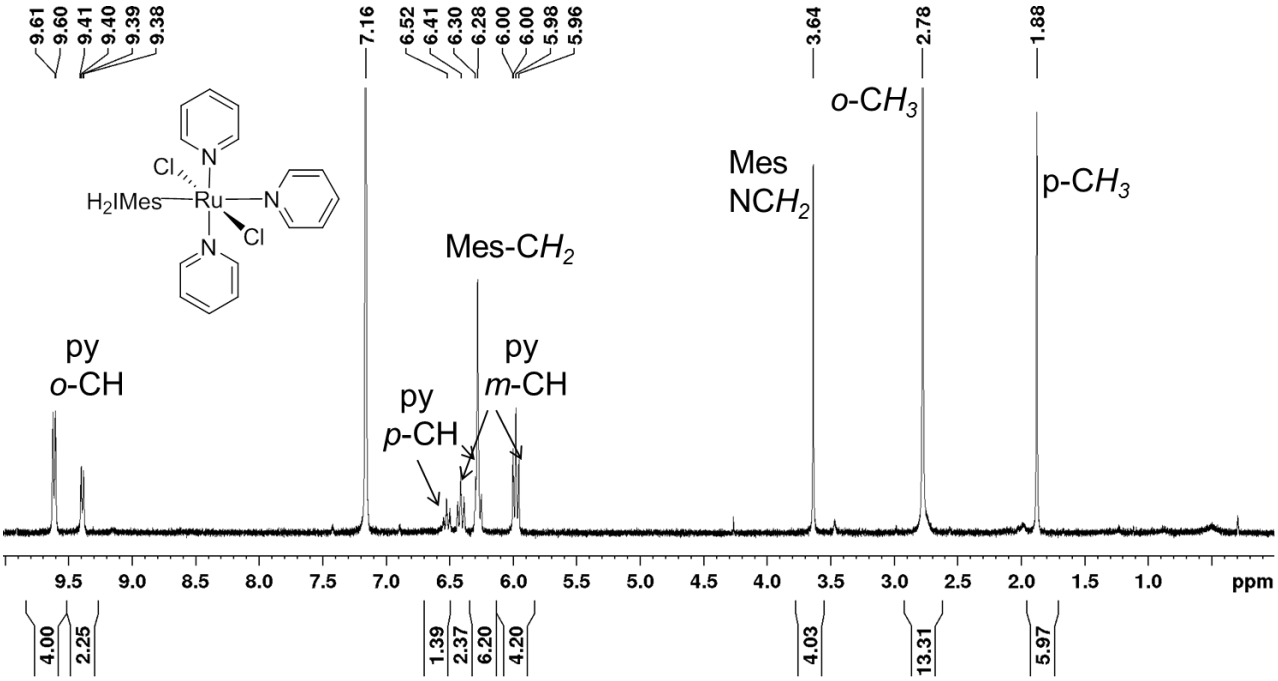

Figure A5. Representative ^{1}H NMR spectrum (C_6D_6, 300 MHz) of isolated $RuCl_2(H_2IMes)(py)_3$ **Ru-6**.

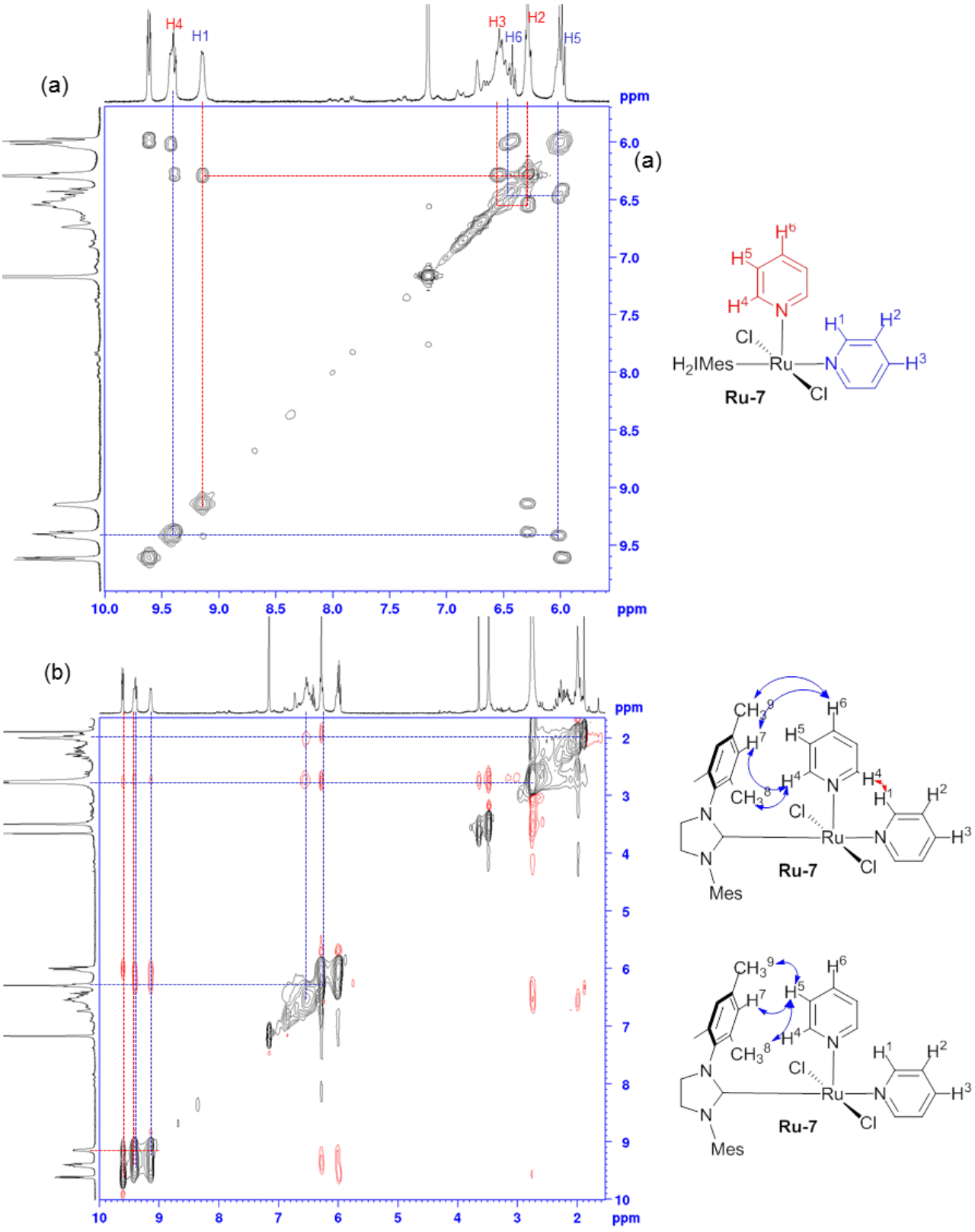

Figure A6. (a)^{1}H-^{1}H COSY spectrum of $RuCl_2(H_2IMes)(py)_2$ **Ru-7** zoomed in to diagnostic pyridine signals (b) Full ^{1}H-^{1}H NOESY spectrum of $RuCl_2(H_2IMes)(py)_2$ **Ru-7**.

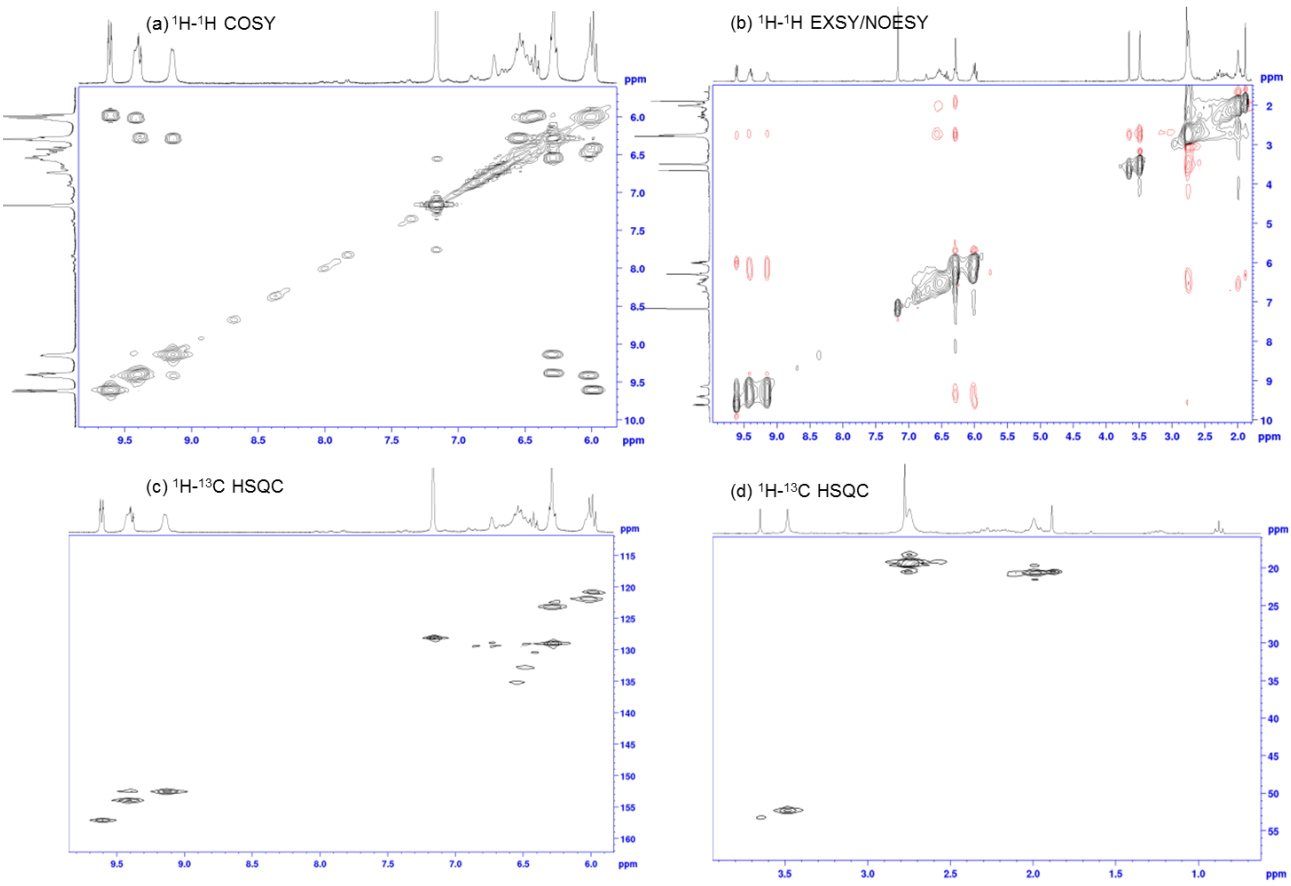

Figure A7. 2D NMR spectra of $RuCl_2(H_2IMes)(py)_2$ **Ru-7**

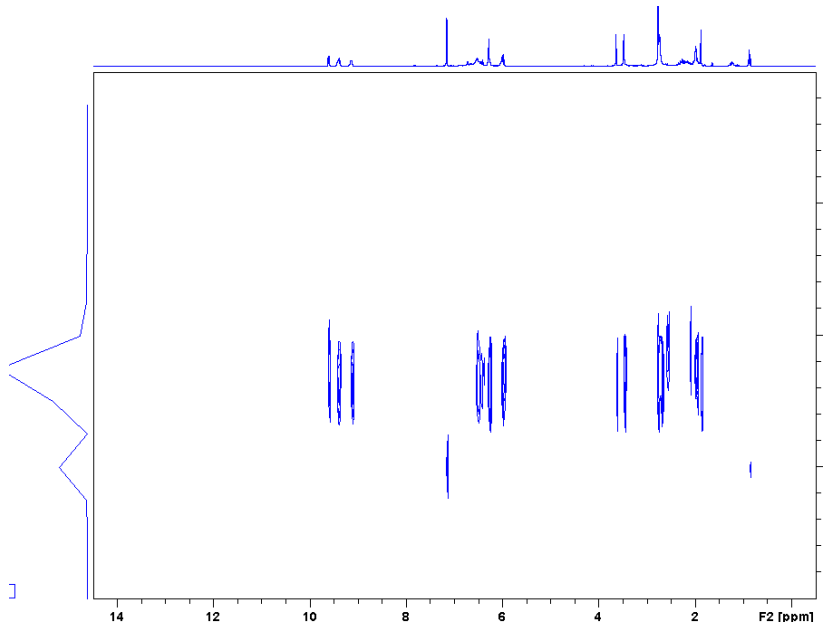

Figure A8. DOSY NMR spectra of $RuCl_2(H_2IMes)(py)_2$ **Ru-7** and $RuCl_2(H_2IMes)(py)_3$ **Ru-6** confirming **Ru-7** is monomeric

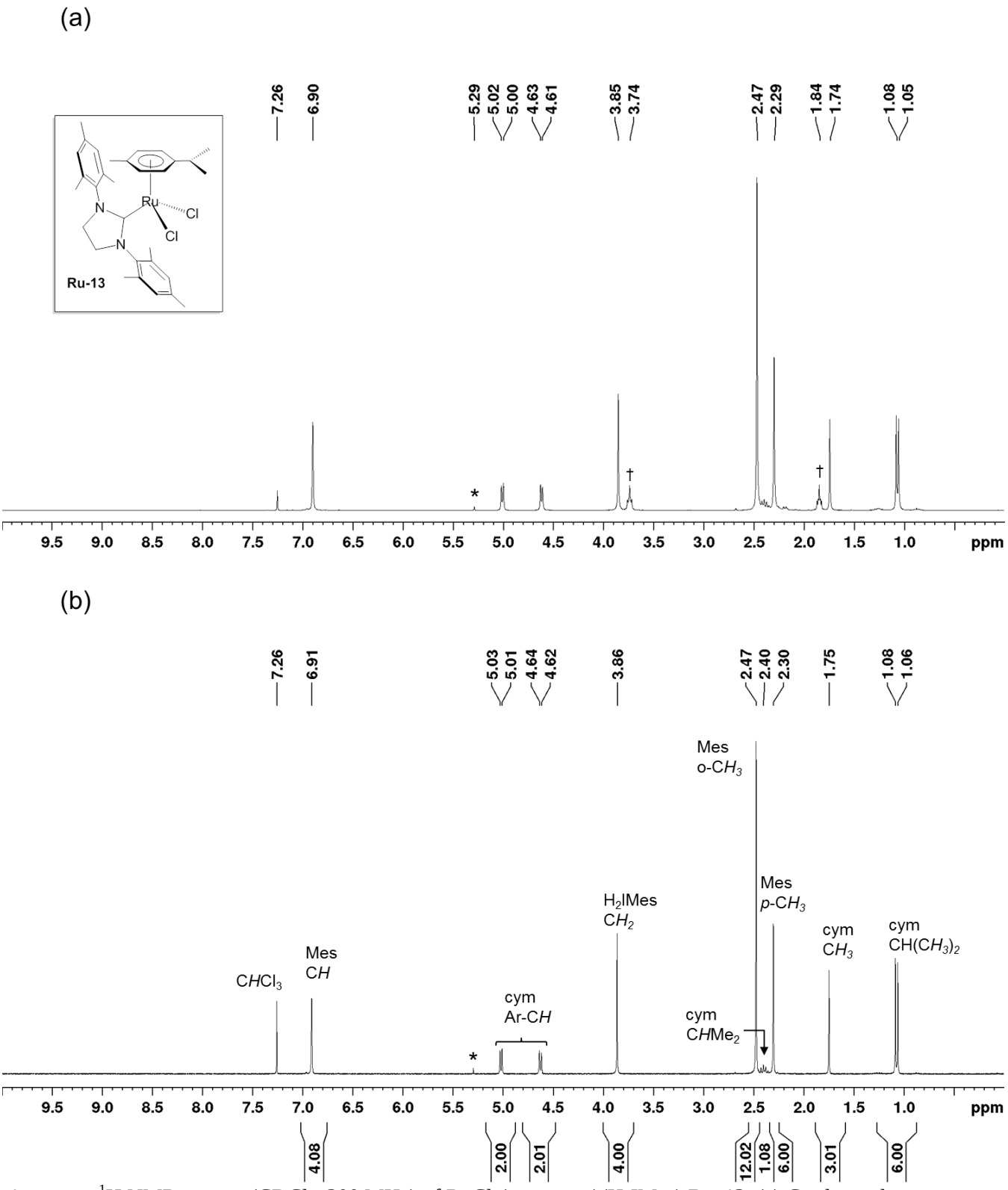

Figure A9. ^{1}H NMR spectra ($CDCl_3$, 300 MHz) of $RuCl_2$(*p*-cymene)(H_2IMes) **Ru-13**. (a) Crude product. Residual solvent is denoted: (*) CH_2Cl_2; (†) THF. (b) After precipitation. For the ^{1}H spectrum of clean **Ru-13** in C_6D_6, see Fig. A13.

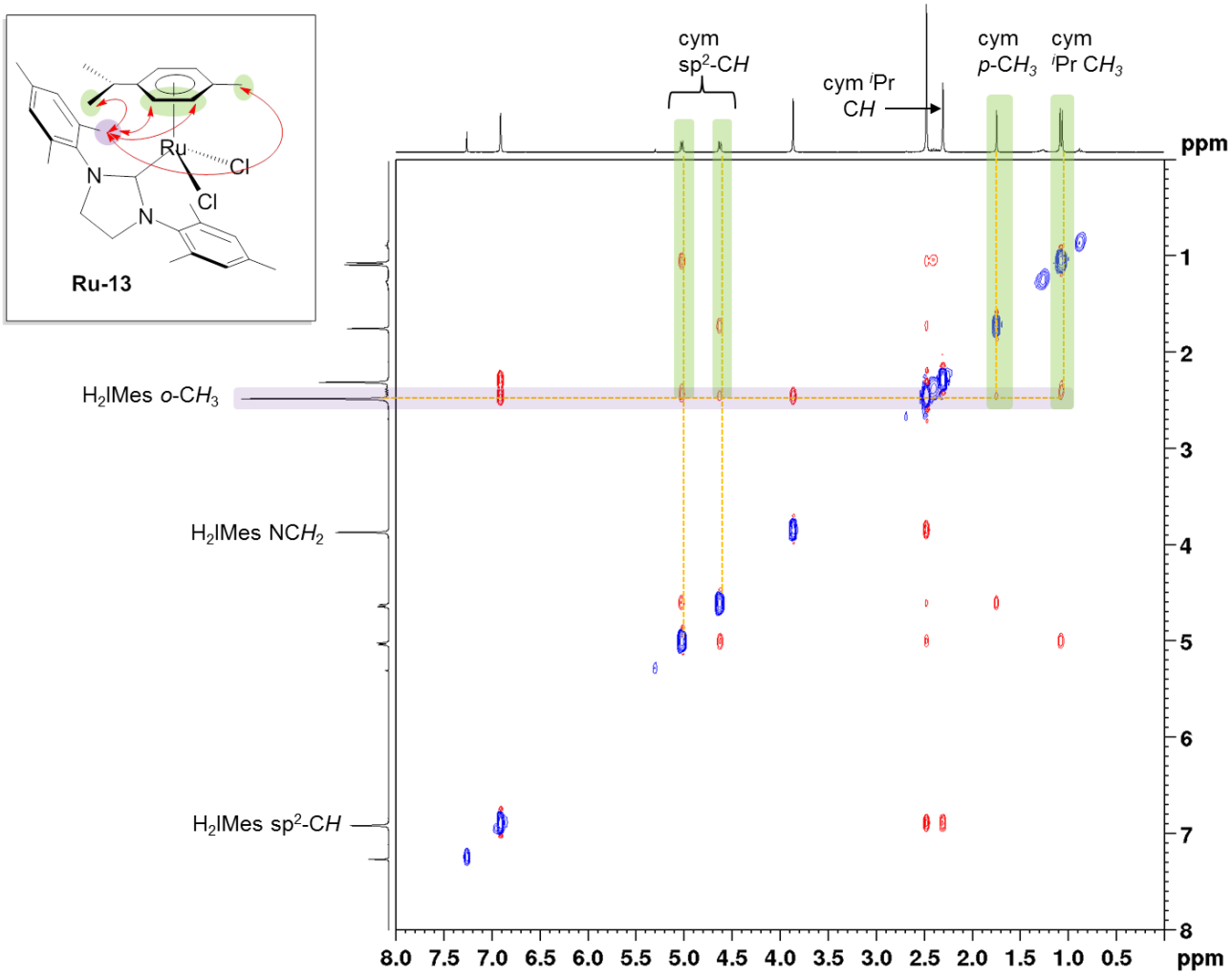

Figure A10. ^{1}H-^{1}H NOESY spectrum ($CDCl_3$, 300 MHz, 1 s mixing time) of **Ru-13**, highlighting correlations between the mesityl and *p*-cymene protons. For simplicity, correlations are shown (red arrows) for only one group where nuclei are equivalent by rotation.

The 1-D NMR spectra shown on the axes are not projections of the contour plot, but were measured prior to the NOESY experiment to exclude artifacts arising from sample decomposition.

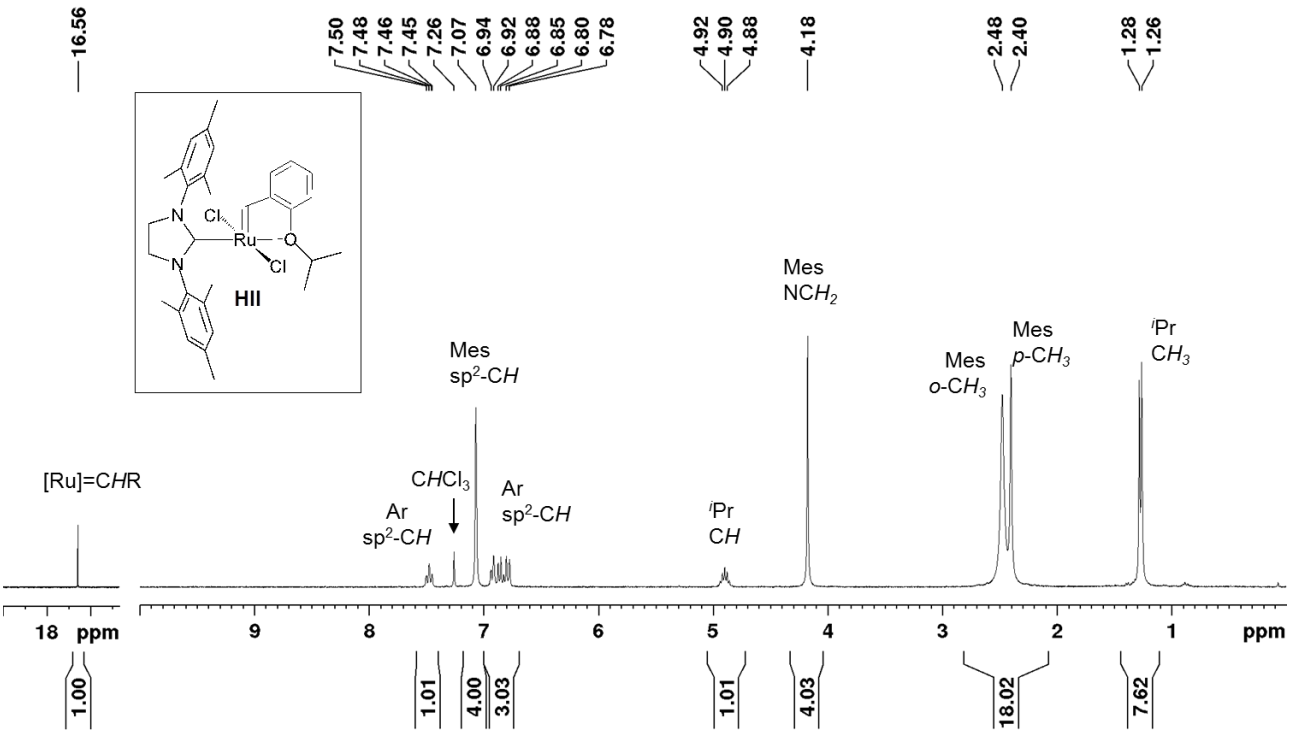

Figure A11. ^{1}H NMR spectrum ($CDCl_3$, 300 MHz) of $RuCl_2(H_2IMes)(=CH\text{-}o\text{-}C_6H_4OiPr)$, **HII**.

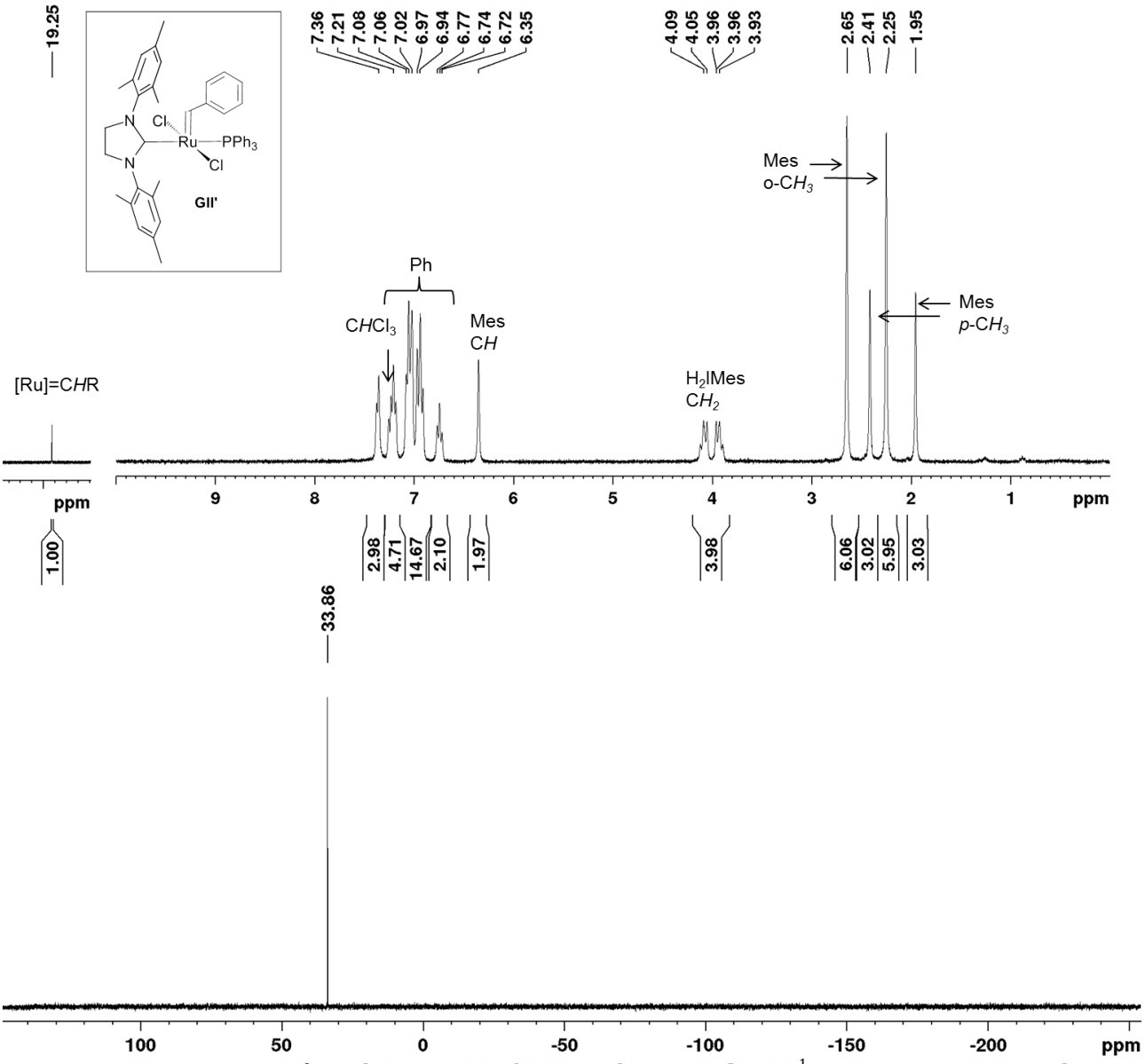

Figure A12. NMR spectra of $RuCl_2(H_2IMes)(PPh_3)(=CHPh)$ **GII-PPh$_3$**. (a) ^1H NMR spectrum **(**$CDCl_3$, 300 MHz). (b) $^{31}P\{^1H\}$ NMR spectrum **(**$CDCl_3$, 121 MHz).

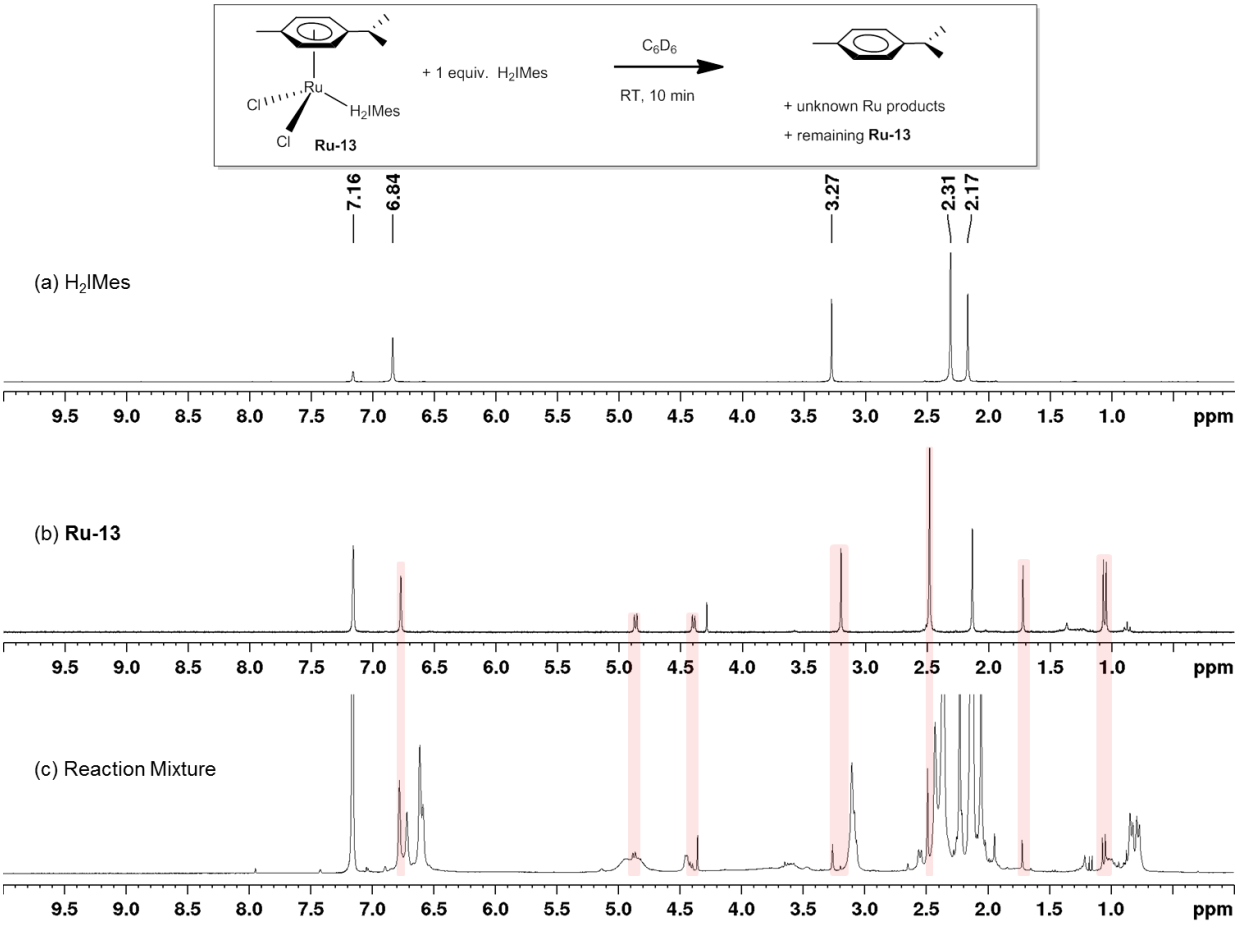

Figure A13. Probing the decomposition of $RuCl_2$(*p*-cymene)(H_2IMes) **Ru-13** with H_2IMes. ^{1}H NMR spectra (C_6D_6, 300 MHz) of: (a) Free H_2IMes. (b) **Ru-13**. (c) Reaction after 10 min. Red indicates **Ru-13** signals.

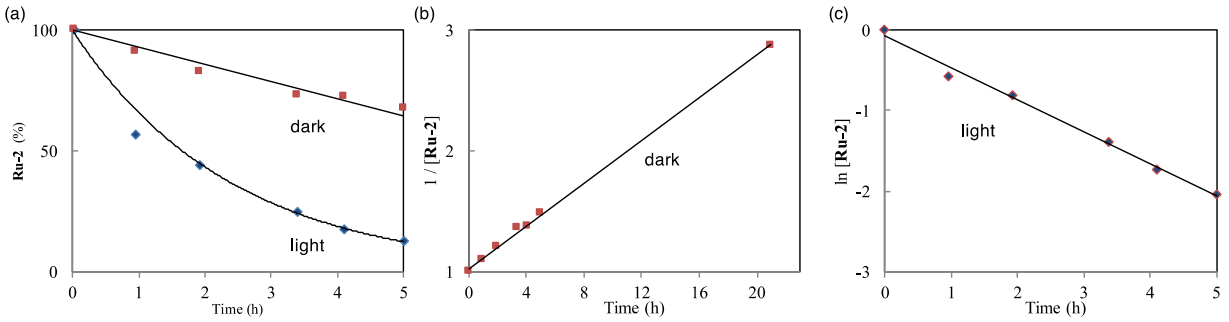

Figure A14. Decomposition of **Ru-13** (20 mM; C_6D_6, RT). (a) Conversion-time plots for foil-wrapped sample, and sample exposed to fluorescent light. Lines are provided an aid to visualization, not curve fits. (b) Plot showing second-order dependence for decomposition of **Ru-13** in the dark. (c) Plot showing first-order dependence for decomposition of **Ru-13** by light.

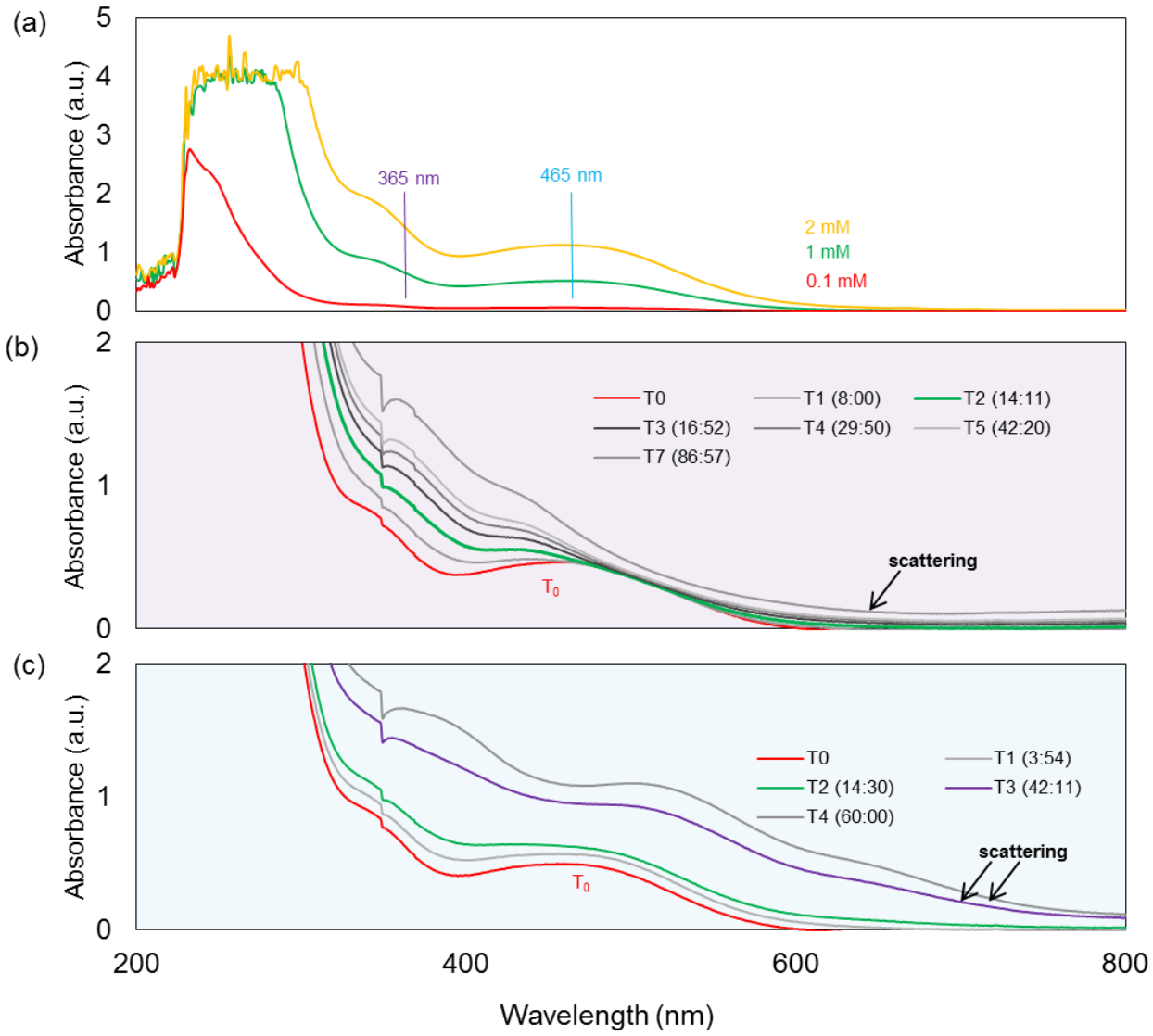

Figure A15. UV-vis spectra of **Ru-13** in CH_2Cl_2. (a) Initial spectrum. (b) After UV irradiation (365 nm, 6882 mW•m^{-2}; 1 mM) for the time periods shown: units are minutes. (c) After visible light irradiation (465 nm, 1669 mW•m^{-2}; 1 mM) for the time periods shown. "T0" designates starting spectrum.

Table A2. Overall Yields in Synthesis of **HII** By Leading Routes**.**

Prior Work					This Work				
Step	Product	Precursor	Yield (%)	Ref	Step	Product	Precursor	Yield (%)	Ref
1	$RuCl_2(PPh_3)_3$	$RuCl_3$	74[a]	1	1	$[RuCl_2(p\text{-cymene})]_2$	$RuCl_3$	87	2
2	**GI**	$RuCl_2(PPh_3)_3$	75[a]	3	2	**Ru-2**	$[RuCl_2(p\text{-cymene})]_2$	96	This work
3	**GII**[b]	**GI**	90-96	4,5	3	**HII**	**Ru-2**	82	This work
4	**HII**[b]	**GII**	85-97	6,7	**NET**			**68**	
NET			**42-52**						
Alternative reaction sequence (differs after Steps 1 & 2).									
3	**HI**	**GI**	67	8					
4	**HII**[b]	**HI**	92-96	4,5,9					
NET			**34-36**						
Alternative indenylidene route (differs after Step 1).									
2	**In0**	$RuCl_2(PPh_3)_3$	quant	10					
3[c]	**InII'**	**In0**	88-90	11,12					
4	**HII**	**InII'**	40	11					
NET			**35-36**						

[a]Isolated yield after extracting PPh_3. [b] High-yield routes to **HII** and **GII** are summarized in ref [5], Table 1. The Amberlyst route is omitted, given reproducibility issues (see ref [5]).

Table A3. Overall Yields in Synthesis of **GII'**.

Prior Work					This Work			
Step	Product	Precursor	Yield (%)	Ref	Step	Product	Yield (%)	Ref
1	$RuCl_2(PPh_3)_3$	$RuCl_3$	74[a]	1	1	$[RuCl_2(p\text{-cymene})]_2$	87	2
2	**GI**	$RuCl_2(PPh_3)_3$	75[a]	3	2	**Ru-2**	96	This work
3	**GII**[b]	**GI**	90-96	4,5	3	**GII'**	81	This work
4	**GIII**	**GII**	80-85	13[c]				
5	**GII'**	**GIII**	73	13				
NET			**29-33**				**68**	

[a]Isolated yield after extracting PPh_3. [b] High-yield routes to **HII** and **GII** are summarized in ref 5 (Table 1). The Amberlyst route is omitted from the table above, given the reproducibility issues discussed in ref 5. [c] The range indicated is given in the text of ref 13.

(b) Comparative Calculations of Atom Economy

$$\textbf{Atom economy} = \frac{\textbf{MW desired product}}{\Sigma\ \textbf{MW reactants}} \times 100$$

Table A4. Synthesis of HII By Leading Routes Discussed.[a]

	Σ MW	AE
New Route (this work)		
$RuCl_3$ + α-phellandrene + H_2IMes + $N_2CHC_6H_4O^iPr$ ⟶ **HII** MW 207.4 136.2 306.5 176.2 MW 626.6	826	76%
Prior Synthesis: Phenyldiazomethane Route		
$RuCl_3$ + 6 PPh_3 + $PhCHN_2$ + 2 PCy_3 + H_2IMes + $H_2C{=}CHC_6H_4O^iPr$ ⟶ **HII** MW 207.4 6 x 262.3 118.1 2 x 280.4 306.5 162.2 MW 626.6	2929	21%
Improvement in AE in new route		**3.6x**
Prior Synthesis: Indenylidene Route		
$RuCl_3$ + 6 PPh_3 + $HCC(OH)Ph_2$ + $H_2IMes{\bullet}HO^tBu$ + $H_2C{=}CH(CH_2)_3HC{=}CHC_6H_4O^iPr$ ⟶ **HII** MW 207.4 6 x 262.3 208.3 380.5 230.4 MW 626.6	2526	25%
Improvement in AE in new route		**3.1x**

[a]The extent of water-solvation of $RuCl_3$ is highly variable: the solvate is omitted here and below.

Table A5. Synthesis of GII' By Routes Discussed.

	Σ MW	AE
New Route (this work)		
$RuCl_3$ + α-phellandrene + H_2IMes + $PhCHN_2$ + PPh_3 ⟶ **GII'** MW 207.4 136.2 306.5 118.1 262.3 MW 830.8	1031	81%
Prior Route		
$RuCl_3$ + 6 PPh_3 + $PhCHN_2$ + 2 PCy_3 + H_2IMes + 2 py + PPh_3 ⟶ **GII'** MW 207.4 6 x 262.3 118.1 2 x 280.4 306.5 2 x 79.1 262.3 MW 830.8	3187	26%
Improvement in AE in new route		**3.1x**

References

(1) Hallman, P. S.; Stephenson, T. A.; Wilkinson, G. *Inorg. Synth.* **1970**, *12*, 237–40.
(2) Bennett, M. A.; Huang, T.-N.; Matheson, T. W.; Smith, A. K. *Inorg. Synth.* **1982**, *21*, 74–78.
(3) Schwab, P.; Grubbs, R. H.; Ziller, J. W. *J. Am. Chem. Soc.* **1996**, *118*, 100–110. Isolated yields of clean **GI** are typically on the order of 75%.
(4) Sauvage, X.; Demonceau, A.; Delaude, L. *Adv. Synth. Catal.* **2009**, *351*, 2031–2038.
(5) Nascimento, D. L.; Davy, E. C.; Fogg, D. E. *Catal. Sci. Technol.* **2018**, 1535–1544.
(6) Bujok, R.; Bieniek, M.; Masnyk, M.; Michrowska, A.; Sarosiek, A.; Stepowska, H.; Arlt, D.; Grela, K. *J. Org. Chem.* **2004**, *69*, 6894–6896.
(7) Garber, S. B.; Kingsbury, J. S.; Gray, B. L.; Hoveyda, A. H. *J. Am. Chem. Soc.* **2000**, *122*, 8168–8179.
(8) Kingsbury, J. S.; Harrity, J. P. A.; Bonitatebus, P. J.; Hoveyda, A. H. *J. Am. Chem. Soc.* **1999**, *121*, 791–799.
(9) Bieniek, M.; Michrowska, A.; Gulajski, L.; Grela, K. *Organometallics* **2007**, *26*, 1096–1099.
(10) Fürstner, A.; Guth, O.; Duffels, A.; Seidel, G.; Liebl, M.; Gabor, B.; Mynott, R. *Chem. – Eur. J.* **2001**, *7*, 4811–4820.
(11) Randl, S.; Gessler, S.; Wakamatsu, H.; Blechert, S. *Synlett* **2001**, 430–432.
(12) Urbina Blanco, C. A.; Manzini, S.; Gomes, J. P.; Doppiu, A.; Nolan, S. P. *Chem. Comm* **2011**, *47*, 5022—5024.
(13) Sanford, M. S.; Love, J. A.; Grubbs, R. H. *Organometallics* **2001**, *20*, 5314–5318.